

# ANALYSIS OF ENERGY BASED SIGNAL DETECTION

**JANNE  
LEHTOMÄKI**

Faculty of Technology,  
Department of Electrical and  
Information Engineering,  
University of Oulu

OULU 2005





*JANNE LEHTOMÄKI*

**ANALYSIS OF ENERGY BASED  
SIGNAL DETECTION**

Academic Dissertation to be presented with the assent of  
the Faculty of Technology, University of Oulu, for public  
discussion in Raahensali (Auditorium L10), Linnanmaa,  
on December 9th, 2005, at 12 noon

OULUN YLIOPISTO, OULU 2005

Copyright © 2005  
University of Oulu, 2005

Supervised by  
Professor Markku Juntti

Reviewed by  
Associate Professor Peter Händel  
Professor Marco Lops

ISBN 951-42-7924-7 (nid.)  
ISBN 951-42-7925-5 (PDF) <http://herkules.oulu.fi/isbn9514279255/>  
ISSN 0355-3213 <http://herkules.oulu.fi/issn03553213/>

OULU UNIVERSITY PRESS  
OULU 2005

## **Lehtomäki, Janne, Analysis of energy based signal detection**

Faculty of Technology, University of Oulu, P.O.Box 4000, FIN-90014 University of Oulu, Finland,  
Department of Electrical and Information Engineering, University of Oulu, P.O.Box 4500, FIN-  
90014 University of Oulu, Finland  
2005  
Oulu, Finland

### ***Abstract***

The focus of this thesis is on the binary signal detection problem, i.e., if a signal or signals are present or not. Depending on the application, the signal to be detected can be either unknown or known. The detection is based on some function of the received samples which is compared to a threshold. If the threshold is exceeded, it is decided that signal(s) is (are) present. Energy detectors (radiometers) are often used due to their simplicity and good performance. The main goal here is to develop and analyze energy based detectors as well as power-law based detectors.

Different possibilities for setting the detection threshold for a quantized total power radiometer are analyzed. The main emphasis is on methods that use reference samples. In particular, the cell-averaging (CA) constant false alarm rate (CFAR) threshold setting method is analyzed. Numerical examples show that the CA strategy offers the desired false alarm probability, whereas a more conventional strategy gives too high values, especially with a small number of reference samples.

New performance analysis of a frequency sweeping channelized radiometer is presented. The total power radiometer outputs from different frequencies are combined using logical-OR, sum and maximum operations. An efficient method is presented for accurately calculating the likelihood ratio used in the optimal detection. Also the effects of fading are analyzed. Numerical results show that although sweeping increases probability of intercept (POI), the final probability of detection is not increased if the number of observed hops is large.

The performance of a channelized radiometer is studied when different CFAR strategies are used to set the detection threshold. The proposed iterative methods for setting the detection threshold are the forward consecutive mean excision (FCME) method with the CA scaling factors in final detection decision (FCME+CA), the backward consecutive mean excision (BCME) method with the CA scaling factors in detection (BCME+CA) and a method that uses the CA scaling factors for both censoring and detection (CA+CA). Numerical results show that iterative CFAR methods may improve detection performance compared to baseline methods.

Finally, a method to set the threshold of a power-law detector that uses a nonorthogonal transform is presented. The mean, variance and skewness of the decision variable in the noise-only case are derived and these are used to find a shifted log-normal approximation for the distribution of the decision variable. The accuracy of this method is verified through simulations.

*Keywords:* channelized radiometers, intercept receivers, power-law detectors, radiometers, signal detection, threshold settings



## Preface

Research for this thesis has been carried out in the Centre for Wireless Communications (CWC) and the Telecommunication Laboratory, Department of Electrical and Information Engineering, University of Oulu, Oulu, Finland. I wish to thank the Director of the Telecommunication Laboratory, Prof. Pentti Leppänen, former Director of CWC, Docent Ian Oppermann, and the Director of CWC, Prof. Matti Latva-aho, for giving me an opportunity to perform this research.

I wish to express my deep gratitude to my supervisor, Prof. Markku Juntti, for his guidance and encouragement.

Most of the work on this thesis was conducted in a research project sponsored by the Finnish Defence Forces Technical Research Centre. The scientific advisory board for defence (Maanpuolustuksen tieteellinen neuvottelukunta, MATINE) and PANU project partners (Nokia, Elektrobit, Finnish Defence forces and Tekes) also sponsored some parts of the work. I would like to thank the manager of the project, Dr. Harri Saarnisaari, and other persons who participated in the project. From CWC, I would like to mention my co-authors Johanna Vartiainen and Sami Koivu.

During my postgraduate studies, I had the privilege of being a student in the Graduate School in Electronics, Telecommunications and Automation (GETA). The director of GETA, Prof. Iiro Hartimo, and the coordinator of GETA, Marja Leppäharju, are warmly thanked. I also thank Tekniikan Edistämissäätiö (TES), Nokia Foundation, and Tauno Tönningin säätiö for supporting the thesis work.

I wish to thank the reviewers of the thesis, Professor Peter Händel from the Royal Institute of Technology and Professor Marco Lops from the University of Cassino for their insightful comments. Special thanks are due to Johanna Vartiainen and Harri Saarnisaari who (in addition to my supervisor) read and commented on the manuscript. Their comments and the comments from the reviewers of the thesis improved the readability and clarity of the thesis. The anonymous reviewers and the co-authors of the original papers are also gratefully acknowledged.

I thank all personnel in the CWC and Telecommunication Laboratory for providing a pleasant working environment.

Oulu, November 8, 2005

Janne Lehtomäki



## Symbols and abbreviations

|              |  |
|--------------|--|
| $\mathbf{A}$ | Transformation matrix  |
| $B$          | Number of quantization bits  |
| $\mathbf{C}$ | Set of local decisions in all hops and channels  |
| $C_{ij}$     | Local decision based on the radiometer output  |
| $E_H$        | Received signal energy per hop   |
| $E_{ij}$     | Energy of the FH signal in the time-frequency area corresponding to the radiometer output $j$ in hop $i$ |
| $f_{V'}$     | Probability density function of $V'$   |
| $H_0$        | Noise-only hypothesis  |
| $H_1$        | Signal(s)-and-noise hypothesis   |
| $I_\nu$      | Modified Bessel function of the first kind   |
| $k_M$        | Final detection threshold  |
| $M$          | Number of preliminary decisions per a decision   |
| $M_C$        | Integer value corresponding to time-frequency product  |
| $N$          | Number of samples per block  |
| $N_C$        | Number of radiometers  |
| $N_H$        | Number of non-overlapping hop channels   |
| $n_k$        | Noise process sample   |
| $N_R$        | Number of reference samples  |
| $N_{eff}$    | Total number of radiometer outputs within a hop  |
| $p_0$        | Probability of false alarm per hop   |
| $p_1$        | Probability of detection per hop   |
| $p_I$        | Probability of intercept per hop   |
| $P_k$        | $k$ th raw moment of the power-law decision variable   |
| $P_r$        | Clean sample rejection rate  |
| $P_D$        | Probability of detection   |
| $P_{FA,DES}$ | Desired probability of false alarm   |
| $P_{FA}$     | Probability of false alarm   |
| $P_{FC}$     | Probability of false censoring   |
| $P_M$        | Probability of miss  |
| $Q_D$        | Individual radiometer's probability of detection   |
| $Q_{FA}$     | Individual radiometer's probability of false alarm   |
| $Q_m$        | Generalized Marcum's Q function  |

|                    |   |
|--------------------|---|
| <b>R</b>           | Set of normalized radiometer outputs                        |
| $R$                | Dynamic range   |
| $r_k$              | Receiver signal at time instant $k$                         |
| $\tilde{r}_k$      | Quantized received signal                                   |
| $R_{i,j}$          | Normalized (scaled with $2/N_0$ ) radiometer output         |
| $s_k$              | Sample of a typically unknown signal to be detected         |
| $T'$               | Integer-valued detection threshold                          |
| $T_H$              | Hop duration  |
| $T_k$              | Censoring scaling factor in step $k$                        |
| $T_R$              | Individual radiometer's integration time                    |
| $T_{CA}$           | Cell-averaging scaling factor                               |
| $T_{CME}$          | Consecutive mean excision scaling factor                    |
| $T_{f2,v}$         | Decision statistic of a contiguity-based power-law detector |
| $T_{OS,k}$         | Order statistics scaling factor                             |
| $T_v$              | Decision statistic of transform domain power-law detector   |
| $V$                | Decision variable of energy detector                        |
| $V'$               | Equivalent energy detection decision variable               |
| <b>W</b>           | Matrix with window coefficients in the diagonal             |
| $W$                | Decision variable   |
| $W_H$              | Hop bandwidth   |
| $W_i$              | Per hop decision variable                                   |
| $W_R$              | Individual radiometer's bandwidth                           |
| $x$                | Ratio of step size and standard deviation of noise          |
| $Z$                | Radiometer output in test cell                              |
| $Z_i$              | Radiometer outputs in the reference cells                   |
| $Z_{CA}$           | Cell-averaging reference statistic                          |
| $\eta$             | Hard-decision threshold for individual radiometers          |
| $\tilde{\delta}$   | Randomization factor  |
| $\gamma$           | Threshold scaling factor                                    |
| $\gamma_H$         | Instantaneous hop SNR                                       |
| $\tilde{\gamma}_H$ | Average hop SNR   |
| $\Gamma$           | Gamma function  |
| $\Lambda$          | Likelihood ratio  |
| $\lambda_i$        | Non-centrality parameter of reference cells                 |
| $\lambda_S$        | Total non-centrality parameter                              |
| $\Omega$           | Signal-to-noise ratio                                       |
| $\Phi$             | FFT matrix  |
| $\Psi$             | Covariance matrix   |
| $\sigma^2$         | Noise variance  |
| $\Delta$           | Quantization step   |
| $\Upsilon$         | Quantization operator                                       |
| $\vartheta_k$      | Reference samples   |
| ACMLD              | Automatic censored mean level detector                      |
| ADC                | Analog-to-digital converter                                 |
| AGC                | Automatic gain control                                      |

|      |                                     |
|------|-------------------------------------|
| AOS  | Adaptive order statistic            |
| AWGN | Additive white Gaussian noise       |
| BCME | Backward consecutive mean excision  |
| BI   | Binary integration                  |
| BMWD | Binary moving window detection      |
| BPM  | Bit position modulation             |
| CA   | Cell averaging                      |
| CCA  | Censored cell averaging             |
| CDF  | Cumulative distribution function    |
| CFAR | Constant false alarm rate           |
| CMLD | Censored mean level detector        |
| DOA  | Direction-of-arrival                |
| DS   | Direct sequence                     |
| ES   | Electronic support                  |
| FCME | Forward consecutive mean excision   |
| FFH  | Fast frequency hopping              |
| FFT  | Fast Fourier transform              |
| FH   | Frequency hopping                   |
| GLRT | Generalized likelihood ratio test   |
| GOS  | Generalized order statistic         |
| IF   | Intermediate frequency              |
| IID  | Independent identically distributed |
| LRT  | Likelihood ratio test               |
| MML  | Multiple-hop maximum likelihood     |
| NP   | Neyman-Pearson                      |
| OS   | Order statistic                     |
| OSCA | Order statistics cell averaging     |
| OSGO | Order statistics greatest of        |
| PDF  | Probability density function        |
| PLD  | Power-law detector                  |
| PMF  | Probability mass function           |
| POI  | Probability of intercept            |
| ROC  | Receiver operating characteristic   |
| SFH  | Slow frequency hopping              |
| SLE  | Sum-of-largest-envelopes            |
| SLES | Sum-of-largest-envelopes-squared    |
| SNR  | Signal-to-noise ratio               |
| STAP | Space-time adaptive processing      |
| STFT | Short time Fourier transform        |
| TH   | Time hopping                        |
| TM   | Trimmed mean                        |
| UMP  | Universally most powerful           |
| UWB  | Ultra-wideband                      |
| VI   | Variability index                   |
| VTM  | Variably trimmed mean               |



# Contents

|  |    |
|--|----|
| Abstract   |    |
| Preface  |    |
| Symbols and abbreviations  |    |
| Contents   |    |
| 1 Introduction . . . . .   | 13 |
| 1.1 Signal detection . . . . .                                   | 13 |
| 1.2 Energy detector . . . . .                                    | 16 |
| 1.3 Aims and outline of the thesis . . . . .                     | 17 |
| 1.4 Author's contribution to the original publications . . . . . | 19 |
| 2 Literature review . . . . .                                    | 20 |
| 2.1 Total power radiometer . . . . .                             | 20 |
| 2.2 Decision strategies for a total power radiometer . . . . .   | 22 |
| 2.3 Channelized radiometer . . . . .                             | 23 |
| 2.4 CFAR methods . . . . .                                       | 24 |
| 2.4.1 Fixed censored CFAR . . . . .                              | 28 |
| 2.4.2 Excision CFAR . . . . .                                    | 29 |
| 2.4.3 Automatic censored CFAR . . . . .                          | 30 |
| 2.5 Power-law detector . . . . .                                 | 33 |
| 2.5.1 General . . . . .  | 34 |
| 2.5.2 Extended power law detector . . . . .                      | 35 |
| 3 System models . . . . .  | 36 |
| 3.1 Digital receiver model . . . . .                             | 36 |
| 3.2 Channelized radiometer model . . . . .                       | 38 |
| 3.2.1 Local radiometer outputs . . . . .                         | 39 |
| 3.2.2 FH detection assumptions . . . . .                         | 40 |
| 3.2.3 CFAR analysis assumptions . . . . .                        | 40 |
| 4 Threshold setting for a quantized radiometer . . . . .         | 43 |
| 4.1 Radiometer with quantization . . . . .                       | 43 |
| 4.2 Noise level estimation based on quantized samples . . . . .  | 45 |
| 4.3 Exact randomized decision rule . . . . .                     | 46 |
| 4.4 Performance analysis of the CA-CFAR strategy . . . . .       | 46 |
| 4.5 Numerical results . . . . .                                  | 49 |

|       |  |    |
|-------|--|----|
| 4.6   | Conclusions . . . . .  | 50 |
| 5     | Sweeping channelized radiometer . . . . .                            | 52 |
| 5.1   | Sweeping channelized radiometer . . . . .                            | 52 |
| 5.2   | Decision strategies . . . . .  | 54 |
| 5.2.1 | Likelihood ratio of un-quantized data . . . . .                      | 54 |
| 5.2.2 | Suboptimal methods . . . . .   | 55 |
| 5.2.3 | Likelihood ratio of quantized data . . . . .                         | 55 |
| 5.3   | Efficient calculation of the un-quantized likelihood ratio . . . . . | 56 |
| 5.4   | Performance analysis . . . . .                                       | 58 |
| 5.4.1 | Logical OR-sum decision rule . . . . .                               | 58 |
| 5.4.2 | Sum-sum decision rule . . . . .                                      | 59 |
| 5.4.3 | Max-sum decision rule . . . . .                                      | 59 |
| 5.5   | Performance under fading . . . . .                                   | 61 |
| 5.6   | Numerical results . . . . .  | 62 |
| 5.7   | Conclusions . . . . .  | 64 |
| 6     | CFAR strategies for channelized radiometer . . . . .                 | 66 |
| 6.1   | Performance analysis . . . . .                                       | 66 |
| 6.1.1 | Cell-averaging detector . . . . .                                    | 66 |
| 6.1.2 | Order statistics detector . . . . .                                  | 67 |
| 6.2   | Automatic censored CFAR detection . . . . .                          | 67 |
| 6.2.1 | Analysis of the stage (A) . . . . .                                  | 68 |
| 6.2.2 | Stage (B) . . . . .  | 70 |
| 6.3   | Numerical results . . . . .  | 70 |
| 6.3.1 | Clean sample rejection rate . . . . .                                | 70 |
| 6.3.2 | Automatic censored CFAR . . . . .                                    | 75 |
| 6.4   | Conclusions . . . . .  | 81 |
| 7     | Power-law based intercept receiver . . . . .                         | 82 |
| 7.1   | Properties of the decision variable . . . . .                        | 82 |
| 7.2   | Shifted log-normal approximation . . . . .                           | 84 |
| 7.3   | Contiguity-based detector . . . . .                                  | 85 |
| 7.4   | Numerical results . . . . .  | 86 |
| 7.5   | Conclusions . . . . .  | 89 |
| 8     | Conclusions and future work . . . . .                                | 92 |
|       | References . . . . .   | 94 |

# 1 Introduction

*”As far as the laws of mathematics refer to reality, they are not certain; and as far as they are certain, they do not refer to reality.” –Albert Einstein*

In classical hypothesis testing, the goal is to decide between the null hypothesis and the alternative hypothesis. For example, the null hypothesis could be ”some cars are not red”. In this case, the alternative hypothesis could be ”all cars are red”. To make a decision, it would be possible to go to a street and observe, say, 10 cars. The number of observed red cars is counted and the count is denoted with  $T$ . If  $T = 10$ , it is quite probable, based on the available observations, that the alternative hypothesis is true. Otherwise, the null hypothesis should be chosen.

Hypothesis testing is an old problem. It can be viewed to have been initiated by Bayes in 1764 [1]. Significant contributions were given by Neyman & Pearson (NP) in 1933 [2].

If the null and alternative hypotheses are defined in terms of signal(s), the hypothesis testing problem can be called binary signal detection. Binary refers to fact that there are two possible hypotheses. Actually, the number of hypotheses can be larger than two. However, in this thesis, the topic is binary signal detection, which has a multitude of important applications.

In Section 1.1, a brief overview to general binary signal detection theory and some signal detection applications are presented. Often, an energy detector is used for making detection decisions. This is discussed in Section 1.2. Section 1.3 presents the aims and outline of the thesis. In Section 1.4, the author’s contribution to the original publications is summarized.

## 1.1 Signal detection

The binary signal detection problem can be formulated as an hypothesis testing problem. There are two possible hypotheses,  $H_0$  and  $H_1$ ,

$$\begin{aligned} H_0 : & r_k = s_{1,k} + n_k & k = 0, 1, \dots, N - 1 \\ H_1 : & r_k = s_{2,k} + n_k & k = 0, 1, \dots, N - 1, \end{aligned} \tag{1}$$

where  $r_k$  is the received signal sample at time instant  $k$ ,  $n_k$  is the noise process sample,  $s_{1,k}$  is a sample of a signal present in the case of  $H_0$ ,  $s_{2,k}$  is a sample of a signal present in the case of  $H_1$ , and  $N$  is the total number of samples used for one decision. The samples can be real-valued or complex-valued. Signal detection theory has been extensively studied over several decades. Books [3, 4, 5, 6] form a small sample upon which this section is mainly based on. For example, in telecommunications, antipodal signaling uses  $s_{1,k} = -s_k$  and  $s_{2,k} = s_k$ , where  $s_k$  is a known signal waveform [7]. With antipodal signaling one information bit can be transferred at a time. In this thesis, transmission of information is not studied. Rather, the problem is to find out if there is a signal or signals present or not, i.e.,

$$\begin{aligned} H_0 : & \quad r_k = n_k & k = 0, 1, \dots, N-1 \\ H_1 : & \quad r_k = s_k + n_k & k = 0, 1, \dots, N-1, \end{aligned} \quad (2)$$

where the noise is assumed to be a white zero-mean Gaussian process with known or unknown variance. The signal can be, for example, deterministic with unknown parameters, like arrival time, phase, and amplitude; or deterministic but completely unknown [4]. This type of binary signal detection finds numerous applications in engineering.

- Electronic support (ES) receivers are used to search, locate and identify sources of electromagnetic radiation [8, 9, 10]. The detection of the presence of unknown signal(s) is an important goal in ES, and also in spectrum monitoring, which can be used for detecting unlicensed transmitters. In both applications the signal to be detected can range from analog to digital and from narrowband to wideband. Quite often some parameters of the single channel ground and airborne radio system (SINCGARS) are used when analyzing ES systems [11].
- Pulsed radar transmits and receives electromagnetic pulses. If there is a target present, the received signal will contain noise and a distorted echo of transmitted waveform. The distance of the target is directly related to delay between transmitting and receiving the pulse. The search or surveillance problem is to decide if the received signal contains only noise or noise and a signal [12].
- Methods similar to those described above for electromagnetic pulses can be used with underwater acoustic pulses. The device converting acoustic signals into electrical signals is called a hydrophone. A passive sonar processes the received electrical signal(s) and decides if it contains only noise, or noise and a signal generated by a ship or a submarine. It is also possible to use active sonars, which are similar to radars: they transmit an acoustic pulse and then listen for an echo [13].
- A cognitive radio is a radio that can alter its parameters, such as frequency, dynamically based on the environment and/or user demands. Spectrum sensing cognitive radio refers to a situation whereby the frequency spectrum is observed. Based on the spectrum information, signal detection methods can be used for finding signal-free frequency bands [14, 15, 16].

Detection is based on some function  $T$  of the received samples which is compared to a threshold  $\gamma$ . If the threshold is exceeded, it is decided that  $H_1$  is true. Let  $\mathbf{r}$  denote the received samples as a column vector. The probability of a false alarm  $P_{\text{FA}}$  is the probability that  $H_1$  is selected even when  $H_0$  is actually true, i.e.,  $P_{\text{FA}} = P(T(\mathbf{r}) > \gamma; H_0)$ . For example, in the case of a sonar, a false alarm occurs when it falsely decided that a

ship or a submarine is present. Depending on the sensitivity of the situation, a false alarm can have serious consequences. In the NP framework, the probability of a false alarm is required to have a fixed value. Here, the desired false alarm probability is denoted with  $P_{\text{FA,DES}}$ . The probability of a miss  $P_{\text{M}}$  is the probability that  $H_0$  is selected when  $H_1$  is true. The probability of detection  $P_{\text{D}} = 1 - P_{\text{M}}$  is the probability that  $H_1$  is selected when it is really true, i.e.,  $P_{\text{D}} = P(T(\mathbf{r}) > \gamma; H_1)$ . In the sonar application,  $P_{\text{D}}$  is the probability that an alarm occurs when a ship or a submarine is present. The best detector in the NP sense is the one with the highest probability of detection subject to the constraint on the false alarm probability. In addition to signal detection, the NP framework can also be used in synchronization in telecommunications [17]. Assume that the probability density functions (PDF) under both hypotheses are available. According to the NP theorem (when ignoring possible randomization), the optimal detector uses the likelihood ratio test (LRT):

$$T = \Lambda(\mathbf{r}) = \frac{p(\mathbf{r}; H_1)}{p(\mathbf{r}; H_0)} > \gamma, \quad (3)$$

where  $p(\mathbf{r}; H_j)$  is the PDF under hypothesis  $j$ ,  $\Lambda(\cdot)$  is the resulting likelihood ratio and the threshold  $\gamma$  is chosen so that  $P_{\text{FA}} = P(\Lambda(\mathbf{r}) > \gamma; H_0) = P_{\text{FA,DES}}$ .

In practice, the PDFs under hypotheses  $H_0$  and  $H_1$  often depend on some unknown parameters, i.e., the test at this point is a composite one. It can be reduced to a simple one if and only if the parameters are random and their PDFs are known. Then, the unknown parameters can be integrated out and the resulting optimal NP test is [4, p. 198]

$$T = \Lambda(\mathbf{r}) = \frac{\int p(\mathbf{r}|\theta_1; H_1) p(\theta_1) d\theta_1}{\int p(\mathbf{r}|\theta_0; H_0) p(\theta_0) d\theta_0} > \gamma \quad (4)$$

where  $p(\mathbf{r}|\theta_i; H_i)$  is the PDF under  $H_i$  and  $\theta_i$  are unknown parameter vectors.

However, often prior uncertainty is such that the parameters must be modelled as non-random, unknown quantities. In this case, no optimum test can be usually defined. In some special cases, the NP test can be reduced to be such that it does not depend on the unknown parameters; then it is called the uniformly most powerful (UMP) test. An alternative is to estimate the unknown parameters using the maximum-likelihood approach. If these parameters are used in the LRT instead of the actual (but unknown) parameters, the resulting test is called the generalized likelihood ratio test (GLRT): [4, p. 200]

$$T_{\text{GLRT}} = \frac{\max_{\theta_1} p(\mathbf{r}; \theta_1, H_1)}{\max_{\theta_0} p(\mathbf{r}; \theta_0, H_0)} > \gamma \quad (5)$$

The GLRT is a suboptimal detector that often has a satisfactory performance.

Assume that the probability of a false alarm is required to have a fixed value, as in the NP framework. Now, to be able to set the proper detection for any test requires knowledge of the PDF of the decision variable under  $H_0$ . If it is unknown, it is best if additional reference observations of the noise process are available. This is the so called two-channel or two-input problem [18]. If the noise PDF has an unknown form, nonparametric methods can be used [18]. However, the noise PDF is usually known except with some scaling factors. For example, if the noise is a white zero-mean Gaussian process, only the noise variance is unknown. In the radar literature, several threshold setting strategies have been proposed for the two-channel problem. These detectors are usually called a constant false

alarm rate (CFAR) [19]. Quite often, some of the reference samples are corrupted. This means that they have signal or interference components in addition to just noise. The severity of performance degradation depends on the CFAR method and the amount of corruption, see Section 2.4 for further details.

In some applications, such as telecommunications, it is possible to assign prior probabilities to possible hypotheses. In the Bayesian approach to hypothesis testing, costs are assigned to different types of errors and the decision rule is based on minimizing the expected cost (risk) [4]. It can be shown that the detector minimizing the Bayes cost also uses the likelihood ratio. However, the detection threshold is in general different from that used in the NP framework, since it depends on the costs and the prior probabilities. If the costs are available, but the priors cannot be realistically assigned, then the min-max criterion can be applied. It minimizes the maximum possible risk [3].

## 1.2 Energy detector

Assume that noise is complex or a real white Gaussian process, and that signal is also a white Gaussian process. As a consequence, a detector measuring energy is optimal: it is the LRT [4]. On the other hand, assume that the signal samples  $s_k$  are unknown parameters and noise is a white Gaussian process. In this case, the GLRT results also in the energy detector. Often, the energy detector is called a radiometer or quadratic detector.

An energy detector corresponding to the signal model in (2) calculates the decision variable

$$V = \sum_{k=0}^{N-1} |r_k|^2, \quad (6)$$

where  $r_k$  is the received infinite precision discrete signal. Often, it is quantized to produce a digital signal  $\bar{r}_k$ , which can be used instead of  $r_k$  in (6). Fig. 1 shows a zero-IF (intermediate frequency) receiver with two analog-to-digital converters (ADC) that are used for sampling and quantizing the in-phase and quadrature signals.

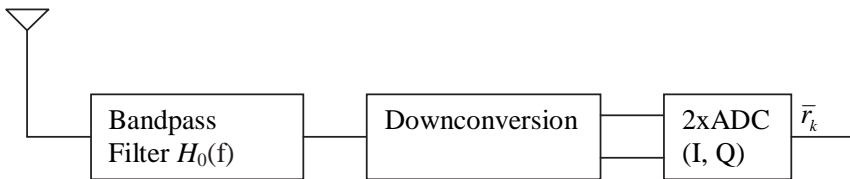


Fig. 1. Zero-IF receiver front-end.

An analog total power radiometer calculates the energy receiver over the last  $T_R$  sec-

onds, i.e.,

$$V = \int_{t-T_R}^t |y(t)|^2 dt, \quad (7)$$

where the signal  $y(t)$  has been filtered with a bandpass filter with bandwidth  $W_R$ , see Fig. 2. The form (6) can be viewed to be an approximation of the above continuous time result. The radiometers are used for detection by alerting when  $V$  exceeds the detection threshold  $\eta$ , which is set according to the statistical properties of radiometer outputs when only noise is present.

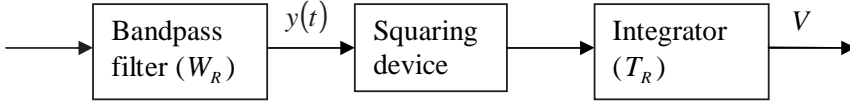


**Fig. 2. Total power radiometer.**

The energy detector/radiometer can be used in several applications, some of which are mentioned here. In ES, the radiometer can be used for detecting spread-spectrum signals [9]. In cognitive radio, the energy detector can be used for finding signal-free frequency bands [14]. It should be noted that a simple energy detector is not always enough, it may be necessary to have several cooperating sensing nodes, not necessarily using an energy detector, performing distributed detection [20]. In radio astronomy, a radiometer can be used for measuring the signal power. In telecommunications, a non-coherent ultra-wideband (UWB) [21] receiver may be implemented using energy measurements. For example, in the case of bit position modulation (BPM), the bit decision is based on the measured energies in the possible bit positions [22].

The channelized radiometer is a multichannel receiver that has several total power radiometers covering different frequency bands. It is especially useful for detecting frequency hopping (FH) spread-spectrum signals [9].

### 1.3 Aims and outline of the thesis

In this thesis, the focus is on the binary detection problem. The main goal is to develop and analyze energy based detectors as well as their generalization — a power-law detector. To support this goal, the existing results are reviewed in Chapter 2 and the signal model is presented in Chapter 3.

The received signal is usually quantized in practical equipment and the detection decision is based on the quantized received signal. A proper threshold setting may be difficult, especially when quantization is used and the noise variance is unknown. The analysis

of the quantized radiometer found in the literature lacks accurate results. Further study is required to determine its properties and limitations. This is the problem considered in Chapter 4, which is based on original publication [23]. There, the false alarm probability of a quantized radiometer using different threshold setting strategies is analyzed. The input is assumed to follow the Gaussian distribution.

In a practical signal detection system, the instantaneous bandwidth may be limited. To cover a wider bandwidth, the receiver may use frequency sweeping. In frequency sweeping, the center frequency is changed as a function of time. The performance analysis of multichannel receivers with frequency sweeping available in the literature is quite limited and will be the subject of Chapter 5. The chapter is mainly based on original publication [24], and partly on [25, 26, 27]. An analysis of the effects of frequency sweeping on a channelized radiometer is presented. It is assumed that the signal to be detected uses slow frequency hopping (SFH) and that sweeping is faster than hop dwell time. Different methods to make decisions based on the available total power radiometer outputs are analyzed. These methods are based on using logical-OR, sum and maximum operations. The performance of a logical-OR based channelized radiometer is calculated by applying the results derived in [11]. In addition to these practical methods, also the optimum detector is analyzed. Optimal detection statistics conditioned on the normalized radiometer outputs are presented.

The threshold depends on the noise statistics, which is often assumed to be known when a channelized radiometer is investigated [9, 10, 11]. If the noise statistics are known, the ideal detection threshold can be determined. However, if the noise statistics are unknown, CFAR strategies can be used. There, the threshold is determined using reference cells. Several CFAR strategies have been proposed and analyzed in the radar literature [19]. However, in channelized radiometer literature, these methods have not been previously studied, except cell-averaging CFAR (CA-CFAR) [28]. Further study comparing different radar CFAR strategies in the context of the channelized radiometer is required. This is the topic in Chapter 6, which is based on original publication [29]. In that publication, novel automatic CFAR methods based on the consecutive mean excision (CME) methods are also presented.

The threshold setting of a power-law detector has been so far limited to a case without windowing, which is used in practice to reduce the spectral leakage. In Chapter 7, the threshold setting of a power-law detector with windowing is studied. The chapter is mainly based on original publication [30], and partly on [31]. The results presented there enable the use of the windowed fast Fourier transform (FFT), and other nonorthogonal transforms, with the power-law detector. As in interference excision [32], windowing causes windowing loss. However, it is cost-effective if the same transform can be used in many applications. The actual performance loss depends on the window used and the signal to be detected. The performance loss when the signal is a sinusoidal or a direct-sequence (DS) signal is studied.

Finally, Chapter 8 concludes the thesis. Therein, the main results and contributions of the thesis are summarized.

## 1.4 Author's contribution to the original publications

The thesis is in part based on eight original publications [23, 24, 25, 26, 27, 29, 30, 31]. In [23], the impact of a uniform quantizer on the false alarm probability of the total power radiometer is theoretically analyzed using exact methods. Several possibilities to set the detection threshold are studied and compared. In [24, 27], analysis of the effects of frequency sweeping on a channelized radiometer is presented. Different methods of making a decision, based on the available total power radiometer outputs, are analyzed. Exact results for the sum-sum channelized radiometer are found by calculating the relevant discrete density functions. The performance of a maximum-sum based channelized radiometer is found with a novel application of the shifted log-normal approximation instead of using the normal approximation that was applied in the original publication [25]. An efficient method for calculating the numerically demanding likelihood ratio used in optimal detection is proposed and its accuracy is studied. The effects of the sweeping speed on the detectors mentioned above are analyzed. Numerical results are presented for two cases. Case (a) has a large number of observed hops, and case (b) has a small number of observed hops. The effects of fading on the logical OR-sum, sum-sum and maximum-sum based detectors are analyzed. In [29], methodologies and ideas from the radar literature are applied to the channelized radiometer. Novel automatic CFAR methods based on the consecutive mean excision (CME) methods are also presented. In [30], a method to set the threshold of a power-law detector that uses a nonorthogonal transform is presented. The mean, variance and skewness of the decision variable in the noise only case are derived and these are used to find a shifted log-normal approximation to the distribution of the decision variable. In [31], the performance of the power-law based intercept receiver in detection of spread spectrum signals was studied. In [26], it is proposed that a power-law statistic can be used to combine channelized radiometer outputs.

The publications have been conceived and written by the author, and the author produced all analytical and simulation results presented in the publications. The other authors provided criticism, comments, and some ideas. For clarity, and to enable uniform treatment, the thesis is presented as a monograph and the original publications are not reprinted.

## 2 Literature review

This chapter gives a literature overview of different energy or power based detection methods. The total power radiometer is discussed in Section 2.1, and different decision strategies for processing the local decisions are briefly presented in Section 2.2. A channelized radiometer is the topic in Section 2.3. CFAR methods are introduced in Section 2.4, including the excision CFAR and the automatic CFAR. Finally, the power-law detector is discussed in Section 2.5.

### 2.1 Total power radiometer

In his landmark paper in 1967 [33], Urkowitz analyzed the distributions of the continuous time radiometer output in the noise-only case, and when a deterministic signal is present. His work was based on sampling the received bandlimited waveform within the integration interval, and then using the sinc-interpolation to reconstruct the signal from the samples. This results in an approximation, because the sampling theorem requires that samples outside the integration interval are also used. However, usually the difference is not significant. Urkowitz discusses also the prolate spheroidal functions. Shnidman [34] and Urkowitz [33] have noted that the radiometer distributions correspond to a radar using noncoherent integration with the constant target model [35], [12, Chapter 10]. Mills & Prescott [36] present several classical radiometer models. They can be used to approximate radiometer performance instead of using the exact results. A quote below from Urkowitz [33] discusses the consequences of assuming a deterministic signal:

"Although this paper has taken the view that the unknown signal is of deterministic form, there is nothing in it which changes results for any signal, known or unknown, deterministic or random, provided the probability of detection is considered a conditional probability of detection where the condition is a given amount of signal energy, then its detection probability is given by the results of this paper, regardless of where the signal comes from."

In addition to the total power radiometer, there are also Dicke radiometers and correlation radiometers [9]. A list of twenty-seven references studying radiometers, for example,

in radio astronomy, has been compiled by Dillard & Dillard [9, p. 42–47]. In classical radiometer applications, the input is assumed to be a Gaussian signal, and the goal is to accurately measure the signal power or variance. In these applications, so called sensitivity can be used for performance evaluation [37]. Here, we use the radiometer for detection purposes.

Dillard & Dillard [9] note that the radiometer is useful for detecting many spread spectrum signals when the exact signal structure is not known. The relationship between a radiometer having a time-bandwidth product  $T_R W_R = 1$  and the envelope detector has been discussed by Urkowitz [33]. Sonnenschein & Fishman [38] have studied the effects of noise level uncertainty on the radiometer. Noise level uncertainty refers to a situation where the noise variance is only approximately known. Cai *et al.* [39] have studied radiometer performance in a noise fluctuating channel, where the noise level is changing due to, for example, changes in temperature. Gevargiz *et al.* [40] have studied a total power radiometer with narrow-band interference rejection before detection. Interference excision before the radiometer has also been studied by Davidovici & Kanteratis [41]. Dillard & Dillard [9, p. 32–34, p. 112] have analyzed a system using one radiometer that is continuously swept and the center frequency is changed with a constant slope. Polydoros & Weber [42] have studied optimal detection of DS and time hopping (TH) signals. Performance was compared with that of the radiometer. McKinstry & Buehrer [43] used a radiometer for detecting the presence of an UWB signal. It was noticed that using higher order modulation methods, and/or coding, makes detection more difficult. Gardner [44] discusses the drawbacks of radiometry, and argues that cyclic-feature detection may have better performance, see also [16]. Laboratory measurements with the radiometer and some other detectors have been reported by Hill & Felstead [45]. Sousa [46] has studied the crosscorrelation radiometer. It attempts to overcome difficulties the total power radiometer has with noise power uncertainty. Eaddy *et al.* [47] showed that the optimum detector of colored Gaussian signals in white Gaussian noise can be well approximated with the radiometer.

Usually in radiometer studies, a non-fading additive white Gaussian noise (AWGN) channel is assumed. The simple AWGN channel can be used, for example, for modelling air-to-air channels. However, in many practical situations fading occurs. MacMullan [48] studied the effects of movement between the intercept receiver and the signal source on a total power radiometer detecting FH signals. It was assumed that the channel consists of a direct component and a reflected component. Kostylev [49] and Digham *et al.* [50] have also studied the use of a radiometer for detecting unknown signals in a fading channel. In addition to Rayleigh fading, Digham also considers Nakagami fading channels and independent identically distributed (IID) diversity paths.

Expressions for the mean and variance of the quantized total power radiometer outputs with a white Gaussian input, taking into account the effects of the bandpass filter and saturation, have been derived in 1973 by Ohlson & Swett [51]. Although the goal therein was to measure the signal power, as in [52], the mean and variance can also be used for evaluating the detection performance of a quantized radiometer with the Gaussian approximation [14]. Koivu *et al.* [53] have studied the performance of a quantized radiometer with simulations. The detection threshold of an analog total power radiometer was used. In Koivu *et al.* [54], a quantized total power radiometer was studied, and the noise level was estimated, based on quantized noise-only reference samples. The strategy

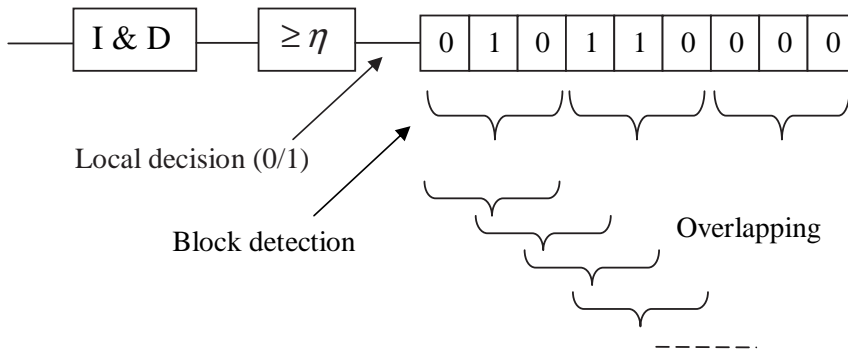
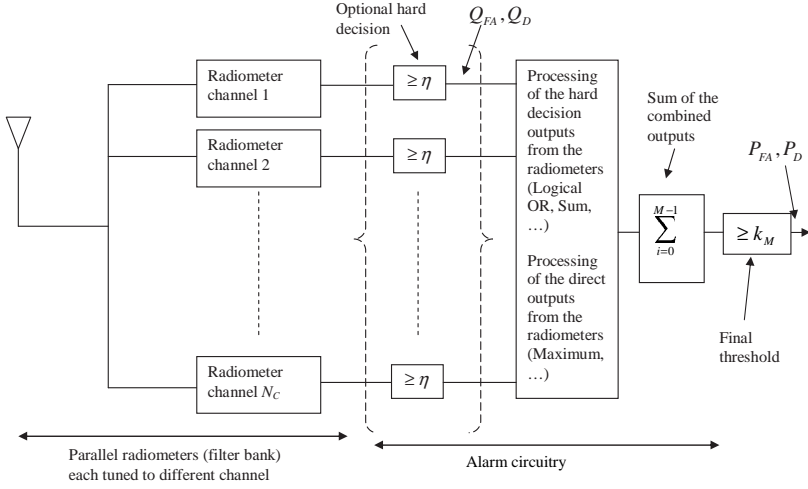


Fig. 3. Detection in non-overlapping (block) and overlapping systems,  $M = 3$ .

used there is similar to CA-CFAR, but with a different scaling factor. Gandhi [55] has theoretically studied the effects of quantization in CA-CFAR signal detection. The order statistic CFAR (OS-CFAR) detector was also studied. However, an analog square-law device was assumed so that the input follows the exponential distribution.

## 2.2 Decision strategies for a total power radiometer

In the integrate-and-dump (I+D) case, the radiometer output is sampled periodically every  $T_R$  seconds [9]. It is also possible to use continuous integration, where the radiometer output is not sampled. Instead, an alarm occurs when the measured energy crosses a threshold in an upward direction [56]. Assume that I+D is used. Now, the radiometer outputs measure energies which are compared to a threshold. These decisions can be used directly or it is also possible to use various other decision strategies that make a decision based on the preliminary decisions in several integration intervals. Binary integration (BI) is a well known postdetection method for processing the preliminary decisions, for example, in radar or radiometer applications [12, 9, 57, 58]. This was analyzed in the 1950s by Schwartz [59] and Harrington [60]. In BI,  $M$  preliminary decisions (1 or 0) corresponding to an observation period are added, and the sum is compared to a second threshold  $k_M$ . Binary integration is also called double-threshold detection, binomial fixed sample-size testing, coincidence detection and  $k$ -out-of- $b$  detection [12, 9]. Binary integration can be used, for example, for detecting TH signals [9]. One advantage of using BI is that even very strong interference in a few radiometer intervals does not cause a false alarm, depending of course on the second threshold. The observation periods for different final decisions can be either overlapping or non-overlapping, see Fig. 3. Torrieri [58] calls the non-overlapping system "block detection". Using overlapping limits misalignment between the signal to be detected and the observation period, in contrast with block detection



**Fig. 4. A channelized radiometer.**

[58]. In the overlapping system, there are at least two possible detection strategies. It is possible to always alarm when the sum of the preliminary decisions exceeds  $k_M$  [61]. It is also possible to alarm only when the sum exceeds  $k_M$  in the upwards direction. The latter method is called binary moving window detection (BMWD) [56]. Dinneen & Reed [62] present some additional methods.

## 2.3 Channelized radiometer

The basic idea in channelized receivers is to use several parallel narrowband receivers. Tsui [63, Chapter 7] notes that channelization can be applied to many receiver designs. When channelization is applied to the total power radiometer, the resulting structure is called the channelized radiometer [11, 9, 58, 64, 65]. It uses multiple radiometers, i.e., it integrates energy in many frequency bands simultaneously. It can be used, for example, for detection of a FH signal. Fig. 4 shows the structure of a channelized radiometer based detection system. The system has  $N_C$  radiometers which form a channelized radiometer, each with bandwidth  $W_R$  and integration time  $T_R$ . The description of the alarm circuitry is left to Section 3.2. Basically, the local or preliminary decisions from the individual radiometers are combined using, for example, a logical-OR operation. It is possible to sum several combined outputs. These combined outputs from different integration intervals are summed. The output is compared with the second threshold  $k_M$ . Mills & Prescott [64, 65] have studied detecting FH networks using the channelized radiometer. Nem-sick & Geraniotis [28] have studied CA type algorithms in the context of the channelized radiometer. The Gaussian approximation was used and some further processing of the decisions was performed to separate the alarms caused by single channel signals and jam-

mers. The Woodring-Edell combining method uses the likelihood ratio [66]. The optimum noncoherent detector for fast frequency hopping (FFH) signals [67] is closely related to the channelized radiometer using Woodring-Edell combining. The difference is that envelope detectors are used instead of bank of radiometers. In [67], a simplified detector called a multiple-hop maximum likelihood (MML) is also introduced. It corresponds to a channelized radiometer using logical-OR function.

In a practical channelized radiometer implementation, instantaneous bandwidth may be smaller than the signal bandwidth. This may happen especially when the signal to be detected is a spread spectrum signal, e.g., a FH signal. On the other hand, in some implementations, the number of radiometers may be limited. In systems with limited bandwidth, the simplest possibility is to use the same center (carrier) frequency at all times. Another possibility is to change the center frequency of the receiver, i.e., to perform frequency sweeping [9, p. 32],[68]. Rapid sweeping has been used for detecting SFH signals in [68], where the performance of a sweeping sum based envelope receiver implemented with the FFT was analyzed. Here, rapid sweeping refers to a situation where the duration that the receiver stays at a certain frequency is small relative to the time that the signal frequency is unchanged. This can be referred to as "sweeping faster than hop dwell time". Probability of intercept (POI) of multichannel receivers using rapid sweeping has been studied in [69, 70]. Dillard & Dillard [9, p. 32–34, p. 112] have analyzed a system using one radiometer that is continuously swept and the center frequency is changed with a constant slope. The approximate results are given there for a system using BMWD. Miller *et al.* [11] have analyzed systems where the bandwidth of each radiometer  $W_R$  can be increased to improve the intercept probability, for a fixed number of radiometers. It was found that the performance of the channelized radiometer depends more on the number of radiometer channels  $N_C$  than of the covered hopping band.

For detecting TH signals, a similar structure to that of the frequency channelized radiometer can be used. Instead of using a radiometer with different frequency bands, radiometers with different time-intervals are used [9, 56]. In this case, the logical OR operation would be performed on the local decisions in each hopping interval. An upper bound to the performance can be found by assuming time synchronism. This type of structure is sometimes called a time channelized radiometer [43] or multi-radiometer system [71].

A compressive receiver is an alternative to channelized receivers. Its use for detecting FFH signals has been studied by Snelling & Geraniotis [72]. In a compressive receiver, the signal is mixed with a chirp-type signal and is filtered with a pulse compression filter.

## 2.4 CFAR methods

For threshold setting, it is necessary to know the PDF of the decision variable under  $H_0$ . Usually the noise is known except for some scale factors. The unknown scale factor can often be taken into account by using a threshold based on some reference samples. In some situations, it is necessary to take into account also a "shape" parameter [73]. However, here we consider only the scale factor, as usual. Ideally, the reference samples should be "signal-free", i.e., they should contain only noise components. The methods based on using reference samples are often called CFAR. In the radar literature, numerous CFAR

methods have been proposed and studied, some of which are specific to the radar problem wherein, for example, clutter level changes can occur. In the radar problem, CFAR can be implemented based on range cells, angle cells, or Doppler shift cells. Usually, the range cells are used for radar CFAR [74]. Denote the value of the cell where the local detection decision should be made with  $Z$ , and let the values of the reference cells, i.e., the reference samples, be  $Z_i$ , where  $i = 1, 2, \dots, N_R$  and  $N_R$  is the number of reference cells. In the radar problem, it is usually assumed that the cells are independent and follow the exponential distribution with PDF

$$f(z) = \frac{1}{2\lambda} e^{-z/2\lambda}, \quad z \geq 0, \quad (8)$$

where, if the cell contains only noise,  $\lambda = \mu$  and  $\mu$  is background noise power. If the cell contains also signal(s),  $\lambda = \mu(1 + S)$  and  $S$  is the average signal-to-noise ratio [19, 75].

The thresholds of different CFAR methods can be expressed with

$$\eta = Tg(Z_1, Z_2, \dots, Z_{N_R}), \quad (9)$$

where  $T$  is a scaling factor, and  $g$  is a function that defines the properties of the CFAR method. For example, Ritcey [76] notes that it is possible to use the weighted sum of the ordered samples. This method is sometimes called the generalized order statistic (GOS) CFAR detector [77] or  $L$ -CFAR [75]. The threshold is

$$\eta = T_{\text{GOS}} \sum_{i=1}^{N_R} \varrho_i Z_{(i)}, \quad (10)$$

where reference values have been sorted in ascending order so that  $Z_{(1)} \leq Z_{(2)} \leq \dots \leq Z_{(N_R)}$ ,  $\varrho_i$  are the weights of the GOS filter, and  $T_{\text{GOS}}$  is the GOS scaling factor. The probability of detection, assuming the exponential model, is [75]

$$P_D = \prod_{i=1}^{N_R} \frac{1}{1 + \frac{T_{\text{GOS}} \xi_i}{1+S}}, \quad (11)$$

where

$$\xi_i = \frac{1}{N_R + 1 - i} \sum_{k=i}^{N_R} \varrho_k \quad (12)$$

and the probability of false alarm is obtained using (11) with  $S = 0$ . Most conventional CFAR detectors can be expressed as special cases of the GOS-CFAR. In CA-CFAR,  $\varrho_i = 1$ , i.e., it calculates the sum of the reference cell values. By calculating the false alarm probability using the methods described above, it is found that to obtain the desired false alarm probability  $P_{\text{FA,DES}}$ , the scaling factor should be

$$T_{\text{CA}} = (P_{\text{FA,DES}})^{-1/N_R} - 1. \quad (13)$$

In [78], it has been shown that a detector using the CA-CFAR is UMP, assuming the exponential distribution and signal-free reference cells. However, CA-CFAR is known to have poor performance in nonhomogeneous backgrounds [19], which refer to situations

where part of the reference cells are not signal-free, or the noise power varies between cells. The former usually means that there are multiple targets. The latter is called clutter transitions (in radar literature). The OS-CFAR has been proposed in [79]. There,

$$\varrho_i = \begin{cases} 1 & \text{if } i = k \\ 0 & \text{otherwise} \end{cases} \quad (14)$$

where  $k$  is a fixed parameter that controls the properties of OS-CFAR. The OS-CFAR is significantly more robust against multiple targets than the CA-CFAR. However, in radar applications, it can have problems with clutter edges [19]. In adaptive order statistic (AOS) CFAR, the order parameter  $k$  of the OS-CFAR is changed if a clutter edge is detected [80]. Rickard & Dillard [81] have proposed the censored cell averaging (CCA) detector, where  $N_R - k$  of the largest cell values are censored, i.e.,

$$\varrho_i = \begin{cases} 1 & \text{if } i = 1, 2, \dots, k \\ 0 & \text{otherwise} \end{cases} \quad (15)$$

Ritcey [76] has proposed the censored mean level detector (CMLD). The CMLD uses weights

$$\varrho_i = \begin{cases} 1 & \text{if } i = 1, 2, \dots, k - 1 \\ N_R - k + 1 & \text{if } i = k \\ 0 & \text{otherwise} \end{cases} \quad (16)$$

The scaling factor for CMLD is given by  $T_{\text{CMLD}} = -1 + (P_{\text{FA,DES}})^{-1/k}$  [76]. Holm & Ritcey [82] and Lops [75] have shown that the weights (16) are optimal for a system censoring  $N_R - k$  samples, assuming the reference cells contain only noise. For no censoring, the CA-CFAR comes out as the optimum solution. In [82], it was additionally shown that the probability of detection of the CMLD-CFAR converges to the probability of detection of the fixed-threshold NP test when  $k$  becomes large. Gandhi & Kassam [19] have proposed the trimmed mean (TM) CFAR, which censors some fixed amount of the largest and the smallest cell values. Ozgunes *et al.* [83] have proposed the variably trimmed mean (VTM) CFAR detector. There the number of smallest cell values to be censored is fixed. However, the number of largest values to be censored is data-dependent. Generally, VTM-CFAR can give some performance improvement over the OS-CFAR in clutter edge and multiple target environments [83]. Assume that  $Z_{(k)}$  is the smallest value to be included in the reference set. Now, those cell values that fall within the interval

$$[Z_{(k)}, (1 + \nabla) Z_{(k)}]$$

are used as the reference set. The  $\nabla$  is a design parameter. The threshold for the test cell is the average of the reference set multiplied by a scaling factor  $T$ . The scaling factor  $T$  corresponding to the desired false alarm probability can be calculated using [83, Eq. (22)]. With  $\nabla = 0$ , VTM reduces to OS( $k$ ), with  $\nabla = \infty$ , it reduces to TM that does not censor any of the largest cell values [83].

The most interesting radar CFAR publications consider noncoherent integration. In this case, the cell values follow the same distributions as the channelized radiometer outputs, at least in the noise-only case. Shnidman [84] has presented the scaling factors for the CA-CFAR detector. Lim & Lee [85] have analyzed an OS-CFAR detector with noncoherent

integration, and have found the proper scaling factors. Han & Lee [86] have also studied an OS-CFAR detector with noncoherent integration, where, the order statistics cell averaging (OSCA) and order statistics greatest of (OSGO) methods have been analyzed for general fluctuating targets. These methods divide the cells into two groups. The cells before the test cell (leading) and the cells after the test cell (lagging). The OSCA uses the sum of some order statistics in the leading and lagging windows and the OSGO uses the maximum of those. Kim *et al.* [77] have analyzed the GOS-CFAR detector with noncoherent integration. Shnidman [84] has studied the detection performance of the CA-CFAR detector in the constant target case, which corresponds to the channelized radiometer model by Urkowitz [33]. Shnidman [57] has recently studied binary integration combined with noncoherent integration.

Smith & Varshney have presented an interesting CFAR processor based on a variability index (VI) [87]. It is designed especially for situations with clutter edge, but can also be used when multiple targets are present. The VI is based on calculating the ratio of variance estimate and the squared mean estimate. Depending on the VI of the leading and lagging windows, and also on the ratio of means in leading and lagging windows, reference samples can be the samples in the leading window, lagging window, or in both windows. The sum of the reference samples is multiplied with the CA-CFAR scaling factor corresponding to the size of the reference set and the desired false alarm probability. Due to the design of the VI-CFAR, detection performance degrades if targets are present in both windows.

A clutter map CFAR has been analyzed by Nitzberg [88]. It uses a detection threshold based on the temporal average of the previous values of the resolution cell to be tested. The averaging can be efficiently implemented using a forgetting factor technique [88]. Lops & Orsini [89] have studied scan-by-scan averaging CFAR. It is based on mapping several range cells into a map cell. The number of range cells per a map cell is usually relative small, so that the background is usually homogeneous. The background estimate is based on previous values of the range cells in the map cell. Nonlinear processing, for example taking the maximum, can be used when updating the background estimate [89]. Lops [75] has proposed and analyzed processing the range cells in each map cell with a spatial  $L$ -filter. Background estimation was done by filtering in time. A given number of the largest samples can be censored by using zeros in the  $L$ -filter.

Corrupted reference samples have signal or interference components in addition to just noise. As stated above, especially the CA-CFAR is known to have an unsatisfactory performance when some of the reference cells are corrupted. There are at least two methods for combatting the effects of interference. First, it is possible to use fixed censoring, where some of the largest reference cell values are ignored. Fixed censoring is used, for example, in CCA-CFAR, CMLD-CFAR, TM-CFAR and GOS-CFAR. The effects of corrupted reference samples on systems using fixed censoring are briefly discussed in Section 2.4.1. Secondly, it is possible to use automatic censoring. Here, automatic refers to the fact that the number of censored cells is not fixed. Instead, it is determined based on the actual values of the reference cells. Automatic CFAR methods are discussed in Sections 2.4.2 and 2.4.3.

### 2.4.1 Fixed censored CFAR

The effects of interference on fixed censoring methods are discussed with emphasis is on the CMLD-CFAR method. Assume that the number of reference cells is  $N_R = 32$  and that CMLD-CFAR is used with  $k = 24$  (the weights are given by (16)). For simplicity, assume additionally that the interference is infinitely strong. In this case, the interference reduces the dimensionality of the reference set. Because eight of the highest reference cell values are ignored, the maximum number of cells with interference is also eight. Assume that the scaling factor is chosen assuming that there are  $l_D$  cells with interference. Note that usually it is assumed that  $l_D = 0$ , i.e., the scaling factor is designed for the noise only case. Now, Fig. 5 shows the actual false alarm probabilities of detectors designed for different values of  $l_D$ . It corresponds to [76, Fig. 5]. For example, it can be observed that a system designed for  $l_D = 0$  obtains exactly the desired false alarm probability only when the actual number of interfering targets is  $l_A = 0$ . When  $l_A > 0$ , the probability of false alarm will be smaller than the desired value. On the other hand, if the system is designed using  $l_D = 8$ , the desired probability of false alarm is obtained exactly when  $l_A = 8$ . However, if  $l_A < 8$ , the probability of false alarm will be higher than the desired value, which is a serious breach of the NP requirements.

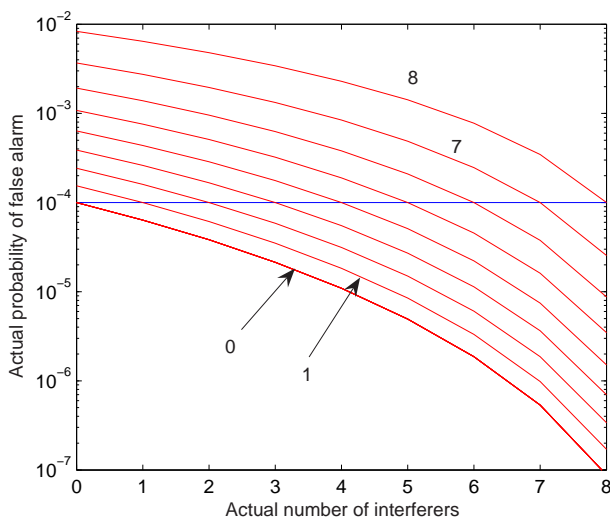


**Fig. 5. Actual probability false alarm, CMLD-CFAR,  $N_R = 32$ ,  $k = 24$ , and  $P_{FA,DES} = 10^{-4}$ . The curves are indexed with the assumed number of interfering targets  $l_D$ .**

### 2.4.2 Excision CFAR

Excision CFAR is an automatic CFAR method that has been proposed in 1973 by Urkowitz & Perry <sup>1</sup> [90]. Those cell values that are higher than some secondary threshold are censored before calculating the mean. This method, called the excision CFAR, was mathematically analyzed by Goldman & Bar-David [91]. The PDF of the normalized mean of the samples surviving excision was found. It depends on the ratio of the excision threshold  $B_E$  to  $2\lambda$ , denoted with  $\alpha$ , but not on the absolute values. An example of the PDF is shown in Fig. 6. When  $\alpha$  is very large, the PDF is the chi-square PDF (scaled with  $1/2N_R$ ) with  $2N_R$  degrees of freedom, as expected [91]. Using similar techniques, the probability of a false alarm is derived. It depends on the scaling factor used for setting the detection threshold  $\gamma_D$ ,  $N_R$  and  $\alpha$ . The excision threshold can be represented with  $B_E = 2\alpha\lambda$ . It depends on the  $\lambda$ , which therefore should, unfortunately, be known. Therefore, strictly speaking, this is not actually CFAR, since some prior information about the noise variance is needed in order to avoid too heavy (or too light) censoring. Assuming only noise is present in the reference cells, small values of  $\alpha$  result in performance loss. This is due to censoring reducing the effective size of the reference set [91]. If the  $\alpha$  is very large, the proper scaling factor  $\gamma_D = T_{CA}N_R$ , where  $T_{CA}$  is conventional CA-scaling factor and the multiplication with  $N_R$  is due to calculating a mean instead of a sum. The same value of  $\gamma_D$  is used for all values of surviving samples. Fig. 7 shows the probability of a false alarm as a function of the parameters  $\alpha$  and  $\gamma_D$  when  $N_R = 20$ . It can be observed

<sup>1</sup>RCA systems technology memo STM-11011, May 18, 1973, also US Patent 3995270, by Perry and Urkowitz

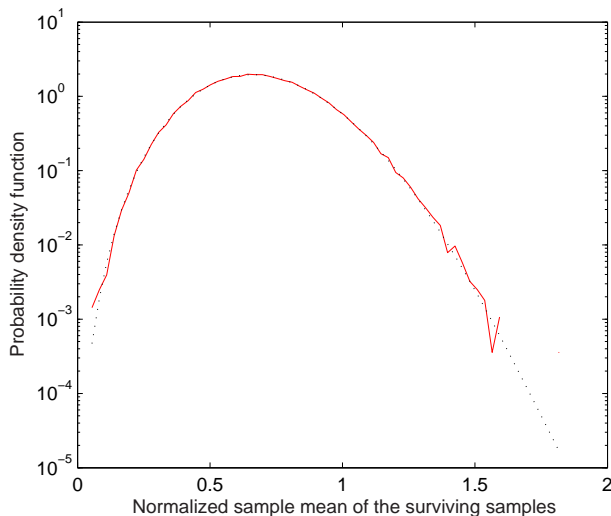


Fig. 6. PDF of the normalized mean of the surviving samples,  $\alpha = 2$  and  $N_R = 8$ .

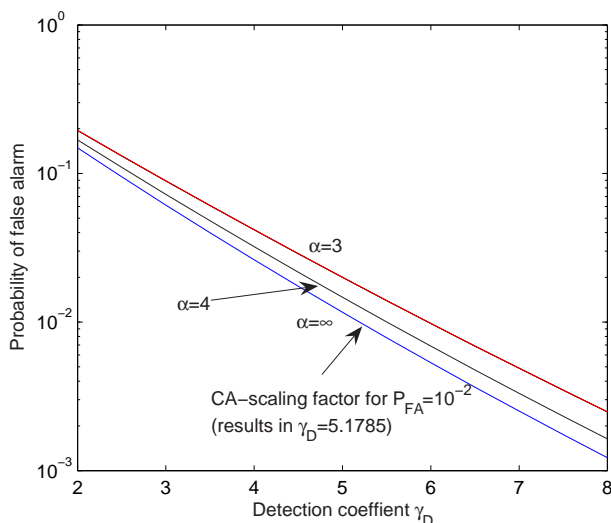


Fig. 7. Probability false alarm,  $N_R = 20$ .

that the CA-scaling factor gives exactly the required false alarm probability for situations where  $\alpha$  is very large. The smaller  $\alpha$  is, the larger the proper scaling factor  $\gamma_D$  for a fixed false alarm probability is. In addition to these results, Goldman [91] finds the expressions for the probability of detection of a constant target and also studies binary integration of the local decisions. It is suggested to choose  $\gamma_D$  based on infinite  $\alpha$  [91]. Assume that ten local decisions are binary integrated and that the BI threshold is five. Now,  $\gamma_D$  corresponding to the final false alarm probability  $10^{-3}$  is 2.5612. This result can be obtained using binomial inverse and the CA-scaling factor. As long as  $\alpha$  is sufficiently large, the obtained false alarm probability will be close to the required value. Goldman suggests choosing the actual detection threshold before normalization based on the minimum tolerable  $\alpha$ , so that  $B_E = 2 \lambda_{\max} \alpha_{\min}$ , where  $\lambda_{\max}$  is the maximum expected  $\lambda$ . However,  $B_E$  should not be too large, otherwise interference is not censored. Also, he suggests estimating the real value of  $\alpha$ , and using that when choosing  $\gamma_D$ . Conte *et. al.* [92] have extended Goldman's results to include fluctuating targets. Goldman [93] has also analyzed the performance of the excision CFAR in the presence of interferers with a fluctuating target model.

### 2.4.3 Automatic censored CFAR

Barbooy *et al.* [94] have proposed an automatic CFAR method, whereby the reference cell censoring is done with an iterative backwards method. Barkat & Himonas [95, 96] have proposed automatic censored CFAR detectors, which automatically estimate the number

of largest reference samples to be censored using an iterative forward method. Reference cell censoring has also been considered in the space-time adaptive processing (STAP) literature [97]. In the  $k$ th iteration of the forward methods, the following test is performed [95, 96]:

$$Z_{(k+1)} \geq T_k \sum_{i=1}^k Z_{(i)}, \quad (17)$$

where  $Z_{(k)}$  are the reference values sorted in ascending order and  $T_k$  is the censoring scaling factor at the  $k$ th step. If the test is true it is decided that  $Z_{(k+1)}$  and all the larger values are corrupted. The first test is  $Z_{(2)} \geq T_1 Z_{(1)}$ . If this test is true, it is decided that the reference cells corresponding to  $Z_{(2)}, \dots, Z_{(N_R)}$  are corrupted. Otherwise, the test is performed again with  $k$  incremented by one. This is continued until the test is true for some value of  $k$  or it is decided that all the reference cells are signal-free. The "automatic censored mean level detector" (ACMLD) scaling factors are designed for some value of probability of false decision,  $P_{FC}$ , in each test during the iteration process. In [95, 96] the exponential distribution is assumed. In this case, it is possible to take advantage of the special properties of the ordered statistics of the exponential distribution in the derivation of the scaling factors, corresponding to the desired  $P_{FC}$ . In [96], it has been assumed that all the reference cells contain only noise. Alternatively, in [95] it has been assumed that the interfering signals in the reference cells are infinitely strong and  $Z_{(k+1)}$  is the last remaining signal-free cell. The scaling factor  $T_k$  derived in [95] can be viewed to be a special case of the  $T_k$  in [96] with  $N_R = k+1$ . According to [96, Eq. (18)], the probability of a false decision at the  $k$ th iteration is (assuming some conditions are satisfied)

$$P_{FC} = \binom{N_R}{k} \frac{1}{[1 + T_k (N_R - k)]^k}. \quad (18)$$

Strictly speaking, the result (18) is valid only assuming that test  $k$  is always reached. A simulation was performed using ACMLD scaling factors given by (18), see Fig. 8. It can be observed that with the ACMLD scaling factors, the probability of a false decision is rather close, but not equal, to the required value. The difference between the desired and obtained values depends on the test number. When  $k = 1$ , the desired and obtained values are actually exactly the same. It can also be observed that if the tests are always performed, i.e., iteration is not stopped even if the current test is true, the probability of false decision is equal to the desired value.

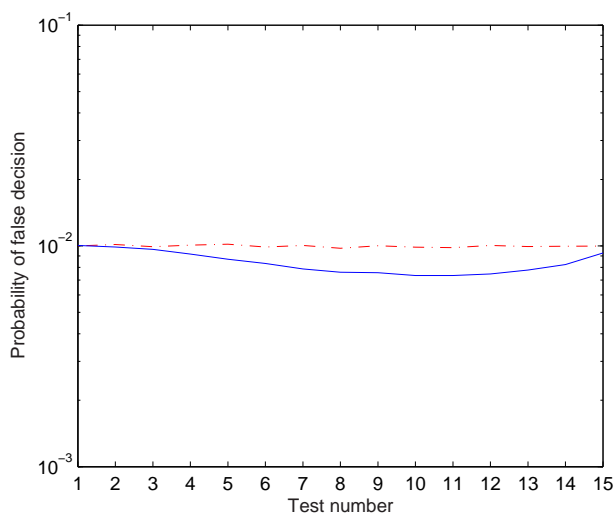


**Fig. 8.** Probability of a false decision, ACMLD scaling factors, homogeneous background,  $N_R = 16$  and desired  $P_{FC} = 10^{-2}$ . All tests are always performed (dash-dotted line), normal operation (solid line).

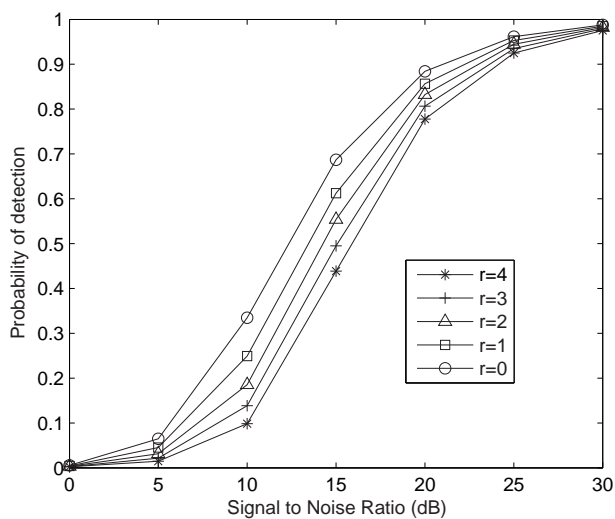


**Fig. 9.** Probability of detection,  $N_R = 16$ ,  $P_{FA,DES} = 10^{-4}$ , desired  $P_{FC} = 10^{-4}$ , and  $r$  is the number of interfering targets in the reference cells. Scaling factors used: ACMLD & TM.

After censoring, it is possible to use either TM-CFAR or CA-CFAR scaling factors. The CA-CFAR scaling factors have better performance. However, the false alarm probability may be higher than desired, depending on how well the censoring method works. Fig. 9 shows simulation results corresponding to those presented in [96, Fig. 11]. The TM-CFAR scaling factors were used for final detection and the ACMLD scaling factors [96] were used for iterative censoring. In simulations, it was noticed that ACMLD surprisingly often censors a large number of reference cells even when they all are actually clean. This may be related to the fact that ACMLD always starts iteration using only the smallest cell. The false alarm rates were found to be somewhat higher than desired, even with the TM-CFAR scaling factors. This can be partly explained as follows. For example, when iteration is stopped in the first test, then the smallest cell is usually very small. The TM-CFAR gives exactly the desired false alarm probability if it is always performed with data-independent parameters and assuming a homogeneous background. If it is performed with unusually small values, the false alarm probability will be higher. For example, the false alarm probability corresponding to Fig. 9 with no interfering targets was about  $2 \cdot 10^{-4}$ , i.e., twice the desired false alarm probability. With CA-CFAR scaling factors, the false alarm probability was over six times larger than the desired value.

CME algorithms have been proposed in [32, 98, 99]. The forward CME (FCME) proposed by Saarnisaari *et al.* [98, 99] is an iterative excision method quite similar to the ACMLD. The differences are that the FCME can start iteration directly with, for example, four reference cells; the iteration scaling factors are based on different type of approach and they are very simple to calculate; and that the FCME can be used also when the cells follow chi-square distribution with more than two degrees of freedom. The backward CME (BCME) proposed by Henttu & Aromaa [32] initially uses all the reference cells and operates backwards, removing samples from the clean set. Saarnisaari *et al.* [99] have noted that CME algorithms are related to "diagnostic methods" used in statistics. Vartiainen [100] and Juntti *et al.* [101] have recently produced overviews of the CME algorithms and their applications. Usually, CME algorithms are used for interference excision. For example, Vartiainen *et al.* [102] have studied CME based interference excision in DS systems.

Very recently, Farrouki & Barkat [103] have proposed iterative ordered data variability based censoring in CFAR.

## 2.5 Power-law detector

In this section, the power-law detector (PLD) is discussed. It can be used as an alternative to energy detection and it has good performance with various signal types.

### 2.5.1 General

The PLD is based on the summing powers of received samples. For example, when used with the signal model (2), the PLD calculates

$$f_v = \sum_{k=0}^{N-1} |r_k|^{2v}, \quad (19)$$

where  $v$  is the power-law parameter. Obviously  $v = 1$  corresponds to energy detection (6). Usually  $v$  is a positive integer, which is often the choice also in practical implementations, because calculation of integer powers can be significantly faster than the calculation of non-integer powers. In mathematics, a similar concept called "power sum" is defined with [104]

$$S_p = \sum_{k=0}^{N-1} r_k^p, \quad (20)$$

which corresponds to a power-law detector with  $v = p/2$ , if  $p$  is even and the signal is real-valued.

PLD can be used with time-domain samples [105] or with the FFT of the received signal [106, 107]. More generally, any function of the received (time-domain) signal could be used. However, in this case the problem of selecting the detection threshold may be difficult.

An optimal power-law parameter has been determined for detecting a real-valued Gaussian burst in real-valued Gaussian noise by Fawcett & Maranda [105]. An optimal detector would consist of a bank of energy detectors with different integration times [105]. However, usually this is not practical. The power-law detector can be used instead. Numerical inversion of the characteristic function was used to find the probabilities of a false alarm and detection. The optimal power-law parameter depends on the relative burst length. It is well known that when detecting a Gaussian burst with a burst length equal to the number of samples in the detection interval, the optimal PLD is equal to the energy detector. When the relative burst length decreases, the optimal power-law parameter increases. The signal samples corresponding to the burst do not need to be consecutive, i.e., the power-law detector does not depend on the order of the samples. Therefore, the power-law detector can be used as a method for detecting a Gaussian burst with unknown duration and location or a series of bursts.

Frey & Andescavage [108] have studied the problem of detecting a bursty target in multiplicative noise. This problem is more general than the one considered in [105]. It was observed that the power-law detector is optimal for several noise distributions. This motivates one to use the power-law detector, although usually it is not optimal when the burst length is smaller than the observation duration.

In [108], the Cornish-Fisher approximation was used to find the detection threshold. The Cornish-Fisher approximation requires one to find cumulants or moments. Closed form expressions for moments are available for various noise distributions, for example, lognormal or Gamma-Weibull. The required signal-to-noise ratio (SNR) to obtain a probability of detection of 0.5 was then found using Gaussian approximation.

Nuttall [106] has proposed a power-law detector that uses frequency-domain samples instead of time-domain samples. These frequency-domain samples can be, for example,

magnitude-squared FFT bins corresponding to the received baseband signal. The power-law detector was proposed as a method for detecting a signal that is present in an unknown number of bins / frequencies. The signal has an unknown structure, i.e, the set of occupied bins does not have any known structure. The power-law detector was derived from the optimum processor using approximations. The FFT is used without windowing, resulting in an orthogonal transform. When only noise is present, the samples follow exponential distribution. When the signal is present, it is assumed that the FFT bins containing a signal still follow the exponential distribution, but with an higher average value than in the noise-only situation. As stated in [107], there is no particular reason for taking this signal model as a fact. However, it is a quite flexible model and the detectors derived using this model seem to perform well [107]. It can be seen that the assumed signal model is actually the same as that typically used with radar performance studies— without noncoherent integration and with a Swerling I or II fluctuation model [84]. Therefore, the power-law detector could also be viewed as a method for determining if a target is present in some of the radar resolution cells under investigation but without information about the location of the target(s) within the investigated cells.

Very recently, the power-law detector has been used in signal detection in cognitive radios [109]. Therein, the results given in [38] for radiometer with noise uncertainty were extended for the power-law detector / "moment detector" with noise uncertainty.

### ***2.5.2 Extended power law detector***

Knowledge on noise variance is required for setting the proper detection threshold for the conventional power law detector. This limits its application possibilities. Wang & Willett [107] have extended the power law detector. First, a CFAR version of the power-law detector is developed, so that the knowledge of the noise level is not required. Second, a few adjacent FFT bins are combined to have better match for the signal. Third, the use of wavelet transforms instead of the FFT is considered. The CFAR method proposed in [107] is based on using non-overlapped non-windowed spectrogram outputs. It is assumed that the noise level can be different in each bin and that there are  $L-1$  noise only measurements corresponding to each bin in the current interval. In [107], the frequency-domain samples in the current interval are normalized with the average of the values of the reference cells. The output SNR is proposed for choosing the power-law parameter. Threshold setting for these detectors was done in [107] using the Gaussian and saddle-point approximations. The Gaussian approximation requires one to find the mean and variance under the noise-only hypothesis  $H_0$ . In [107], it was found that the saddle-point approximation has much better accuracy than the Gaussian approximation.

CFAR power-law detectors can be viewed to perform a homogeneity test (do all the samples follow the same distribution). This is similar to outlier detection, except that the actual location of the outlier(s) does not matter. Chen *et al.* [110] have studied homogeneity testing of an exponentially distributed data set. A new statistic was derived and its performance was compared to that of the power-law detector. Recently, homogeneity testing has been used in an automatic CFAR detection system in [103].

### 3 System models

In this chapter, system models are presented and discussed. First, the digital receiver model and the possible detection functions are presented in Section 3.1. Then the channelized radiometer model is defined and the instantaneous radiometer outputs are statistically analyzed in Section 3.2.

#### 3.1 Digital receiver model

Assume the general digital model (2), except that the signal sequence  $r_k$  has an infinite number of samples. The samples are grouped into blocks of  $N$  samples and the received signal vector in block  $m$  is

$$\mathbf{r}_m = [ r_{0+mM_O} \quad r_{1+mM_O} \quad \cdots \quad r_{N-1+mM_O} ]^T, \quad (21)$$

where the parameter  $M_O$  controls the overlapping between blocks. If  $M_O = N$ , there is no overlapping. If  $M_O = N/2$ , there is 50% overlapping. An example is shown in Fig. 10. The FFT of the samples  $\mathbf{r}_m$  can be presented with

$$\mathbf{x}_m = \mathbf{\Phi} \mathbf{W} \mathbf{r}_m, \quad (22)$$

where the FFT size  $N_{\text{FFT}} = N$ ,  $\mathbf{W}$  is a  $N \times N$  matrix with coefficient of the used window  $w_n$  in the diagonal and  $\mathbf{\Phi}$  is an  $N \times N$  matrix with the elements  $\Phi_{k,n} = e^{-j2\pi kn/N}$ . More generally, the received signal vector in block  $m$  can be transformed with an arbitrary  $N \times N$  transformation matrix  $\mathbf{A}$ , i.e.,

$$\mathbf{x}_m = \mathbf{A} \mathbf{r}_m. \quad (23)$$

The spectrogram calculates squared FFT magnitudes in different blocks. In sonar applications, the spectrogram is called a "lofargram". The frequency-domain power-law detector uses non-overlapping ( $M_O = N$ ) non-windowed ( $\mathbf{W} = \mathbf{I}_{N \times N}$ ) spectrogram outputs [107]. A receiver similar to the channelized radiometer can be implemented by summing some adjacent time and/or frequency spectrogram values in order to increase the

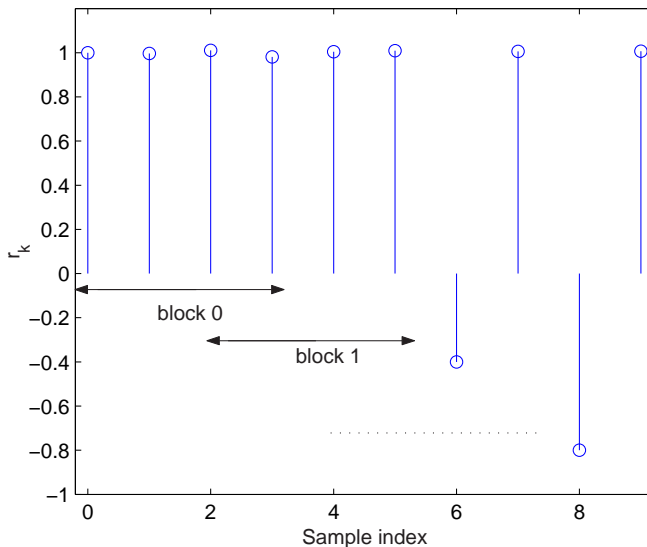


**Fig. 10. Grouping of samples into blocks,  $N = 4$  and  $M_O = 2$ .**

time-bandwidth product [16]. An example is shown in Fig. 11. However, there are some problems associated with this approach. If no windowing is used, spectral leakage will be a problem [111]. On the other hand, if windowing is used, there will be energy loss. It may be possible to mitigate these issues by using overlapping windows [112] or by using more general time-frequency analysis methods.

A general block-based detection statistic is a function of the received samples, i.e.,  $D_m = f(\mathbf{r}_m)$ , where  $m$  is the block index. In what follows, we ignore  $m$  if detection decisions are based on single blocks, e.g., BI is not applied and we do not need to separate the blocks. The time-domain power-law detector makes local detection decisions based on

$$f_v(\mathbf{r}) = \sum_{k=0}^{N-1} |r_k|^{2v}. \quad (24)$$

The transform based PLD uses a decision variable

$$T_v(\mathbf{x}) = \sum_{k=1}^N |x_k|^{2v}, \quad (25)$$

where  $x_k$  is  $k$ th element of the transformed received block vector  $\mathbf{x}$ , which of course depends on the received samples  $\mathbf{r}$ .

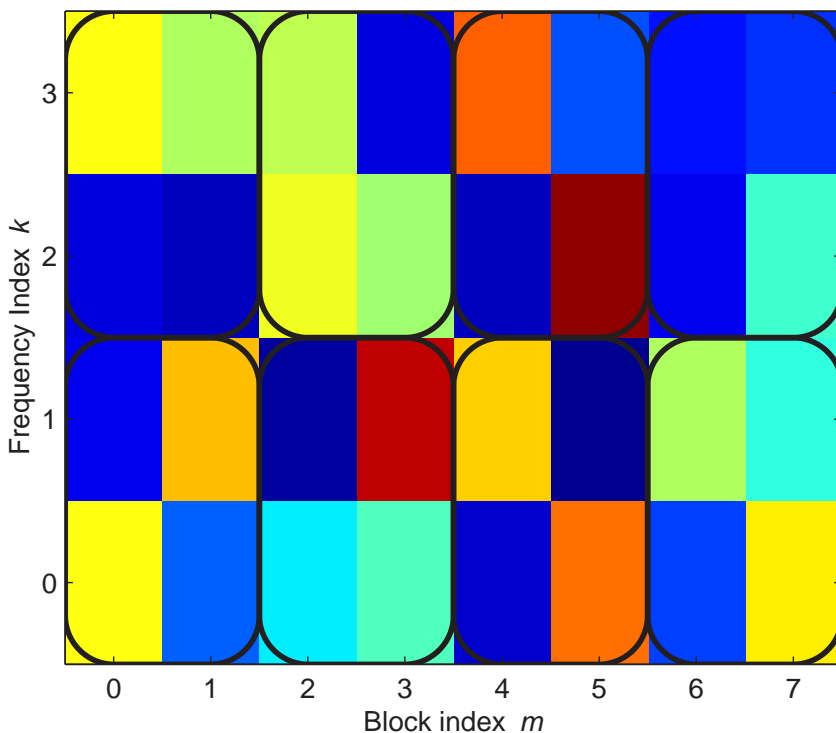


Fig. 11. A receiver combining four adjacent spectrogram outputs,  $N_{\text{FFT}} = 4$ .

### 3.2 Channelized radiometer model

Assume the channelized receiver shown in Fig. 4. It has  $N_C$  radiometers with adjacent frequency ranges, which form a channelized radiometer, each with bandwidth  $W_R$  and integration time  $T_R$ . The time-frequency product of each individual radiometer is  $T_R W_R$ . It is usually assumed that  $T_R W_R$  is an integer [9, p. 57] to simplify analysis, especially in digital implementations. If this is not true, the time-frequency product can be rounded to be an integer for analysis purposes [58, p. 296]. The measured energy in interval  $i$  and channel  $j$  is denoted by  $V_{ij}$ . Let us assume Gaussian white noise with one-sided power spectral density  $N_0$ . If  $N_0$  is known, normalized energies  $R_{ij} = 2V_{ij}/N_0$  can be computed. In the case of hard-decision processing, these energies are compared to a threshold  $\eta$ . After hard-decision, the outputs from different channels are combined with either a logical-OR operation [56],[9, p. 26],[11] or a sum [26, 68]. The radiometer outputs from different channels can also be directly combined by taking the largest output. Let  $M$  denote the total number of radiometer intervals in each observation interval. The combined outputs  $W_i$ , corresponding to the radiometer intervals, are summed to form the final deci-

sion variable  $W$ . The sum  $W$  is compared to a second threshold  $k_M$ . If the sum is larger than or equal to the threshold, and block detection is assumed, it is decided that a signal was present in addition to noise, i.e., hypothesis  $H_1$  is accepted. Otherwise hypothesis  $H_0$  is selected.

### 3.2.1 Local radiometer outputs

The channelized radiometer will be studied assuming that the measured energies in  $H_0$  and  $H_1$  follow the distributions given by Urkowitz [33]. No particular implementation structure is assumed. In the noise-only case, the distribution function of  $R_{ij}$  is assumed to follow the unscaled chi-square distribution with  $2T_R W_R$  degrees of freedom. In the deterministic signal-and-noise case, the distribution is assumed to follow the unscaled non-central chi-square distribution with  $2T_R W_R$  degrees of freedom and non-centrality parameter  $2E_{ij}/N_0$ , where  $E_{ij}$  is the energy of the signal to be detected in the time-frequency area corresponding to the radiometer channel  $j$  in the interval  $i$ . These distributions are actually approximations, at least for some implementation structures. Still, they are usually called exact results [9].

In the case of hard-decision processing, the radiometer outputs are compared to a threshold  $\eta$ . The local decision  $C_{ij}$  based on the (normalized) radiometer output  $R_{ij}$  is

$$C_{ij} = \begin{cases} 1, & R_{ij} > \eta \\ 0, & \text{otherwise,} \end{cases} \quad (26)$$

which have the probability of a false alarm  $Q_{\text{FA}} = P(C_{ij} = 1 | E_{ij} = 0)$ . It is given by [9]

$$Q_{\text{FA}} = \int_{\eta}^{\infty} \frac{x^{T_R W_R - 1} e^{-x/2}}{2^{T_R W_R} \Gamma(T_R W_R)} dx, \quad (27)$$

where  $\eta$  is the threshold and  $\Gamma$  is the gamma function [113, 6.1.1]. The probability of detection  $Q_{\text{D}}$  is the probability that the threshold is exceeded when a signal and noise are present, i.e.,  $Q_{\text{D}} = P(R_{ij} > \eta | E_{ij} > 0) = P(C_{ij} = 1 | E_{ij} > 0)$ . The detection probability is [9]

$$Q_{\text{D}} = Q_{T_R W_R} \left( \sqrt{2E_{ij}/N_0}, \sqrt{\eta} \right), \quad (28)$$

where  $Q_{T_R W_R}()$  is the generalized Marcum's Q function [7, eq. (2-1-122)] with parameter  $T_R W_R$ . The SNR required for a given probability of detection  $Q_{\text{D}}$  can be approximated as [11, Eq. (13a)]

$$E_{ij}/N_0 \approx \frac{1}{2} \left( \left[ \sqrt{\eta - (2T_R W_R - 1)/2} - x_d \right]^2 - (2T_R W_R - 1)/2 \right), \quad (29)$$

where  $x_d = \sqrt{2} \operatorname{erf}^{-1}(1 - 2Q_D)$  and  $\operatorname{erf}$  is the error function, defined as [113, 7.1.1]

$$\operatorname{erf}(z) = \frac{2}{\sqrt{\pi}} \int_0^z e^{-t^2} dt. \quad (30)$$

This result with an exact threshold, i.e., the inverse of the function (27), is a very accurate approximation, especially when  $Q_D$  is relatively high.

### 3.2.2 FH detection assumptions

Assume that the signal to be detected is an SFH signal with  $N_H$  non-overlapping hop channels. The hop bandwidth is  $W_H$  and the hop duration is  $T_H$ . All the signal energy is assumed to be contained within the hop bandwidth and the signal energy is assumed to be approximately evenly distributed over the hop duration [9]. For simplicity, we assume synchronism with the hop timing and that the frequency ranges of the individual radiometers match those of the hop channels [68, 66]. Thus,  $T_R = T_H$  (therefore  $M$  is the number of hops per decision) and  $W_R = W_H$ . Also,  $E_{ij} = E_H$ , where  $E_H$  is the received signal energy per hop. When the synchronism assumption is not valid, there is random splitting of the signal energy in time and/or frequency. This can be approximately taken into account by adding energy loss to the required SNR [9, p. 72–77]. According to Dillard [9], the effective energy loss resulting from a random splitting of the signal energy in time into two cells of integration is typically 0.5–2 dB. Asynchronous operation does not always result in SNR loss: if the detection probability is limited by intercept probability, no matter how high the SNR, an asynchronous operation helps because it increases the probability of intercept [11]. The channelized radiometer model and the detection assumptions presented here will be extended to include frequency sweeping (in Section 5.1).

### 3.2.3 CFAR analysis assumptions

A cell is defined to be the time-frequency area corresponding to individual radiometer measurements. In the noise-only case,  $2Z/N_0$ , where  $Z$  denotes the value of the radiometer output in the test cell, is known to follow the central chi-square distribution with  $2M_C$  degrees of freedom [9], where  $M_C = T_R W_R$  is an integer. Denote the reference cell values by  $Z_i$ , where  $i = 1, 2, \dots, N_R$ . The reference cells can, for example, be previous cells in the same frequency (see Fig. 12), the other cells in the same time interval, or their combination (see Fig. 13). Corrupted reference cells can be caused, for example, by other signals, by the presence of the signal to be detected also appearing in the reference area and by interference. Assume that the signal energy in a reference cell  $i$  is  $E_i$ . The random variable  $2Z_i/N_0$  follows the noncentral chi-square distribution with  $2M_C$  degrees of freedom and the non-centrality parameter  $\lambda_i = 2E_i/N_0$  [9]. The total non-centrality

parameter

$$\lambda_S = \sum_{i=1}^{N_R} \lambda_i. \quad (31)$$

The distributions of the cells used here, as in the previous studies of the channelized radiometer, correspond to those used in the radar literature with noncoherent integration and a nonfluctuating target [84, 85].

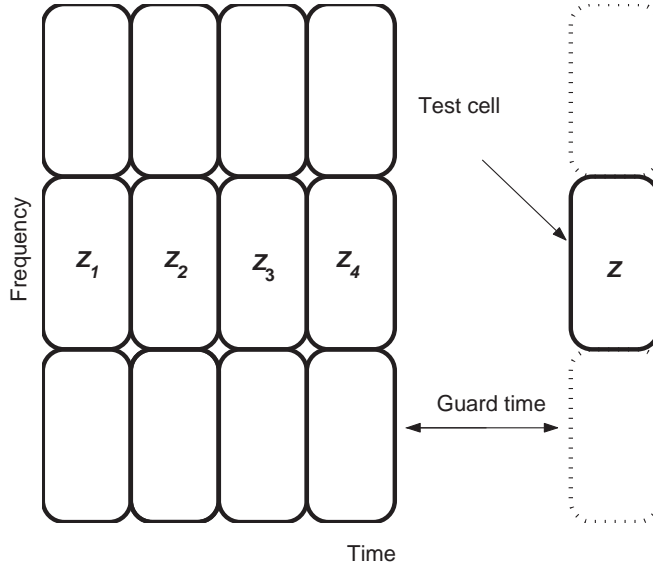


Fig. 12. Reference cells are the previous cells in the same frequency,  $N_R = 4$ .

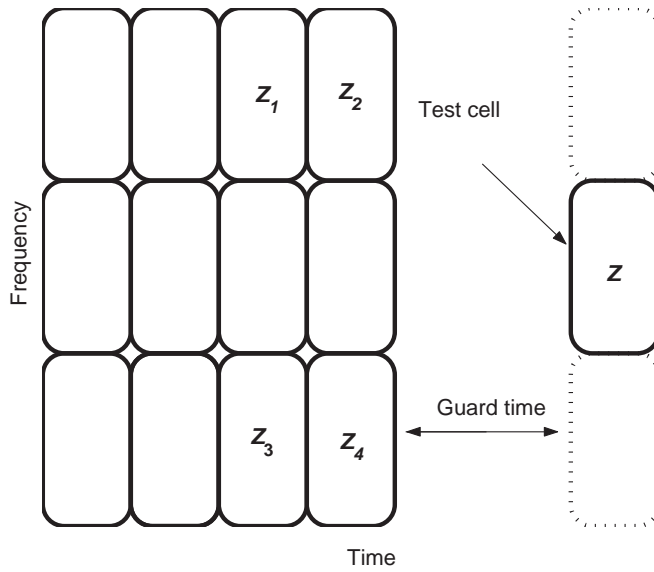


Fig. 13. One possible set of reference cells when  $N_R = 4$ .

## 4 Threshold setting for a quantized radiometer

In this chapter, issues related to threshold setting for a quantized radiometer are considered. First, false alarm probability corresponding to a fixed threshold is found in Section 4.1. Noise variance estimation based on quantized samples is discussed in Section 4.2. In Section 4.3, we use a randomized decision rule that gives exactly the required false alarm probability, assuming that the noise variance is known or an accurate estimate is available. The main goal is to analyze the false alarm probability of a detector that uses the CA-CFAR strategy. The analysis is carried out in Section 4.4. Numerical results are presented in Section 4.5 and the conclusions are drawn in Section 4.6.

### 4.1 Radiometer with quantization

Assume that the receiver shown in Fig. 1, with separate quantization and sampling of the in-phase and quadrature channels, is used. The real and imaginary parts are assumed to be independent zero-mean, white Gaussian random processes with variances  $\sigma^2$ . Assume that  $N/2$  complex samples are collected. These samples can be represented in real variables with

$$\bar{r}_k = \begin{cases} \Upsilon(\operatorname{Re}(r_k)) & k = 0, 2, \dots, N/2 - 1 \\ \Upsilon(\operatorname{Im}(r_{k-N/2})) & k = N/2, \dots, N - 1 \end{cases} \quad (32)$$

where  $\Upsilon$  is assumed to be a deterministic uniform midriser quantization operator. For example, assume  $N = 6$  and  $r_0 = 1 + 2j$ ,  $r_1 = 3 + j$ , and  $r_2 = 4 + 7j$ . Now, the vector containing  $\bar{r}_k$ ,  $k = 0, 1, \dots, 5$ , is

$$[\Upsilon(1) \quad \Upsilon(3) \quad \Upsilon(4) \quad \Upsilon(2) \quad \Upsilon(1) \quad \Upsilon(7)]^T.$$

Here, the focus is on general purpose receivers using uniform quantization, i.e., the optimum quantization levels and boundaries are not searched. Actually, assuming the noise variance is known, in many cases it would be optimal to quantize the envelope  $|r_k|$  or the squared envelope of the received signal [114]. The quantization operator used here has output levels  $(i + 1/2)\Delta$ , where the quantization levels are indexed with integer values  $i = -2^{B-1}, -2^{B-1} + 1, \dots, 2^{B-1} - 1$ ,  $B$  is the number of quantization bits and  $\Delta$  is

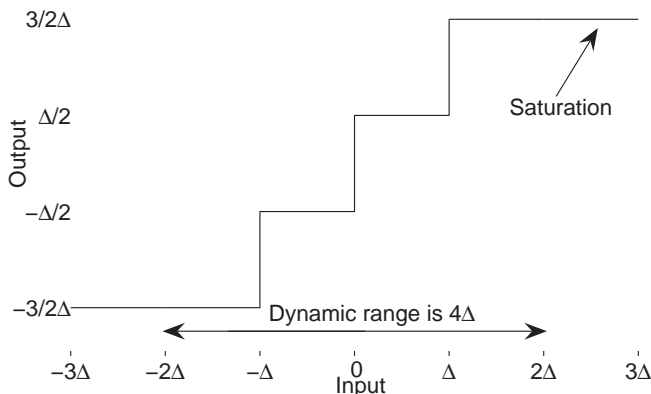


**Fig. 14. Uniform midriser quantizer with  $B = 2$  quantization bits.**

the quantization step so that the dynamic range  $R$  is  $2^B \Delta$  as illustrated in Fig. 14. Uniform quantization is widely used in practice due to its simplicity. In the context of energy detection, half of the quantization levels are "wasted" because the sign information is not needed. The probability that the  $i$ th quantization level of the midriser quantizer is chosen when  $H_0$  is true is [51, 52]

$$P_i(x) = \frac{1}{2} \left[ \operatorname{erf} \left( \frac{(i+1)x}{\sqrt{2}} \right) - \operatorname{erf} \left( \frac{ix}{\sqrt{2}} \right) \right], \quad (33)$$

where  $x = \Delta/\sigma$ ,  $i = -2^{B-1}+1, \dots, 2^{B-1}-2$ . If  $i = 2^{B-1}-1$ ,  $P_i(x) = \frac{1}{2} - \frac{1}{2} \operatorname{erf} \left( \frac{ix}{\sqrt{2}} \right)$ . If  $i = -2^{B-1}$ ,  $P_i(x) = \frac{1}{2} + \frac{1}{2} \operatorname{erf} \left( \frac{(i+1)x}{\sqrt{2}} \right)$ . Let  $i_k$  denote the indices of the chosen quantization levels for the received signal in the current observation interval, where  $k = 0, 1, \dots, N-1$ , i.e, the quantized values are

$$\bar{r}_k = (i_k + 1/2) \Delta. \quad (34)$$

The quantized total power radiometer uses the decision statistic (6) with quantized input (or equivalently (24) with  $v = 1$ ) [51]

$$V = \sum_{k=0}^{N/2-1} |\Upsilon(\operatorname{Re}(r_k)) + j\Upsilon(\operatorname{Im}(r_k))|^2 = \sum_{k=0}^{N-1} \bar{r}_k^2. \quad (35)$$

However, it is more convenient to use the equivalent integer-valued decision variable

$$V' = \frac{V}{\Delta^2} - \frac{N}{4} = \sum_{k=0}^{N-1} (i_k^2 + i_k). \quad (36)$$

Let us denote the probability mass function (PMF) of  $i_k^2 + i_k$  with  $f_s(z)$ , i.e.,

$$f_s(z) = P(i_k^2 + i_k = z), \quad z = 0, 1, 2, \dots, \quad (37)$$

which can be easily found using the probability weights  $P_i(x)$ . Now, the PMF of  $V'$  is

$$f_{V'}(z) = \underbrace{f_s(z) * f_s(z) * \dots * f_s(z)}_N, \quad (38)$$

which can also be calculated by using the recursive method presented by Goldstein and Hansen [115, Appendix].

Let us assume that a fixed threshold  $T$  is used with a quantized total power radiometer. The equivalent integer-valued threshold is  $T' = \lceil T/\Delta^2 - N/4 \rceil$ , where  $\lceil \cdot \rceil$  is the smallest integer greater than or equal to the argument, e.g.,  $\lceil 1.2 \rceil = 2$  and  $\lceil 2.0 \rceil = 2$ . Now, the probability of a false alarm corresponding to the threshold  $T$  is

$$P_{\text{FA}} = \sum_{z \geq T'} f_{V'}(z). \quad (39)$$

One possibility is to use a detection threshold corresponding to an analog total power radiometer [53]. In that case,  $T = \eta\sigma^2$ , where  $\eta = F_{\chi^2, N}^{-1}(1 - P_{\text{FA,DES}})$ ,  $F_{\chi^2, N}$  is the chi-square cumulative distribution function (CDF) with  $N$  degrees of freedom, and  $P_{\text{FA,DES}}$  is the desired false alarm probability [9]. It was found in [53] that the actual probability of a false alarm is different from the desired value, especially when the number of quantization bits is low.

Quantization can be (often approximately) modelled to cause additive noise, uncorrelated with the input process, with variance  $\Delta^2/12$  [116, 117]. In the standard model, quantization noise is assumed to be uniformly distributed (and white) [118, 119]. Note that in some applications, such as when testing ADC using sinusoidal input, the quantization noise is far from uniform [120]. For simplifying the threshold setting, and keeping in mind the central limit theorem, here the quantization noise is assumed to follow the Gaussian distribution instead of uniform distribution [54]. This assumption leads to a threshold  $T = \eta(\sigma^2 + \Delta^2/12)$ , i.e., this approximate threshold depends also on the step size.

## 4.2 Noise level estimation based on quantized samples

Noise level estimation based on quantized reference samples is needed in various applications. For example, the detection threshold used in [53] requires knowledge of the noise level. Also, the randomized decision rule in Section 4.3 requires knowledge of the noise level. The mean of the squared quantized noise-only samples normalized with the known step size  $\Delta$  is

$$\varphi(x) = E\left(\frac{\tilde{r}^2}{\Delta^2}\right) = \sum_{i=-2^{B-1}}^{2^{B-1}-1} \left(i + \frac{1}{2}\right)^2 P_i(x), \quad (40)$$

where the index  $k$  has been dropped because the samples are IID. The maximum value of  $\varphi(x)$  is  $(2^{B-1} - \frac{1}{2})^2$ , in which case the quantization step size is so small that even just

noise causes only the largest output values to be selected. The minimum value is  $\frac{1}{4}$ , in which case the quantization step size is so large that only the smallest output values are selected. The variance of the input signal can be found with (see [121] for explicit results for a three-level quantizer)

$$\sigma^2 = \Delta^2 \left[ \varphi^{-1} \left( E \left( \frac{\bar{r}^2}{\Delta^2} \right) \right) \right]^{-2}. \quad (41)$$

The variance and, equivalently  $x$ , can be estimated by substituting the sample mean in place of the statistical mean, i.e., by using  $1/N_R \sum_{k=0}^{N_R-1} (i_k + 1/2)^2$ , where  $N_R$  is the number of noise-only reference samples.

### 4.3 Exact randomized decision rule

The decision variable (36) has a finite number of possible output values. Therefore, using a randomized decision rule is necessary for obtaining arbitrary false alarm probabilities [122]. It is specified by the threshold  $T'$  and probability  $\delta$ . If the observed  $V'$  is larger than  $T'$ , an alarm occurs always. If  $V' = T'$ , an alarm occurs with probability  $\delta$  (for example, a random number generator is used within the intercept receiver). The proper threshold  $T'$  is the maximum value satisfying

$$\sum_{z \geq T'} f_{V'}(z) \geq P_{\text{FA,DES}} \quad (42)$$

and the corresponding randomization factor is [123]

$$\delta = \frac{P_{\text{FA,DES}} - \sum_{z > T'} f_{V'}(z)}{f_{V'}(T')}. \quad (43)$$

With the randomization factor (43) the exact required false alarm probability is obtained, assuming that  $x$  is known. If it is estimated instead, a large number of reference samples may be necessary so that the false alarm probability is close to the desired value. It may be desirable to choose the quantization step  $\Delta$  so that the randomization factor is zero or one, i.e., no randomization is used [122].

### 4.4 Performance analysis of the CA-CFAR strategy

If the noise variance is unknown and reference samples are available, it is intuitive to use as a threshold  $\gamma\eta\hat{\sigma}^2$ , where

$$\hat{\sigma}^2 = \frac{1}{N_R} \sum_{k=0}^{N_R-1} v_k^2 \quad (44)$$

is the variance estimate based on  $N_R$  zero-mean reference samples  $\vartheta_k$ , and  $\gamma$  is a scaling factor chosen so that, on average, the false alarm probability has the desired value. The ideal situation where power mismatch between reference samples  $\vartheta_k$  and the actual noise is zero is assumed. Power mismatch can occur, for example, if the reference samples are obtained by turning the antenna off. In that case, the reference samples contain only internal thermal noise, whereas the actual received noise includes also external noise.

Let  $U_1$  and  $U_2$  denote two independent chi-square distributed variates with  $v_1$  and  $v_2$  degrees of freedom, respectively. The ratio

$$\frac{U_1/v_1}{U_2/v_2} \quad (45)$$

follows the  $F$  (Fisher) distribution [113, 26.6.]. Its CDF can be expressed using the regularized incomplete beta function [113, 26.5.]

$$\text{FCDF}(x, v_1, v_2) = I_{v_1 x / (v_1 x + v_2)}(v_1/2, v_2/2). \quad (46)$$

The chi-square distribution is a special case of the gamma distribution. The ratio of two gamma variates follows the beta prime distribution [124]. However, here only the chi-square variates are considered.

Using the results in the CA-CFAR literature (see, for example, [29, 84]), the correct scaling factor for a detector without quantization is found to be

$$\gamma = \text{FCDF}^{-1}(1 - P_{\text{FA,DES}}, N, N_R) N / \eta. \quad (47)$$

The scaling factor (47) gives exactly the desired false alarm probability. When the number of reference samples increases, the scaling factor approaches one. In other words, when the number of reference samples is large, less scaling is needed. This behavior is illustrated in Fig. 15.

The scaling factor  $\gamma = 1$  has been used in [54]. The theoretical false alarm probability corresponding to  $\gamma = 1$  without quantization is

$$P_{\text{FA}} = 1 - \text{FCDF}(\eta/N, N, N_R). \quad (48)$$

When quantization is performed, the correct CA-CFAR scaling factor depends on the unknown  $x$ . Therefore, it is not possible to always use the "correct" scaling factor. Instead, for example, the scaling factor  $\gamma = 1$  or the scaling factor (47) is used. We evaluate the exact false alarm probability corresponding to an arbitrary scaling factor  $\gamma$  and  $x$ . Let  $v_k$  denote the indices of the chosen quantization levels for the reference signal, i.e.,  $\bar{\vartheta}_k = \Upsilon(\vartheta_k) = (v_k + 1/2) \Delta$ . Now

$$\begin{aligned} P_{\text{FA}} &= P\left(\sum_{k=0}^{N-1} \bar{r}_k^2 > \frac{\gamma\eta}{N_R} \sum_{k=0}^{N_R-1} \bar{\vartheta}_k^2\right) \\ &= P\left(\sum_{k=0}^{N-1} (i_k + 1/2)^2 \Delta^2 > \frac{\gamma\eta}{N_R} \sum_{k=0}^{N_R-1} (v_k + 1/2)^2 \Delta^2\right) \\ &= P\left(\sum_{k=0}^{N-1} (i_k^2 + i_k) > \frac{\gamma\eta}{N_R} \sum_{k=0}^{N_R-1} (v_k^2 + v_k) + c\right) \\ &= P\left(V' > \frac{\gamma\eta}{N_R} V'_{\text{REF}} + c\right), \end{aligned} \quad (49)$$

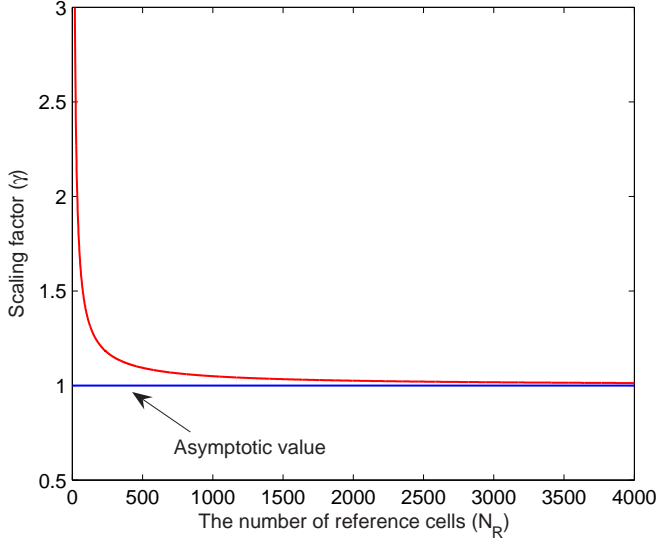


**Fig. 15.** Scaling factor as a function of the number of reference cells,  $N = 512$ ,  $P_{\text{FA,DES}} = 10^{-3}$ .

where  $V'_{\text{REF}} = \sum_{k=0}^{N_R-1} (v_k^2 + v_k)$  and  $c = (\gamma\eta - N)/4$ . The conditional false alarm probability, assuming  $V'_{\text{REF}} = \kappa$ , is

$$P\left(V' > \frac{\gamma\eta}{N_R}\kappa + c\right) = \sum_{z > \frac{\gamma\eta}{N_R}\kappa + c} f_{V'}(z). \quad (50)$$

The probability of false alarm becomes

$$P_{\text{FA}} = \sum_{\kappa} P\left(V' > \frac{\gamma\eta}{N_R}\kappa + c\right) f_{V'_{\text{REF}}}(\kappa), \quad (51)$$

where  $f_{V'_{\text{REF}}}$  denotes the PMF of the  $V'_{\text{REF}}$  found similarly to the PMF of  $V'$ , see (38). Together, (50) and (51) allow the calculation of the theoretical false alarm probability of the quantized total power radiometer using the CA-CFAR threshold setting method.

In [55], similar methods have been used for investigating data quantization effects for exponentially distributed input. The exponential distribution results, for example, from squaring the envelope of a complex Gaussian random variable or from summing the squares of two IID real-valued Gaussian random variables.

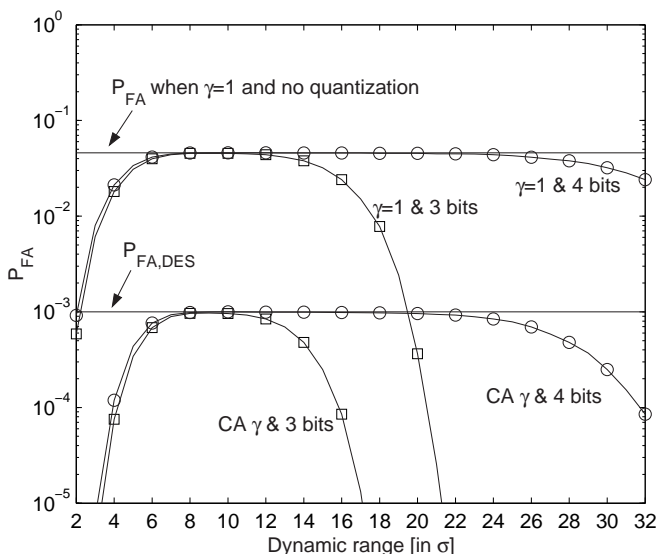


Fig. 16. False alarm probabilities,  $N = 512$  and  $N_R = 256$ .

## 4.5 Numerical results

Fig. 16 shows false alarm probabilities as a function of the dynamic range when  $P_{FA,DES} = 10^{-3}$ ,  $N = 512$  and  $N_R = 256$ . The theoretical false alarm probability corresponding to  $\gamma = 1$  without quantization was calculated using (48). The CA  $\gamma$  refers to the scaling factor (47). It can be seen that when the CA scaling factor is used and  $B = 4$ , the system is operating properly when the dynamic range  $R \in [8\sigma, 20\sigma]$ . When the CA scaling factor is used and  $B = 3$ , it should be that  $R \in [8\sigma, 10\sigma]$ . The scaling factor  $\gamma = 1$  gives significantly higher than desired false alarm probabilities. The results when  $N_R = 2048$  were similar to those in Fig. 16, except that the false alarm probabilities obtained using  $\gamma = 1$  were closer to the desired value, see Fig. 17. Let us now study the situation where the CA  $\gamma$  is used and  $B = 3$ . Fig. 18 shows the false alarm probabilities as a function of the dynamic range with different reference set sizes. It is observed that  $N_R = 8$  is not sufficient. With  $N_R = 64$ , the results are relatively close to the situation with  $N_R = 256$ , which was discussed previously.

Fig. 19 shows the false alarm probabilities when the noise variance before quantization is assumed to be known. The threshold setting strategies analyzed were: (A) the threshold corresponding to an analog radiometer,  $T = \eta\sigma^2$  [53]; (B) the threshold corresponding to the Gaussian quantization noise assumption [54] with  $T = \eta(\sigma^2 + \Delta^2/12)$ ; (C) the randomized decision rule. In addition to the theoretical results found with the method presented in Section 4.1, simulation results are shown. It is seen that threshold (A) is not a good choice. Threshold (B) yields surprisingly good performance, when the dynamic

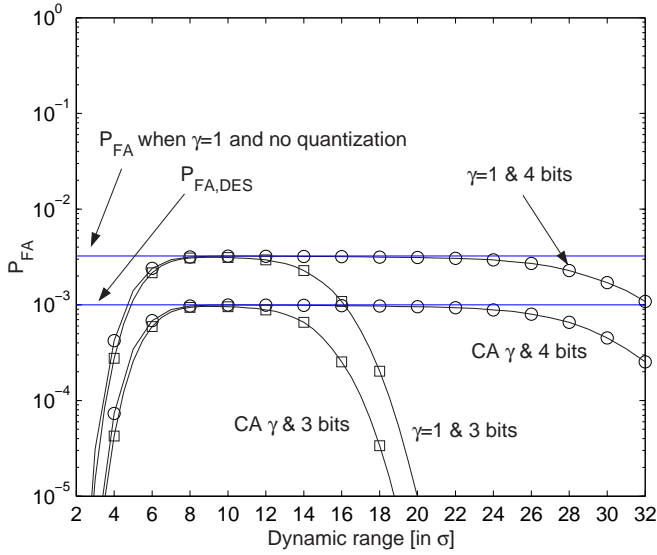
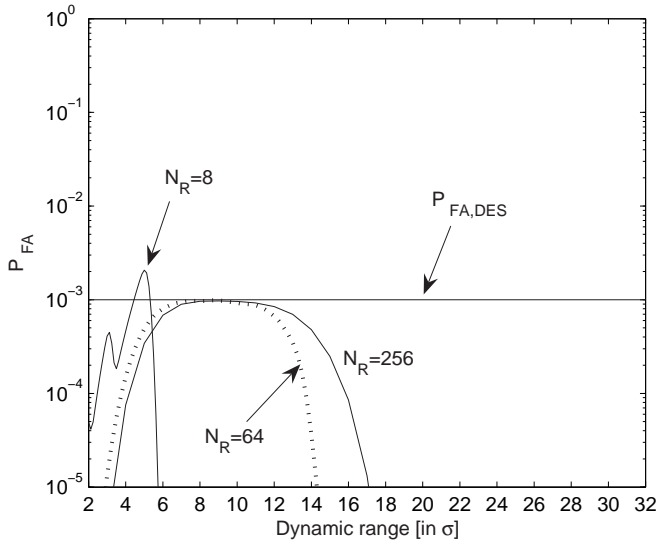


Fig. 17. False alarm probabilities,  $N = 512$  and  $N_R = 2048$ .

range  $R \in [8\sigma, 15\sigma]$ . Strategy (C) gives exactly the desired false alarm probability no matter what the dynamic range is. With four quantization bits threshold (B) gave good results when  $R \in [8\sigma, 30\sigma]$  (results not shown here). It is interesting that 3 or 4 quantization bits have been found to be sufficient also in some other applications, such as carrier frequency recovery [125].

## 4.6 Conclusions

A quantized total power radiometer was studied in two cases: (1) the noise power is unknown; (2) the noise power is known. In case (1), the focus was on analyzing the CA-CFAR threshold setting strategy with different scaling factors. In case (2), three different threshold setting strategies were studied and compared. The threshold corresponding to the Gaussian quantization noise assumption performed surprisingly well. Typically, 3 or 4 quantization bits are required for obtaining the desired false alarm probability in both cases.



**Fig. 18.** False alarm probabilities,  $P_{FA,DES} = 10^{-3}$ ,  $N = 512$  and  $B = 3$ .

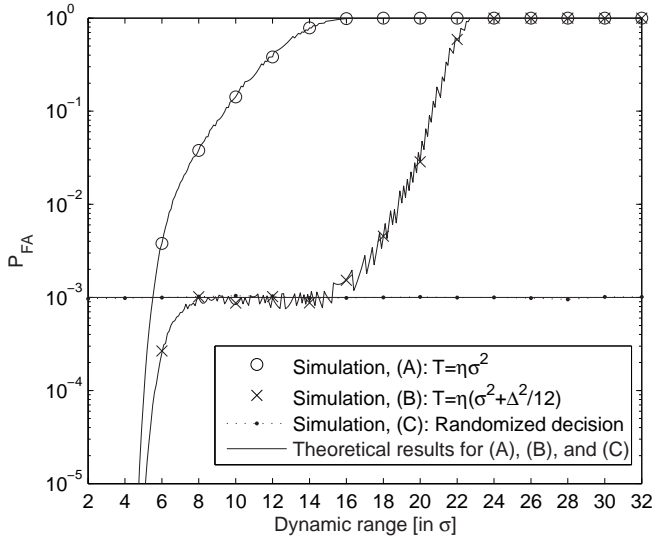


**Fig. 19.** False alarm probabilities,  $P_{FA,DES} = 10^{-3}$ ,  $N = 512$ , three quantization bits ( $B = 3$ ), and  $\sigma^2$  is assumed to be known.

## 5 Sweeping channelized radiometer

In this chapter, the performance of a sweeping channelized radiometer is studied. First, statistical assumptions and the system model are described in Section 5.1. The channelized radiometer system model presented in 3.2 is extended to include sweeping. The decision strategies are introduced and presented in Section 5.2. An efficient method for calculating the likelihood ratio is presented in Section 5.3. Analysis of the logical OR-sum, sum-sum and the max-sum methods is presented in Section 5.4 for a non-fading channel. In Section 5.5, the effects of fading are analyzed. In Section 5.6, the required signal-to-noise ratio SNR is found as a function of the sweeping speed assuming the signal to be detected uses similar parameters as the SINGARS radio. Finally, the conclusions are drawn in Section 5.7.

### 5.1 Sweeping channelized radiometer

Assume that the radiometer bandwidth is equal to the hop bandwidth, i.e.,  $W_R = W_H$ . Typically, the number of radiometers is smaller than the number of hopping frequencies, i.e.,  $N_C < N_H$ . In such a case, the detector can step the received frequency band  $K$  times within each hop to increase the probability of intercept [68, 69]. It would also be possible to increase the radiometer bandwidth, so that  $W_R$  is some multiple of  $W_H$  [11]. The stepping causes the integration time per radiometer output to be reduced to  $T_R = T_H/K$ , where  $T_H$  is the hop duration and  $K$  is the number of detection phases within a hop. The radiometer outputs are sampled before the center frequency is changed. Assume for simplicity time synchronism. Then the total number of radiometer outputs within a hop is  $N_{eff} = KN_C$ . The outputs are indexed so that in the first phase the outputs have indices  $1, 2, \dots, N_C$ ; in the second phase, the outputs have indices  $N_C + 1, N_C + 2, \dots, 2N_C$ , and so on. Due to the assumed synchronism, this detection structure is analytically equivalent to  $N_{eff}$  radiometers with a bandwidth  $W_H$  and integration time  $T_H/K$  [68]. The time-frequency product of each individual radiometer is  $T_R W_R = (T_H/K)W_H$ . In the following, it is assumed that  $T_R W_R$  is an integer or that it is rounded to an integer. Fig. 20 shows the detection structure for the case of  $K = 3$  detection phases per hop duration. Sweeping makes the analytically equivalent instantaneous bandwidth large, but

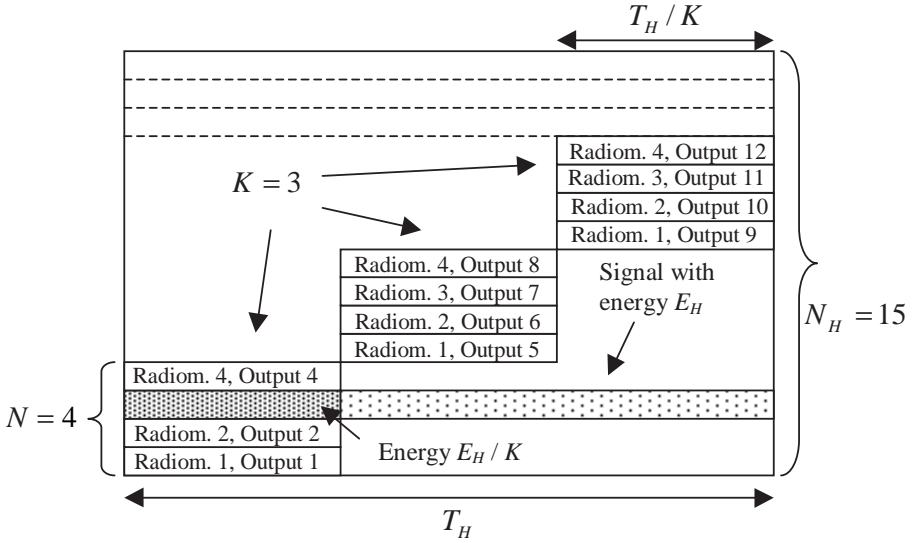


**Fig. 20.** The detection structure in the synchronous case, 15 possible hop channels, 4 radiometers, 3 detection phases, signal intercepted in the first phase by radiometer 3,  $N_{eff} = 12$ .

the integration time is reduced. The POI per hop is  $p_I = N_{eff}/N_H \leq 1$ , because all hop channels are assumed to be equally likely due to the random FH. This result assumes that the search range is fully within the hop range [69]. The results are different in situations where this assumption is not true. For example, the hop range can be fully within the search range or the hop range and search range can overlap [69]. Also, in some systems it is possible to use only a part of the channels for transmission, but this is not considered here. In Fig. 20, channels 1–12 are searched during one hop, and there are 15 possible hop channels. Therefore,  $p_I = 80\%$ . The POI would be the same if channels 2–13, 3–14 or 4–15 were searched instead. Without affecting the results it is possible to combine sweeping faster than hop dwell time and this hop level offset. For example, let us assume that  $N_H = 16$ ,  $N_C = 4$  and  $K = 2$ . Now channels 1–8 can be searched in the first hop, channels 9–16 in the second hop, channels 1–8 in the third hop and so on. If  $K = 1$ , the search pattern could be 1–4, 5–8, 9–12, 13–16. If  $K = 4$ , all the channels are searched during a single hop. Let us assume that the intercept receiver's full scan consists of a searching  $M_{SC}$  channel and let  $L$  denote the number of full scans [70]. The number of hops in these  $L$  full scans is  $M = LM_{SC}/KN_C$ .

The energy of the FH signal in the time-frequency area of the radiometer that intercepts the signal is assumed to be  $E_{ij} = E_H/K$ , where  $E_H$  is the signal energy per hop,  $i$  is the hop index,  $i \in \{1, 2, \dots, M\}$ , and  $j$  is the radiometer output index,  $j \in \{1, 2, \dots, N_{eff}\}$ . In practice, this assumption is an approximation, and the signal may leak some energy also to adjacent radiometers. Let  $R_{ij} = 2V_{ij}/N_0$ , where  $V_{ij}$  is the measured energy, denote the normalized radiometer output, which is scaled with  $2/N_0$ .

The local (quantized) decision  $C_{ij}$  based on the normalized radiometer output is

$$C_{ij} = \begin{cases} 1, & R_{ij} > \eta \\ 0, & \text{otherwise.} \end{cases} \quad (52)$$

The probability of a false alarm for local decisions  $Q_{\text{FA}}$  can be found with (27), and the probability of detection,  $Q_{\text{D}}$  can be found with (28).

## 5.2 Decision strategies

Decision strategies refer to methods used for combining the radiometer outputs in the observation period. Decision strategies for a total power radiometer were discussed in 2.2. There, the binary integration (BI) method was presented. Similar methods can also be used with the channelized radiometer. However, these methods need also to combine radiometer outputs from different channels, in addition to different integration intervals. First, Section 5.2.1 presents the optimal method for combining un-quantized radiometer outputs. Several suboptimal methods, rather similar to the BI, are presented in Section 5.2.2. Finally, in Section 5.2.3, the likelihood ratio of quantized data is briefly discussed.

### 5.2.1 Likelihood ratio of un-quantized data

The optimal detection statistic (average likelihood ratio) conditioned on the observable  $\mathbf{R} = \{R_{ij}\}$ , i.e., the set of normalized radiometer outputs, is [126]

$$\Lambda(\mathbf{R}) = \prod_{i=1}^M \frac{1}{N_H} \sum_{j=1}^{N_H} \Lambda_{ij}(\mathbf{R}_i | f_j), \quad (53)$$

where  $\mathbf{R}_i$  denotes the set of normalized radiometer outputs in the hop  $i$  and  $f_j$  denotes the hypothesis that the signal is present in channel  $j$ . It is assumed that the signal is equally likely to be in any channel and these channels are independent from hop to hop. For the sweeping system, the likelihood ratio  $\Lambda_{ij}$  is 1 if  $N_{\text{eff}} < j \leq N_H$  and if  $j \leq N_{\text{eff}}$  it is ([9, Eq. (A.12)])

$$\Lambda_{ij}(\mathbf{R}_i | f_j) = c \cdot R_{ij}^{-\frac{T_R W_R - 1}{2}} I_{T_R W_R - 1} \left( \sqrt{\frac{2E_H R_{ij}}{K N_0}} \right), \quad (54)$$

where  $I_{T_R W_R - 1}$  is the modified Bessel function of the first kind [113, 9.6] with order  $T_R W_R - 1$  and

$$c = 2^{\frac{T_R W_R - 1}{2}} \left( \frac{E_H}{K N_0} \right)^{-\frac{T_R W_R - 1}{2}} \Gamma(T_R W_R) e^{-\frac{E_H}{K N_0}}. \quad (55)$$

If sweeping is not used, i.e.,  $K=1$ , and  $N_{\text{eff}} = N_H$ , then (53) and (54) form the

classical Woodring-Edell (WE) detector [66]. In this case, the constant term (55) can be ignored.

It can be observed that the optimal detection statistic depends on the signal-to-noise ratio. The signal-to-noise ratio is usually unknown so the optimal detector is not realizable in practice. The signal-to-noise ratio may be estimated after or jointly with detection. It is important to study the optimal detector so that the upper bound on detection performance is found. If details of the signal modulation would be known, more specialized optimal detection methods could be used [66]. It would be possible to evaluate the performance of the optimal detector with approximations similar to those used in [66, 127, 128]. However, simulations are used here.

### 5.2.2 Suboptimal methods

If a sum is used to combine the local decisions, let

$$W_i = \sum_{j=1}^{N_{eff}} C_{ij}. \quad (56)$$

A logical-OR operation can alternatively be used to combine all  $N_{eff}$  local decisions within a hop. In this case,  $W_i = 1$  if at least one  $C_{ij} = 1$ ,  $j \in \{1, 2, \dots, N_{eff}\}$ ; otherwise it is zero. The maximum-based intercept receiver sums per hop maxima of the radiometer outputs [129, 25, 130] so that  $W_i = \max_j \{R_{ij}\}$ . The final decision variable

$$W = \sum_{i=1}^M W_i. \quad (57)$$

These methods are illustrated in Fig. 21. In [129], the envelope detector outputs were combined using the maximum, and the performance was analyzed using the Gaussian approximation. There, the proposed detector was called the sum-of-largest-envelopes (SLE) receiver. In the original publication [25], the channelized radiometer outputs were combined with the maximum. The numerical convolution and the Gaussian approximation were used. This can be viewed to be an extension of the sum-of-largest-envelopes-squared (SLES) receiver [130] in a situation where  $T_R W_R \geq 1$ . It was found in [130] that the SLES receiver has a slightly better detection performance than the SLE receiver.

### 5.2.3 Likelihood ratio of quantized data

An optimal detector conditioned on the observable  $\mathbf{C} = \{C_{ij}\}$ ,  $i \in \{1, 2, \dots, M\}$ ,  $j \in \{1, 2, \dots, N_{eff}\}$ , i.e., the set of local decisions in all hops and channels, has been derived in [68]; there it was derived in the context of the envelope detector, but the result can also be directly applied in the case of the channelized radiometer. It was shown that at low signal-to-noise-ratios, the sum-sum statistic is asymptotically optimal. This does

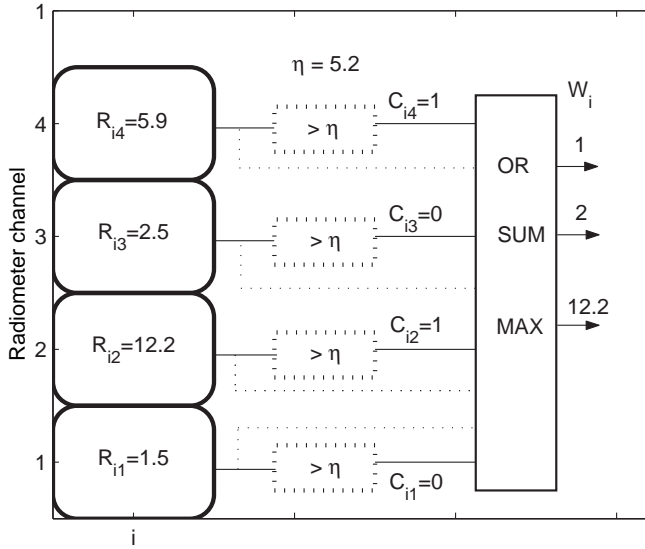


Fig. 21. Per hop operation of the logical OR-sum, sum-sum and the max-sum methods.

not mean that a detector based on the sum-sum performs better than a detector based on the logical-OR. Actually, when only one signal is present, the logical-OR based detector performs slightly better.

### 5.3 Efficient calculation of the un-quantized likelihood ratio

For large values of  $T_R W_R$ , there exists an efficient representation of the Bessel function, namely [113, 9.7.7]

$$I_\nu(z) = \frac{1}{\sqrt{2\pi\nu}} \frac{e^{v\varpi}}{(1+(z/v)^2)^{1/4}} \left\{ 1 + \sum_{k=1}^{\infty} \frac{u_k(t)}{v^k} \right\}, \quad (58)$$

where  $\varpi = (1+(z/v)^2)^{1/2} + \ln(z/v) - \ln(1 + \sqrt{1+(z/v)^2})$ ,  $t = 1/\sqrt{1+(z/v)^2}$  and  $u_1(t) = 1/8t - 5/24t^3$ . For values of  $u_k(t)$  with  $k > 1$  refer to [113, 9.3.9].

We apply the following approximation [131]

$$d_2 = \ln \left\{ 1 + \sum_{k=1}^{\infty} \frac{u_k(t)}{v^k} \right\} \approx \frac{1}{8v}t - \frac{5}{24v}t^3 + \frac{1}{16v^2}t^2 - \frac{3}{8v^2}t^4 + \frac{5}{16v^2}t^6 + \frac{25}{384v^3}t^3 - \frac{531}{640v^3}t^5 + \frac{221}{128v^3}t^7 - \frac{1105}{1152v^3}t^9. \quad (59)$$

By taking the logarithm of the likelihood ratio (54) and using (58)-(59) it is found that

$$\begin{aligned} \ln \Lambda_{ij}(\mathbf{R}_i | f_j) &\approx d_1 + (v^2 + z^2)^{1/2} \\ &- v \ln \left( 1 + \sqrt{1 + (z/v)^2} \right) - \frac{1}{4} \ln \left( 1 + (z/v)^2 \right) + d_2, \end{aligned} \quad (60)$$

where  $v = T_R W_R - 1$ ,  $z = \sqrt{\frac{2E_H R_{ij}}{KN_0}}$ ,

$$d_1 = v \ln 2 + \ln \Gamma(v + 1) - \frac{E_H}{KN_0} - v \ln v - \frac{1}{2} \ln(2\pi v) \quad (61)$$

and  $d_2$  is given by (59). If the term  $d_2$  is ignored, the approximation (60) is still rather accurate. The likelihood ratio can be found with the exponential of (60). Fig. 22 shows the relative error of the individual likelihood ratio  $\Lambda_{ij}(\mathbf{R}_i | f_j)$  calculated with this approximation, i.e., the absolute error divided by the correct value. The parameters used are  $E_H/KN_0 = 30$  and  $T_R W_R = 250$ . It is observed that the approximation (60) with the term  $d_2$  is very accurate. Therefore, when evaluating the performance of the optimal detector with simulations, an exponential of (60) with the term  $d_2$  is used. This method of evaluating the likelihood ratio can be used with a wide range of input values, because first the logarithm of the likelihood ratio is evaluated. Actually, the likelihood ratio is almost linear in a logarithmic scale. This means that potentially even simpler yet still rather accurate expressions could be developed. One way of achieving this would be to use suitable approximations for the terms in (60).

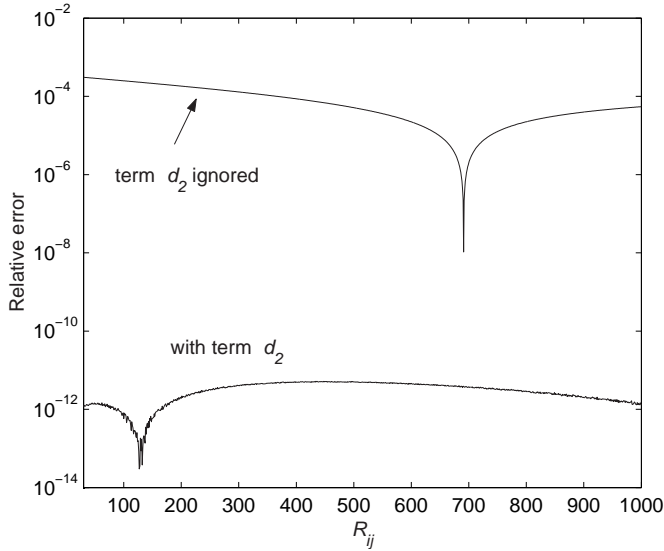


**Fig. 22.** Relative error of the approximation to the individual likelihood ratio  $\Lambda_{ij}(\mathbf{R}_i | f_j)$ ,  $E_H/KN_0 = 30$ ,  $T_R W_R = 250$  and  $j \leq N_{eff}$ .

Numerical effects can also affect the calculation of the final decision variable (53),

which is a product of the sums of the individual likelihood ratios. It is possible to take a logarithm of the final decision variable, which results in a sum of logarithms of sums of the individual likelihood ratios. However, in this case it is still necessary to sum exponentials, because a logarithm cannot be moved inside a sum.

## 5.4 Performance analysis

The statistical properties of the local decisions were discussed in Section 3.2.1. Analysis of the logical OR-sum detector is presented in Section 5.4.1, followed by the sum-sum detector analysis and the max-sum detector analysis in Sections 5.4.2 and 5.4.3, respectively. The analysis of the logical OR-sum detector in Section 5.4.1 is based on [11]. This reference is reviewed here to enable comparisons.

### 5.4.1 Logical OR-sum decision rule

The probability of a false alarm per hop when using logical-OR operation is [11]

$$p_0 = P(W_i = 1 | H_0) = 1 - (1 - Q_{\text{FA}})^{N_{\text{eff}}} \quad (62)$$

because a false alarm occurs if at least one radiometer output exceeds the threshold. The probability of detection per hop is [11]

$$p_1 = P(W_i = 1 | H_1) = p_I \left( 1 - (1 - Q_{\text{D}})(1 - Q_{\text{FA}})^{N_{\text{eff}}-1} \right) + (1 - p_I)p_0, \quad (63)$$

because, at most, one time-frequency cell / radiometer output can have signal energy. The probability of this event is the probability of intercept,  $p_I$ . If the signal is not intercepted, the probability of detection is the false alarm probability. The total probability theorem can be applied to combine these two mutually exclusive events to get the result in (63). Assuming that the hop positions are independent, the final probability of false alarm over  $M$  observed hops is [11, 56]

$$P_{\text{FA}} = P(W \geq k_M | H_0) = \sum_{i=k_M}^M \binom{M}{i} p_0^i (1 - p_0)^{M-i}, \quad (64)$$

where  $k_M$  is the final threshold that is used after summing the last  $M$  logical-OR outputs. The final probability of detection is similarly [11, 56]

$$P_{\text{D}} = P(W \geq k_M | H_1) = \sum_{i=k_M}^M \binom{M}{i} p_1^i (1 - p_1)^{M-i}, \quad (65)$$

where  $p_1$  is the probability of detection per hop and  $k_M$  is the final threshold.

### 5.4.2 Sum-sum decision rule

In [68], a hard decision envelope detector has been studied. Each local decision is based on initial decisions which are based on the magnitudes (envelopes) of the corresponding FFT outputs. These local decisions from all channels and hops are summed and compared to a threshold, i.e., there are three different thresholds. The detector performance was evaluated with the Gaussian approximation. In the sum-sum channelized radiometer considered here, the local decisions  $C_{ij}$  are based on the radiometer outputs. There are only two thresholds to be optimized. For the case studied in [68], a high probability of detection and a large number of hops, the Gaussian approximation gives reasonably good results. However, in most cases, the Gaussian approximation is not very accurate. In the original publication [26], exact results have been used. However, the scenario studied was different and the POI was not taken into account.

Here, an exact method for calculating the probability of detection and false alarm for the sum-sum channelized radiometer is presented. When only noise is present,  $W$  follows the binomial distribution. Therefore, the probability of a false alarm is

$$P_{\text{FA}} = \sum_{i=k_M}^{MN_{\text{eff}}} \binom{MN_{\text{eff}}}{i} Q_{\text{FA}}^i (1 - Q_{\text{FA}})^{MN_{\text{eff}}-i}. \quad (66)$$

In the signal-and-noise case, the PMF of  $W_i$  is

$$f_{W_i}(x) = P(W_i = x | H_1) = p_I f_{W_i}(x | H_{1,inter.}) + (1 - p_I) f_{W_i}(x | H_0), \quad (67)$$

where  $f_{W_i}(x | H_{1,inter.})$  is a convolution of a binomial PMF with parameters  $N_{\text{eff}} - 1$  and  $Q_{\text{FA}}$  and a binomial PMF with parameters 1 and  $Q_{\text{D}}$ . Function  $f_{W_i}(x | H_0)$  is a binomial PDF with parameters  $N_{\text{eff}}$  and  $Q_{\text{FA}}$ . The PMF of the decision variable  $W$  is

$$f_W(x) = \underbrace{f_{W_1}(x) * f_{W_2}(x) * \cdots * f_{W_M}(x)}_M, \quad (68)$$

which can be efficiently calculated with the FFT, and the final probability of detection is found with

$$P_{\text{D}} = 1 - \sum_{x=0}^{k_M-1} f_W(x). \quad (69)$$

### 5.4.3 Max-sum decision rule

Because the conditional PDFs in the signal-and-noise case and the noise-only case are known [129, 25], it is possible to calculate the corresponding raw moments of the per hop decision variable  $W_i$ . Let  $P_k = E(W_i^k | H_0)$  denote the  $k$ th raw moment in the noise-only case and  $P_{k,I} = E(W_i^k | H_{1,inter.})$  denote the  $k$ th raw moment in the signal-and-noise case assuming interception has occurred. The raw moments of the per hop

maximum when taking the POI per hop ( $p_I$ ) into account are  $Z_1^k = p_I P_{k,I} + (1 - p_I) P_k$ . The mean, variance and third central moment can be directly calculated based on the raw moments. For example, in the noise-only case, the mean is  $P_1$ , variance is  $P_2 - P_1^2$ , and third central moment

$$\kappa_3 = 2P_1^3 - 3P_1P_2 + P_3. \quad (70)$$

Now, because the central moments of a sum of independent random variables add up to the order of 3 the mean, variance and the third central moment of decision variable  $W$  are known in both the noise-only case and the signal-and-noise case. Instead of the conventional Gaussian approximation that was used in the original publication [25], the use of the more accurate shifted log-normal approximation that is matched to the first three central moments of the sum [132] is proposed. Here, the shifted log-normal approximation is first used to obtain the threshold and then to obtain the probability of detection. The shifted log-normal approximation is especially useful when the number of observed hops is relatively small. Fig. 23 shows a comparison, corresponding to [25, Fig. 4], between the shifted log-normal and Gaussian approximations. It can be seen that the shifted log-normal approximation is more accurate.

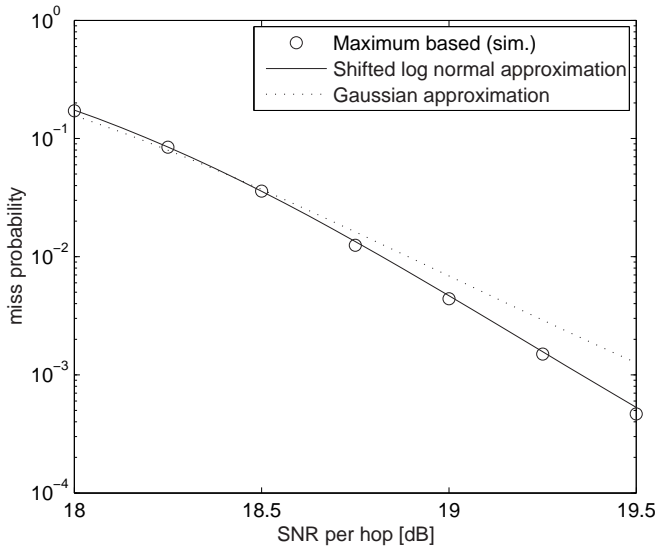


**Fig. 23.** Theoretical (Gaussian and shifted log-normal approximations) and simulated miss probabilities for the maximum based channelized radiometer, 100 hops observed, 464 radiometers in the receiver, the signal has 2320 FH-channels,  $K = 1$  (POI 20%),  $P_{FA} = 10^{-3}$  and the time-frequency product of the radiometers  $T_R W_R = 250$ .

The method presented above requires knowledge of the raw moments of the per hop maximum. In the original publication [25], the first two moments, to be used with the Gaussian approximation, were calculated with numerical integration. It is possible to find

the raw moments analytically by writing out the PDF of the maximum and performing symbolic integration using similar techniques as in [85, 129]. As an example, in the special case  $T_R W_R = 1$ , the following simple result is obtained

$$P_v = N_{eff} 2^v \Gamma(v+1) \times \left[ \sum_{i=0}^{N_{eff}-1} \binom{N_{eff}-1}{i} (-1)^{N_{eff}-1-i} (N_{eff}-i)^{-(v+1)} \right]. \quad (71)$$

However, this process is excessively tedious for practical values of the parameters, i.e., large  $T_R W_R$  and  $N_{eff}$ . Therefore, numerical integration will be used.

## 5.5 Performance under fading

Frequency-nonsselective fading over the used hop channels is assumed. The fading is also assumed to be constant over each hop, and independent from hop to hop. The frequency-nonsselective fading results in multiplicative distortion of the signal [7, p. 772–773]. Let us denote the multiplicative scaling factor by  $\times$ . It is Rayleigh-distributed. The instantaneous SNR is now  $\gamma_H = \times^2 E_H / N_0$ . The instantaneous SNR in each hop is a random variable that follows the chi-square distribution with two degrees of freedom [7, p. 773] with an average value  $\bar{\gamma}_H$ , i.e., the PDF is  $P(\gamma_H) = 1/\bar{\gamma}_H e^{-\gamma_H/\bar{\gamma}_H}$ . The results are given as a function of the average hop SNR, i.e., the average SNR is specified and the instantaneous SNRs in each hop are independently fluctuating around the specified value.

Performance analysis of the logical OR-sum and the sum-sum based receivers requires the finding of each individual radiometer's probability of detection  $Q_D$  assuming that the signal is present in the time-frequency area of the radiometer. The probability of detection for a fixed SNR is given by (28). The probability of local detection when taking into account the fluctuating energy is

$$Q_D = \int_0^{\infty} Q_{T_R W_R} \left( \sqrt{2\gamma_H/K}, \sqrt{\eta} \right) \frac{1}{\bar{\gamma}_H} e^{-\gamma_H/\bar{\gamma}_H} d\gamma_H. \quad (72)$$

By using results of Swerling [133, p. 277], (72) can be written as (see also [84, Eq. (25)], [50, eq.(16)], [49])

$$Q_D = Q_{T_R W_R-1} \left( 0, \sqrt{\eta} \right) + \left[ \left( 1 + \frac{1}{\bar{\gamma}_H/K} \right)^{T_R W_R-1} \times \left( 1 - Q_{T_R W_R-1} \left( 0, \sqrt{\frac{\eta}{1 + \frac{1}{\bar{\gamma}_H/K}}} \right) \right) e^{-\frac{\eta/2}{1 + \frac{1}{\bar{\gamma}_H/K}}} \right]. \quad (73)$$

Shnidman [57] has recently studied binary integration combined with noncoherent integration. Swerling-I plus Swerling-II model is introduced. It corresponds to a special case of the model used here.

In contrast to the nonfading situation, the shifted log-normal approximation was found to have rather poor accuracy in the case of a fading channel and it was not used. Instead,

the performance of the maximum based receiver was evaluated with numerical convolutions similar to those used in the original publication [25]. This requires more numerical computations than the shifted log-normal approximation, but gives the exact performance assuming that numerical convolutions have sufficient accuracy. The distributions are not discrete as they were with the sum based receiver.

## 5.6 Numerical results

It is assumed that the signal to be detected shares some parameters with the SINGCARS radio [11]:  $W_H = 25$  kHz,  $T_H = 0.01$  s and  $N_H = 2320$ . Other parameters used here are  $P_{FA} = 10^{-3}$  and  $N_C = 464$  channels in the receiver. The probability of intercept for these parameters is  $p_I = KN_C/N_H = 0.2K$ . For example, when  $K = 1$ , so that no sweeping is performed,  $p_I = 0.2$ . The other possible values are 0.4, 0.6, 0.8 and 1. Two cases are studied, (a) the number of hops observed per decision  $M = 300$  and (b)  $M = 16$ .

The required energy for the sum-sum receiver, for a given threshold, was calculated by first solving (66) for  $Q_{FA}$  as a function of  $k_M$  and the desired false alarm probability. Then the inverse of the chi-square cumulative distribution function was used to find the threshold  $\eta$  for individual radiometers. Now  $Q_D$  can be found by using (28) (no fading) or (73) (fading). The final probability of detection was found with (69). The required SNR per cell corresponding to the required probability of detection, for a given threshold  $k_M$ , was found with a search. Searching was also used to find the optimal threshold  $k_M$ . The required SNR for a logical OR-sum based channelized radiometer was calculated using procedures similar to those in [11]. Optimal thresholds found with a search were used. The required SNR for a maximum-based receiver was discovered by using the shifted log-normal approximation without fading or with numerical convolutions with fading. The optimal threshold of the maximum-based receiver does not depend on SNR.

The required SNR for the optimal detector was found with simulations. Due to a very large number of random variables to be generated, simulations in case (a) are excessively time consuming. Therefore, the performance of the optimal detector was evaluated only in case (b).

In case (a), also the hard decision envelope detector proposed in [68] is studied. Its performance was evaluated via Gaussian approximations similar to those in [68]. It was assumed that each envelope detector output containing a signal has an equal signal component. In practice, the strength of the signal component varies and the results can be interpreted to be an approximation allowing comparisons with other structures. The results obtained were the same as those in [68]. It would be possible to apply the exact results presented here for the sum-sum detector also for the envelope detector. Since here the focus is on the channelized radiometer this was not pursued here further.

Fig. 24 shows the required energy per hop in case (a) to achieve  $P_D = 0.999$  with the envelope detector [68], the sum-sum based channelized radiometer, the logical OR-sum based channelized radiometer and the maximum based channelized radiometer. It can be observed from Fig. 24 that the sum-sum receiver has practically the same performance as the logical OR-sum receiver. It is anticipated that when multiple signals are present, the

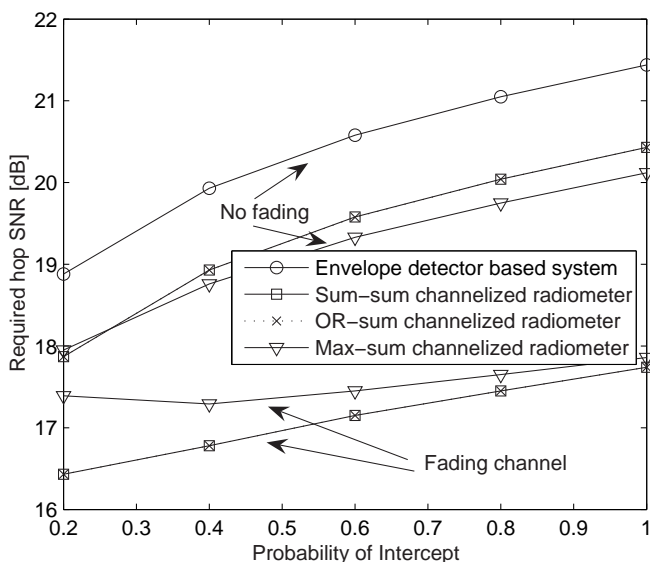


**Fig. 24. Required hop SNR,  $W_H = 25$  kHz,  $T_H = 0.01$  s,  $N_H = 2320$ ,  $M = 300$ ,  $P_D = 0.999$  and  $P_{FA} = 10^{-3}$ .**

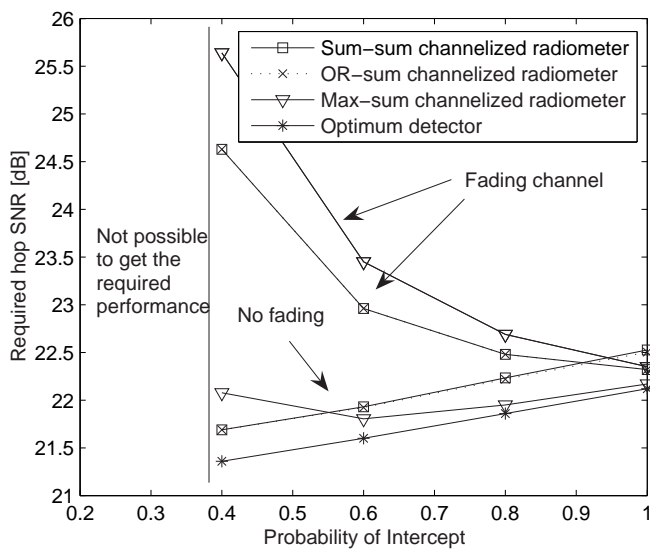
sum-sum based receiver is better than the receiver using the logical OR-sum. Envelope detection is about 1 dB worse than the radiometer based solutions. Without fading, the maximum based intercept receiver is the best of the receivers discussed here, except when POI is 20%. When the channel is fading, the logical OR-sum and sum-sum receivers have better performance than the maximum based intercept receiver. It is seen that when the number of hops observed is large, sweeping does not increase the probability of detection. It is more important to have large detection SNR than to have large probability of intercept. This is in line with the result in [68], obtained for the envelope detector based system. When the channel is fading, the detection SNR is sometimes much higher than the average value. This explains why fading actually improves performance. If the frequency band of the transmitter is unknown, some type of frequency sweeping should be used, at least in the hop level. Otherwise, the probability of intercept can be very low, even zero.

Fig. 25 shows the required energy per hop in case (b) to achieve  $P_D = 0.99$  with the sum-sum based channelized radiometer, the logical OR-sum based channelized radiometer, the maximum based channelized radiometer and the optimum detector using detection statistic (53). It was not possible to achieve the required  $P_D$  without sweeping. This is because without sweeping, the probability that at least one radiometer intercepts the signal in any of the hops is  $1 - (1 - 0.2)^{16}$ , which is 0.97185. Therefore, the maximum probability of detection with any detector is  $0.97185 \cdot 1 + (1 - 0.97185) \cdot 0.001$ , which is smaller than 0.99. It is possible to get the required performance if  $K \geq 2$ , i.e, probability of intercept is larger than or equal to 40%. It can be observed from Fig. 25, that if the probability of intercept exceeds 40% and there is no fading, the maximum based detector is the best of the practical detectors. When the probability of intercept is 100%, the maximum based detector has performance very close to that of the optimal detector. When the channel exhibits fading, the logical OR-sum and sum-sum receivers have better performance than the maximum based intercept receiver. It can be observed that also in this case the sum-sum receiver and the logical OR-sum based receiver have almost equal performance. It was noticed in simulations that the thresholds given by the shifted log-normal approximation are accurate. However, when  $K = 2$ , there was a small difference between the required SNR given by simulations and the approximation (0.08 dB). When  $K > 2$ , the difference was much smaller (0.01–0.02 dB). This is because the shifted log-normal approximation is not such a good fit for the distribution of the decision variable when  $K = 2$  as when  $K > 2$ . In the fading channel, numerical convolutions were used instead of the shifted log-normal approximation. In case (b), fading degrades performance. This is because the number of intercepted hops can be small and possibilities if having a strong signal decrease. When the number of intercepted hops increases, the performance in the case of fading increases. The best performance in the case of fading is achieved when  $K = 5$ .

The same methods can be used also with signals that have other parameters, for example, higher hop rate and larger bandwidth. Actually, the results depend only on the time-bandwidth product, the number of channels in the signal and in the receiver, the number of observed hops and the required  $P_D$  and  $P_{FA}$  per decision. For example, if the hop rate is 10 000 hops/s and the bandwidth of the channels is 2.5 MHz, the time-bandwidth product is 250. If the other parameters do not change, the results are equal to those presented here.

## 5.7 Conclusions

The logical OR-sum channelized radiometer, the sum-sum channelized radiometer, the max-sum channelized radiometer and the optimal detector using frequency sweeping have been analyzed. When sweeping is performed, there are multiple detection phases within each hop, i.e, sweeping is faster than the hop dwell time. The numerical results presented here, for a SFH signal having parameters similar to those of the SINGCARS combat radio, support the following conclusions. If the number of hops observed per decision is large, frequency sweeping degrades the performance compared to a system that does not apply frequency sweeping with or without fading. If the number of hops observed is small, sweeping is often necessary to get the desired performance. Using a sum is only slightly worse than using a logical-OR. Without fading, the maximum based intercept receiver has



**Fig. 25.** Required hop SNR,  $W_H = 25$  kHz,  $T_H = 0.01$  s,  $N_H = 2320$ ,  $M = 16$ ,  $P_D = 0.99$  and  $P_{FA} = 10^{-3}$ .

the best detection performance of the practical receivers discussed here, unless the POI is small. When the POI is large, the performance of the maximum based receiver is close to that of the optimal receiver. In the fading channel, logical OR-sum and sum-sum receivers have better performance than the maximum based receiver.

## 6 CFAR strategies for channelized radiometer

In this chapter, CFAR strategies are studied in the context of the channelized radiometer. One possibility on which this chapter focuses is applying the automatic censored CFAR methods which were introduced in Section 2.4.3<sup>1</sup>. They first perform data-dependent censoring and then calculate the average (or the sum) of the survivors. First, the performance analysis of the CA and OS detectors is extended for the channelized radiometer using exact probabilities in Section 6.1. In Section 6.2, it is proposed that the consecutive mean excision algorithms are applied for the censoring. Using CA scaling factors for censoring is also proposed and a novel clean sample rejection rate analysis is presented. Numerical results comparing the performance of these three methods and the baseline approaches are presented in Section 6.3. Finally, Section 6.4 offers the conclusions.

### 6.1 Performance analysis

Here performance analysis of the CA and OS detectors is extended for the channelized radiometer. The signal model presented in Section 3.2.3 is assumed.

#### 6.1.1 Cell-averaging detector

If the reference cells are uncorrupted, the CA detector's reference statistic  $Z_{CA} = \sum_{i=1}^{N_R} Z_i$  follows the scaled chi-square distribution and  $2Z_{CA}/N_0$  follows the chi-square distribution with  $2M_C N_R$  degrees of freedom. The CA detector gives an alarm when the value of the test cell,  $Z$ , exceeds  $T_{CA} Z_{CA}$ , where  $T_{CA}$  is a scaling factor [19]. Under the noise-only hypothesis  $H_0$ , the probability of a false alarm for the CA detector is

---

<sup>1</sup>In future work, additional CFAR strategies should also be investigated, see Section 8.

$$P_{\text{FA}} = P\left(\frac{Z}{Z_{\text{CA}}} > T_{\text{CA}}; H_0\right) = P\left(\frac{Z/2M_C}{Z_{\text{CA}}/2M_C N_R} > N_R T_{\text{CA}}\right) \quad (74)$$

$$= 1 - \text{FCDF}(N_R T_{\text{CA}}, 2M_C, 2M_C N_R).$$

A sum expression for (74) has been given in [84, Eq. (59)]. The scaling factor  $T_{\text{CA}}$  of the CA detector can be found from

$$T_{\text{CA}} = \text{FCDF}^{-1}(1 - P_{\text{FA,DES}}, 2M_C, 2M_C N_R)/N_R, \quad (75)$$

where  $P_{\text{FA,DES}}$  is the desired probability of false alarm. Because the ratio of two appropriate normalized non-central chi-square variables follows the doubly noncentral  $F$  distribution, the probability of detection under the signal(s)-plus noise hypothesis  $H_1$  is

$$P_{\text{D}} = P\left(\frac{N_0/2}{N_0/2} \frac{(2Z/N_0)/2M_C}{(2Z_{\text{CA}}/N_0)/2M_C N_R} > N_R T_{\text{CA}}; H_1\right) \quad (76)$$

$$= 1 - \text{DNFCDF}(N_R T_{\text{CA}}, 2M_C, 2M_C N_R, 2\Omega, \lambda_S),$$

where  $\Omega = E_{\text{Cell}}/N_0$  denotes the SNR,  $E_{\text{Cell}}$  is the energy contained in the test cell,  $\lambda_S$  is the total non-centrality parameter and  $\text{DNFCDF}^2$  is the CDF of the doubly noncentral  $F$  distribution. A similar application of the doubly noncentral  $F$  distribution has been used in [134]. The performance of the CA detector does not depend on the distribution of the total signal energy or non-centrality amongst the reference cells. If the reference cells are uncorrupted, the probability of detection can be calculated with [84, Eq. (29)] or with  $\lambda_S = 0$  in (76).

### 6.1.2 Order statistics detector

The  $\text{OS}(k)$  detector orders the reference cell values from smallest to largest as  $Z_{(1)} \leq Z_{(2)} \leq \dots \leq Z_{(N_R)}$  and sets the threshold as  $T_{\text{OS}(k)} Z_{(k)}$ , where  $T_{\text{OS}(k)}$  is the scaling factor [19, 85]. The  $T_{\text{OS}(k)}$  can be calculated as shown in [85] or by numerical integration. In the general case, the CDF of  $Z_{(k)}$ ,  $F_{Z_{(k)}}(z)$ , can be found by using the recurrence relations [135]. In [19],  $F_{Z_{(k)}}$  has been found for the special case where the signal energy is uniformly distributed. When  $F_{Z_{(k)}}$  is known, the probability of detection is [19]

$$P_{\text{D}} = T_{\text{OS}(k)} \int_0^{\infty} f(T_{\text{OS}(k)} y) F_{Z_{(k)}}(y) dy, \quad (77)$$

where  $f(\cdot)$  is the PDF corresponding to the distribution of the current test cell.

## 6.2 Automatic censored CFAR detection

As explained in Section 2.4.3, there are two stages in an automatic censored CFAR detector; (A) the censoring of the reference cells, i.e., removing of the corrupted cells from

<sup>2</sup>The DNFCDF can be evaluated, for example, with the Dataplot software from the National Institute of Standards and Technology (<http://www.nist.gov/>).

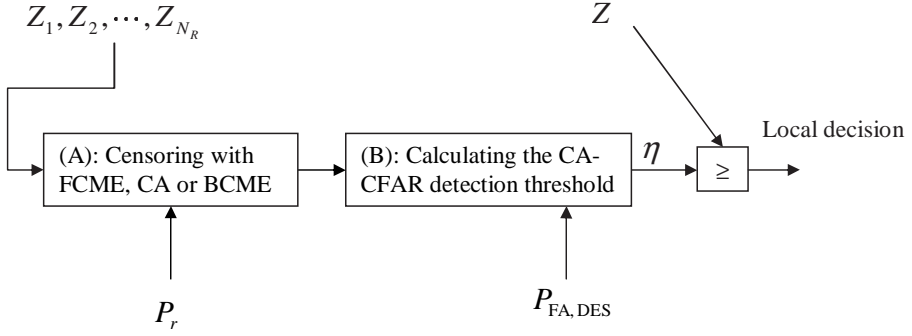


Fig. 26. Automatic censored CFAR.

the reference set, and (B) using the supposedly signal-free reference cells in the calculation of the detection threshold. In Section 2.4.3, the ACMLD scaling factors were described. However, they cannot be used when the time-bandwidth product is greater than two. Therefore, it is proposed that the FCME and BCME algorithms, described also in Section 2.4.3, are used for censoring. After censoring, detection is performed using the CA-CFAR, as shown in Fig. 26.

### 6.2.1 Analysis of the stage (A)

Censoring with forward methods is done by first arranging the reference cell values into ascending order, so that  $Z_{(1)} \leq Z_{(2)} \leq \dots \leq Z_{(N_R)}$ . The test (17) is done in the  $k$ th step. The iteration starts with  $k$  equal to the size of the smallest assumed clean set [98, 99]. The larger the smallest assumed clean set is, the better censoring operates. However, if the assumed clean set is too large, the probability that corrupted samples will be part of the initial clean set increases. The scaling factors  $T_k$  control the properties of the censoring process.

In ACMLD, they are chosen so that the probability of a false decision  $P_{FC}$  has some specified value, see Section 2.4.3. In some applications, it is important to specifically control the clean sample rejection rate  $P_r$  [99]. This is true, especially if censoring is directly applied to CFAR without the second stage. Then the clean sample rejection rate corresponds to the probability of a false alarm. The FCME algorithm, proposed in [98, 99], aims to control the clean sample rejection rate. Because the FCME algorithm can be used with arbitrary time-frequency products, we will use it for censoring the reference cells in stage (A). The FCME uses  $T_k = T_{CME}/k$  and  $T_{CME}$  is found by solving [98]

$$P_r = e^{-(T_{CME}M_C)} \sum_{i=0}^{M_C-1} \frac{1}{i!} (T_{CME}M_C)^i. \quad (78)$$

Listing 6.1. Recursive MATLAB code for finding the probability of passing a test.

```

function out = PrPass(c)
global T NR
k=length(c)-1;
if (k==1)
    out=1/c(2)*(1/c(1)-1/(c(1)+c(2)*(T(1)-1)*(NR-1)/NR));
    return;
end % if

m=1:k;
offset=c(k+1)* ((NR-k)./(NR-m+1).*(T(k).*(k-m+1)-1));
out = (PrPass(c(1:k))-PrPass(c(1:k)+offset))/c(k+1);
return

```

For example, when  $M_C = 8$  and  $P_r = 10^{-4}$ , it is found that  $T_{\text{CME}} = 2.8703$ . The derivation is based on the fact that the probability of a clean sample exceeding the statistical mean of the clean samples multiplied by  $T_{\text{CME}}$  is  $P_r$ . It should be noted that the result (78) is actually an approximation. It is most useful when the number of reference samples  $N_R$  is large. In those cases, the obtained clean sample rejection rate is close to the desired value. We will also study the situation where the CA scaling factors are used in the censoring, i.e.,

$$T_k = \text{FCDF}^{-1}(1 - P_r, 2M_C, 2M_C k)/k, \quad (79)$$

which roughly correspond to the case where corruption is assumed to be infinitely strong and  $Z_{(k)}$  is the last signal-free cell. Previously the CA scaling factors have not been used for censoring. The BCME [32] will also be used here. As a result of the backwards operation, the BCME algorithm sometimes removes too small a number of the corrupted reference cells containing interference. On the other hand, sometimes the FCME algorithm may remove too large a number of the reference cells (depending on the chosen  $P_r$  and the size of the initial set).

Analytical results for the clean sample rejection (given the scaling factors) have not been presented in the literature. First, the probability of passing the test  $k$  can be found by integrating the joint PDF of the order statistics. In the case where  $M_C = 1$ , the result can be conveniently expressed using a recursive function shown in listing 6.1. The global variable  $T$  is a vector containing the scaling factors and  $c$  is the input vector. Now, the probability of passing the test  $k$  is  $\text{PrPass}(\mathbf{1}_{k+1})$ , where  $\mathbf{1}_{k+1}$  is a vector of length  $k+1$  with all components equal to one. This result is exact at least in those situations where all scaling factors are not smaller than one. It would be possible to find the exact result for other cases also. However, in this case the operation of the algorithm does depend on the values of the scaling factors and the analysis is more complicated<sup>3</sup>. Using the above

<sup>3</sup>I am currently preparing a journal paper "On the convergence properties of the FCME algorithm" on this subject

results, the clean sample rejection rate obtained can be found with

$$P_r = (N_R - 1) (1 - \text{PrPass}(\mathbf{1}_2)) + \sum_{k=2}^{N_R-1} (N_R - k) (\text{PrPass}(\mathbf{1}_k) - \text{PrPass}(\mathbf{1}_{k+1})), \quad (80)$$

which should be limited to the maximum value given by the number of samples  $N_R$  minus the initial set size divided by  $N_R$ . This limitation occurs only with very large and impractical values of desired clean sample rejection rate.

### 6.2.2 Stage (B)

In the two-stage system studied here, the final decision is made after censoring with the test  $Z \geq \eta$ , where  $\eta = T_{\text{DET},K} Z_{\text{REF}}$  and  $Z_{\text{REF}}$  is the sum of the values of all the supposedly uncorrupted reference cells and  $K$  is the number of these reference cells. The  $T_{\text{DET},K}$  is the scaling factor used in the detection. If the test is true, the hypothesis  $H_1$  is chosen. Otherwise, it is decided that the noise-only hypothesis  $H_0$  is true. Here, the CA scaling factors [95] are used in the final decision, i.e.,

$$T_{\text{DET},K} = \text{FCDF}^{-1}(1 - P_{\text{FA,DES}}, 2M_C, 2M_C K)/K. \quad (81)$$

The combinations of FCME, CA, and BCME censoring with CA scaling factors in the final decision will be referred as the FCME+CA, CA+CA and BCME+CA, respectively.

## 6.3 Numerical results

For clarity, numerical results are separated into two (sub)sections. In Section 6.3.1, the focus is on the clean sample rejection rate. In Section 6.3.2, the whole two-stage detection is studied. The probabilities of detection and false alarm are presented.

### 6.3.1 Clean sample rejection rate

Fig. 27 shows the obtained versus desired clean sample rejection rates when using the FCME scaling factors and the reference set size is varied,  $M_C = 1$ , and the initial set size is 10%. It can be observed that the simulation results match very well with the theoretical results. The reference cells are assumed to be uncorrupted. The presence of corrupted cells somewhat affects the clean sample rejection rate. However, due to the unknown number of corrupted cells and unknown strengths of corruption, it is not possible to take this into account in the threshold setting process. In addition, in the two-stage detection process, it is the detection and false alarm probabilities in stage (B) that matter. These will be presented in the next section. However, the results in this section are also important,

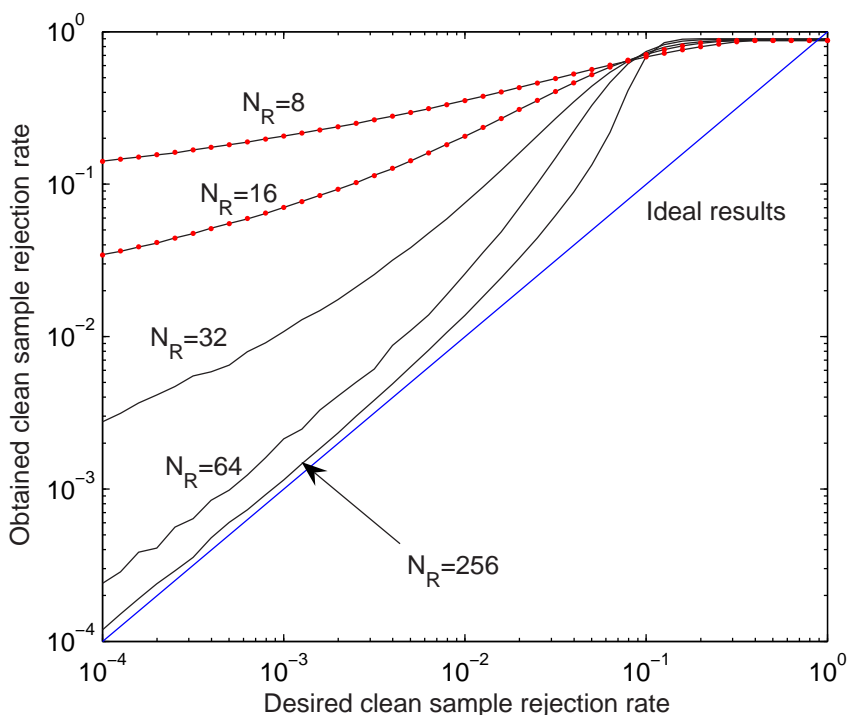


**Fig. 27. Obtained versus desired clean sample rejection rates when using the FCME scaling factors. Dots indicate theoretical results and solid lines are based on simulations. Initial set size is 10%,  $M_C = 1$ .**

especially if in future work these censoring methods will be applied directly to CFAR. Let us return to Fig. 27. Due to the computational requirements of the recursive algorithm, the theoretical results are shown only for the cases  $N_R = 8$  and  $N_R = 16$ . It can be seen that the FCME scaling factors cannot be used when  $N_R$  is small and the initial set size is small. When  $N_R = 64$ , the results are relatively close to the desired values. With  $N_R = 256$ , the difference between the obtained and desired values is small. Fig. 28 shows the corresponding results with CA scaling factors. It can be seen that the clean sample rejection rates obtained are noticeably closer to the desired values than those obtained with the FCME scaling factors, especially when the reference set size is small.

Let us now consider the situation with  $M_C \geq 1$  and the initial set size 25%. As can be seen from Fig. 29, it is now possible to use  $N_R = 16$  with the FCME scaling factors. The larger  $M_C$  is, the closer the obtained clean sample rejection rate is to the desired value. Fig. 30 shows the corresponding results for the CA scaling factors.

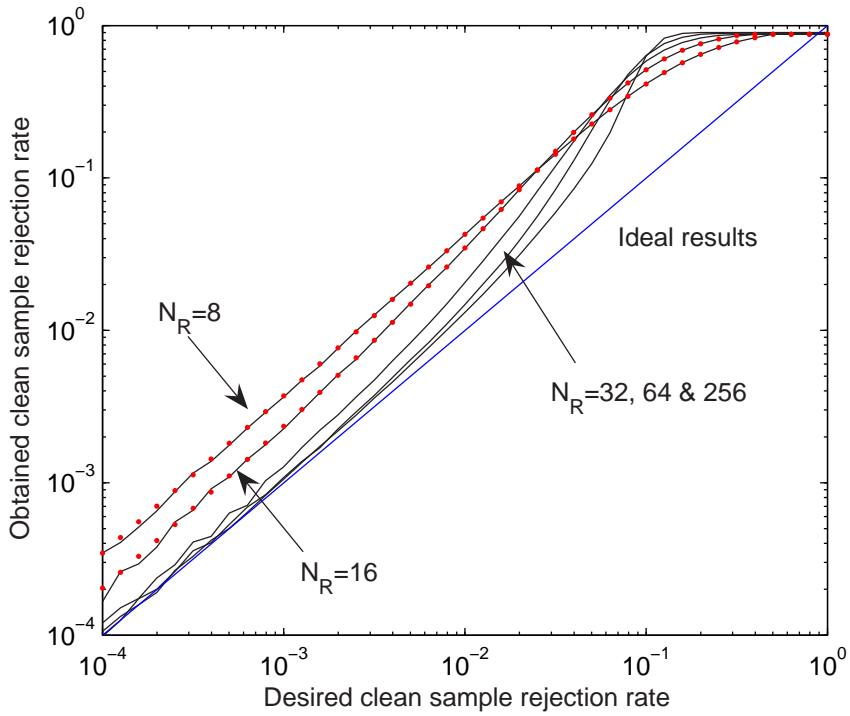


**Fig. 28.** Obtained versus desired clean sample rejection rates when using the CA scaling factors. Dots indicate theoretical results and solid lines are based on simulations. Initial set size is 10%,  $M_C = 1$ .

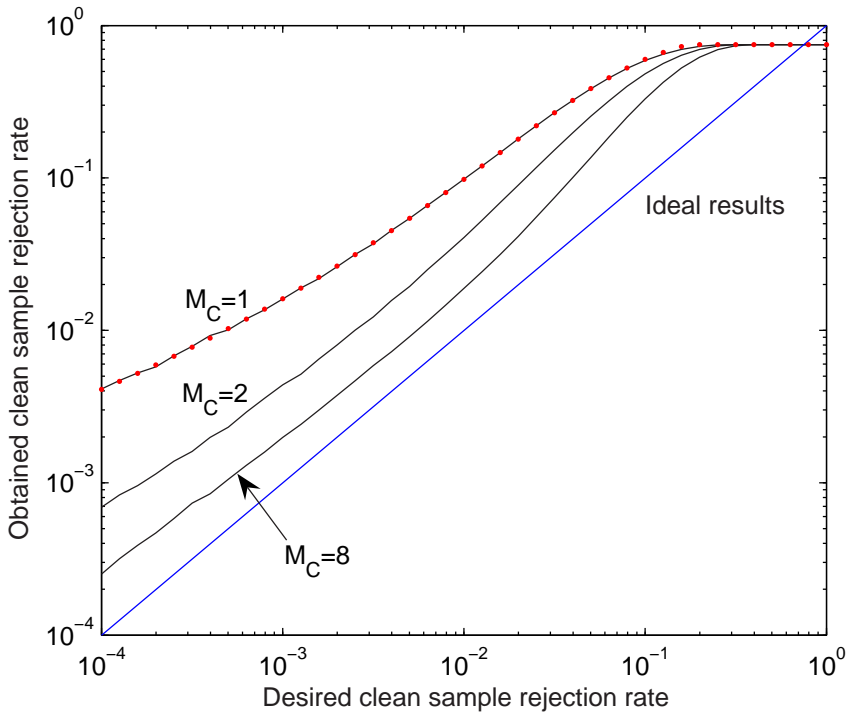


**Fig. 29.** Obtained versus desired clean sample rejection rates when using the FCME scaling factors. Dots indicate theoretical results and solid lines are based on simulations. Initial set size is 25%,  $N_R = 16$ , and  $M_C \geq 1$ .

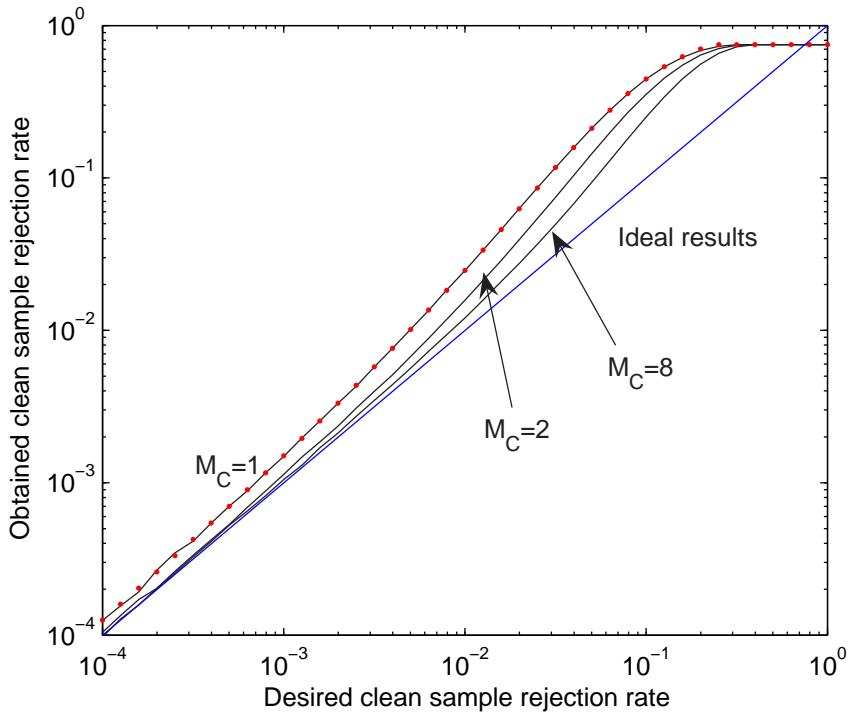


**Fig. 30.** Obtained versus desired clean sample rejection rates when using the CA scaling factors. Dots indicate theoretical results and solid lines are based on simulations. Initial set size is 25%,  $N_R = 16$ , and  $M_C \geq 1$ .

### 6.3.2 Automatic censored CFAR

The properties of the censoring in stage (A) depend on the censoring algorithm and the the censoring parameter  $P_{FC}$  or  $P_r$ . Generally speaking, too small a value of  $P_{FC}$  or  $P_r$  means that some of the corrupted reference cells will not be censored. On the other hand, too large a value means that some of the reference cells containing only noise will be needlessly censored. A numerical example corresponding to the CA scaling factors with different values of  $P_r$  is presented in Figs. 31–32. There are four corrupted reference cells with the same signal strength as in the test cell. It can be seen that  $P_r = 10^{-3}$  seems to be the best choice. However, here  $P_r = 10^{-4}$  will be used for consistency, so that  $P_r = P_{FA,DES}$ .

The corresponding results for the FCME scaling factors are shown in Figs. 33–34. In the case of the FCME scaling factors,  $P_r = 10^{-4}$  seems to be the best choice, because with  $P_r = 10^{-3}$  the false alarm probability is somewhat larger than the desired value.

In these simulations, the thresholds given by the different methods were simulated. The detection and false alarm probabilities were then calculated using the non-central chi-square CDF or the chi-square CDF corresponding to the test cell, respectively. The number of Monte Carlo runs was  $\geq 10^5$ . Therefore, the simulated results are not necessarily valid for extremely low false alarm rates.

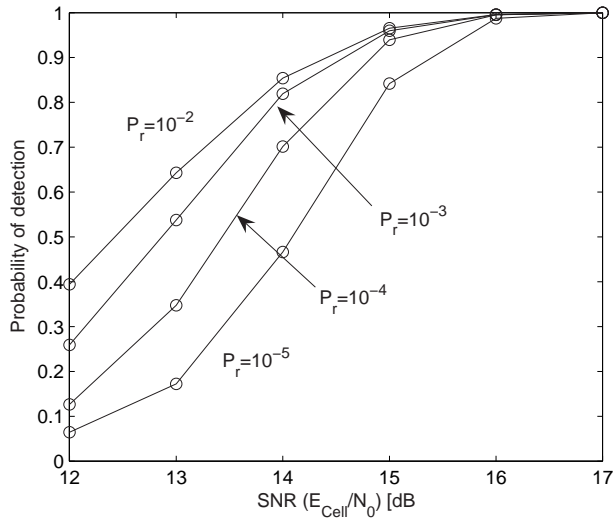


**Fig. 31.** Simulated detection probabilities with the CA scaling factors,  $N_R = 16$ ,  $T_R W_R = 8$ ,  $P_{FA,DES} = 10^{-4}$ , when four reference cells are corrupted with the same signal strength as in the test cell.

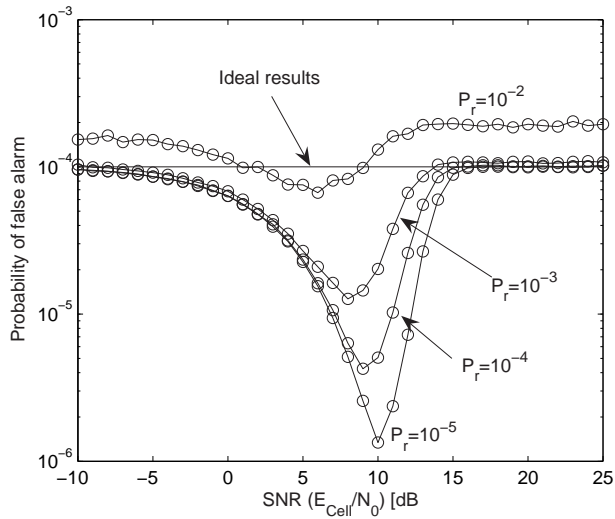


**Fig. 32.** The simulated false alarm probabilities corresponding to Figure 31.

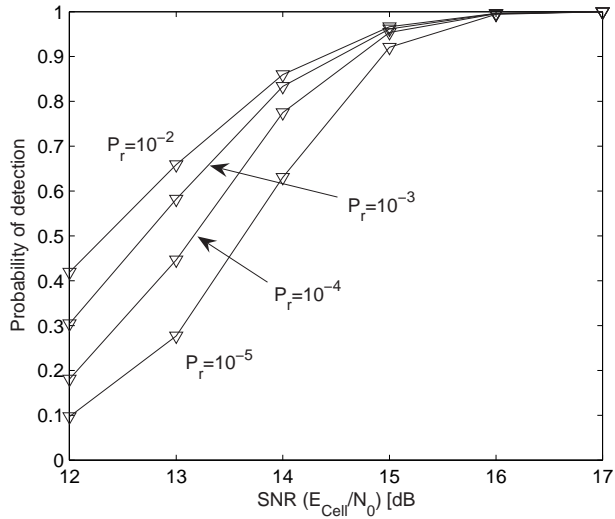


**Fig. 33.** Simulated detection probabilities with the FCME scaling factors,  $N_R = 16$ ,  $T_R W_R = 8$ ,  $P_{FA,DES} = 10^{-4}$ , when four reference cells are corrupted with the same signal strength as in the test cell.

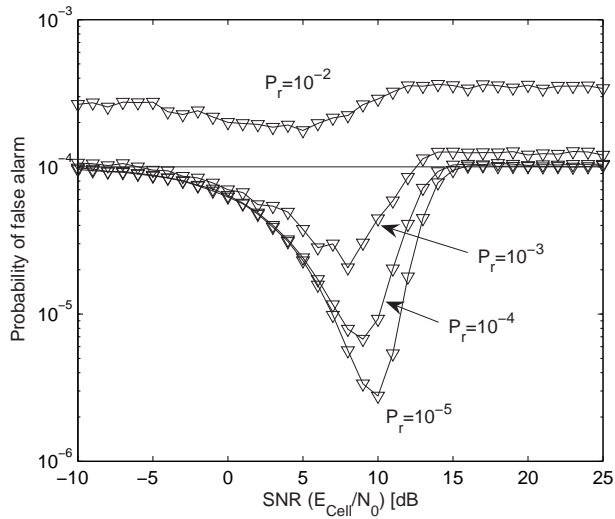


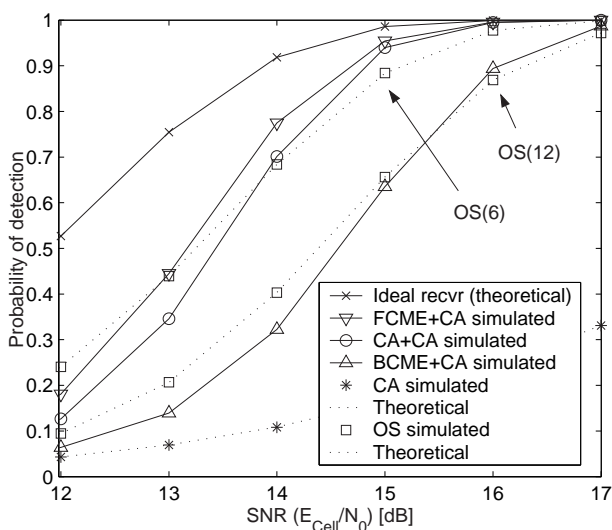
**Fig. 34.** The simulated false alarm probabilities corresponding to Figure 33.

Assume that  $P_r = P_{\text{FA,DES}}$ . Fig. 35 shows the theoretical and simulated detection probabilities with  $N_R = 16$ ,  $T_R W_R = 8$ ,  $k = 6/12$  (OS) and  $P_{\text{FA,DES}} = 10^{-4}$ . There are four corrupted reference cells with the same signal strength as in the test cell. It is observed that the FCME+CA detector has the best performance, unless the SNR is 12 dB or less, closely followed by the OS(6) detector and the CA+CA detector. If the SNR is 12 dB or less, the OS(6) detector has the best performance. Note that with an optimized value of  $P_r$ , FCME+CA and CA+CA would perform better than OS(6) even with small values for the SNR, see the results in the previous subsection. The OS(12) detector and BCME+CA also perform rather well. The conventional CA detector has poor performance, as expected.

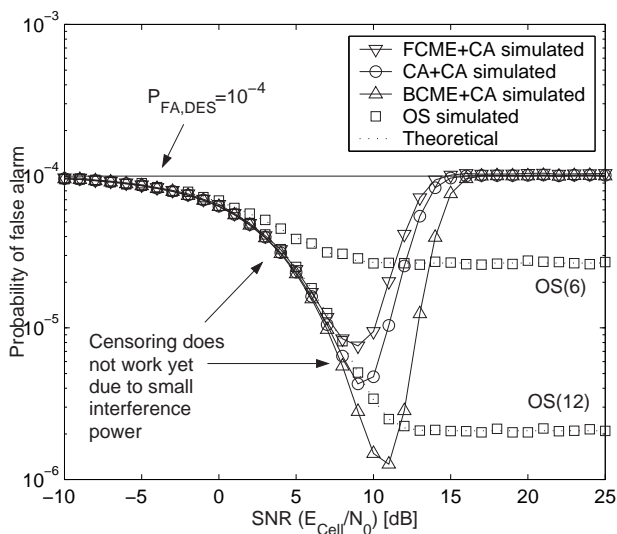
Fig. 36 shows the false alarm probabilities corresponding Fig. 35. It is observed that the false alarm probability of the FCME+CA detector is the largest. However, the desired false alarm probability is not exceeded, i.e., the false alarm probability is controlled. The false alarm probabilities corresponding to the CA detector are small and are not shown. It can be seen that when the SNR and also the interference power is small, the censoring algorithms do not remove corrupted reference cells. The censoring algorithms start to operate when SNR is 10–15 dB. The OS detector's false alarm probabilities converge to certain values. This is because when the SNR is large enough, the effective size of the reference set is decreased by the number of corrupted reference cells. Therefore, if the OS scaling factor would be set assuming  $N_R = 12$  instead of  $N_R = 16$ , the OS detector would achieve exactly the required false alarm probability if the SNR is large enough. However, this detector would give too large false alarm probabilities with small SNR values and also the number of corrupted reference cells is not known *a priori*.

Fig. 37 shows the results of an extreme case, where nine reference cells are corrupted, three with the same signal strength as in the test cell, three with double and three with half the strength or non-centrality. It is seen that the FCME+CA, the OS(6) and the CA+CA detectors are quite good. The OS(12) detector has very bad performance because the number of corrupted reference cells is larger than four. The BCME+CA detector has poor performance and the conventional CA detector is useless. The FCME+CA had about a 20% larger than desired false alarm probability when the SNR was large.

Fig. 38 shows the receiver operating characteristic (ROC) plot, i.e.,  $P_D$  versus  $P_{\text{FA}}$ , when all the reference cells contain noise only. The FCME+CA, CA+CA, BCME+CA and CA detectors have equal performance. The OS detectors are somewhat worse, and the performance loss is smaller with the OS(12) detector. Therefore, the selection of the OS parameter involves a compromise [19] (the OS(6) detector had better performance with interference, Fig. 35). Also, the OS parameter should not be too large (Fig. 37).



**Fig. 35.** The theoretical and simulated detection probabilities with  $N_R = 16$ ,  $T_R W_R = 8$ ,  $k = 6/12$  (OS),  $P_r = P_{FA,DES} = 10^{-4}$ , when four corrupted reference cells are corrupted with the same signal strength as in the test cell. The dotted lines are theoretical results.



**Fig. 36.** The theoretical and simulated false alarm probabilities corresponding to Figure 35.

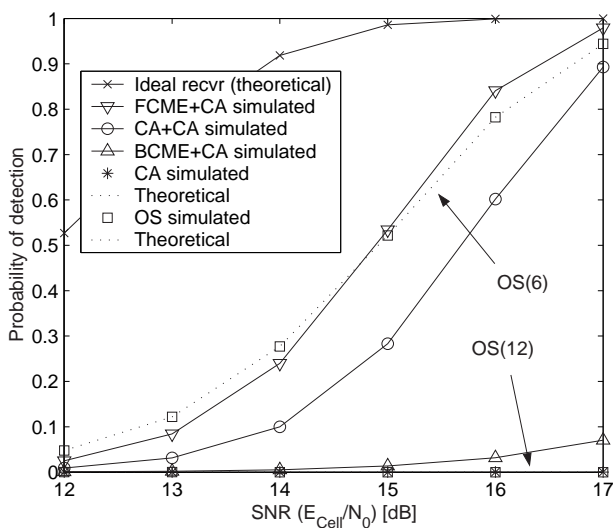


**Fig. 37.** The theoretical and simulated detection probabilities with  $N_R = 16$ ,  $T_R W_R = 8$ ,  $k = 6/12$  (OS),  $P_\tau = P_{\text{FA,DES}} = 10^{-4}$ , when nine reference cells are corrupted; three with the same signal strength as in the test cell, three with double and three with half the strength.

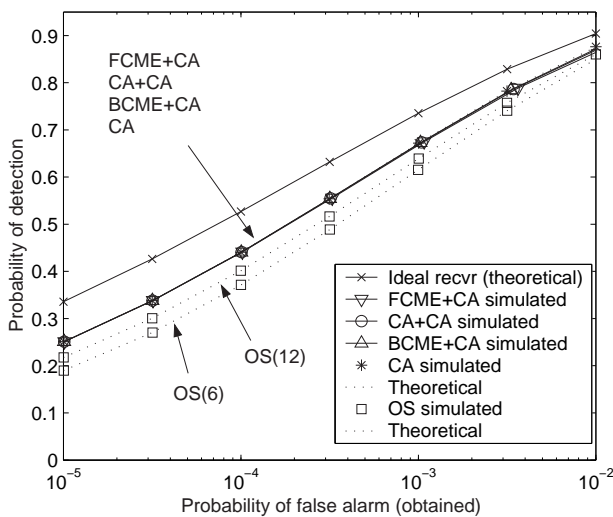


**Fig. 38.** ROC plot showing  $P_D$  versus  $P_{\text{FA}}$  with  $N_R = 16$ ,  $T_R W_R = 8$ ,  $k = 6/12$  (OS), SNR=12 dB and noise-only reference cells. The desired false alarm probability is varied in the range  $[10^{-5} \ 10^{-2}]$  and  $P_\tau = P_{\text{FA,DES}}$ .

## 6.4 Conclusions

The performance of the CA, OS and iterative CFAR signal detection methods (FCME+CA, CA+CA, BCME+CA) were analyzed in the context of the channelized radiometer. The numerical results showed that the iterative CFAR methods can improve the signal detection performance when some reference cells are corrupted and contain signal(s) in addition to noise. In most cases, the FCME+CA detector had the best detection performance, closely followed by the CA+CA detector. In some cases, the FCME+CA provided a somewhat larger false alarm probability than the desired value. The BCME+CA detector had worse performance than both of these methods. The conventional OS detector also performs well, assuming its order parameter  $k$  is correctly chosen. Actually, when the SNR was small, the OS detector had the best performance.

## 7 Power-law based intercept receiver

In this chapter, the threshold setting of a power-law detector (PLD) using windowing will be studied. First, properties of the power-law decision variable are analyzed in Section 7.1. The shifted log-normal approximation will be used for threshold setting, and it is discussed in Section 7.2. Using contiguity in PLD is discussed in Section 7.3. Numerical results are provided in Section 7.4. Finally, Section 7.5 gives the conclusions.

### 7.1 Properties of the decision variable

In the PLD, the detection is made by comparing  $T_v(\mathbf{x})$  (25) to a threshold  $\eta$ . The threshold can be found by using the inverse of the cumulative distribution function of the decision variable. Often the exact distribution of the decision variable cannot be found and approximations need to be used. In detection problems, the conventional Gaussian approximation often lacks the required accuracy. Here, the more accurate shifted log-normal approximation is used. In order to do this, we need to know the mean, variance, and the skewness of the decision variable in the noise-only case, whereas the Gaussian approximation requires only the mean and variance.

It will be assumed that decisions are made based single blocks. Assuming  $H_0$  is true,  $\mathbf{x} = \mathbf{A}\mathbf{n}$ , where  $\mathbf{n}$  is an  $N$ -element noise vector. Noise is assumed to be a zero-mean proper complex white Gaussian process, with independent real and imaginary parts. The covariance matrix of the noise is  $E[\mathbf{nn}^H] = \sigma^2\mathbf{I}_N$ , where " $H$ " denotes conjugate-transpose and  $\sigma^2$  is the total variance. Additionally, the pseudo-covariance vanishes, i.e.,  $E[\mathbf{nn}^T] = \mathbf{0}$ . Vector  $\mathbf{x}$  has zero-mean and the covariance matrix  $\Psi = \sigma^2\mathbf{A}\mathbf{A}^H$ . It is assumed that the covariance matrix  $\Psi$  is positive definite, and that the noise variance is known. If this not the case then the covariance matrix can be singular, however, the characteristic function can still be specified.

For threshold setting with the shifted log-normal approximation, it is necessary to know the mean, the variance, and the skewness of the decision variable. The mean of the decision variable,  $P_1$ , can be found directly by using the result that in the noise-only case  $E(|x_k|^{2v}) = v!(\Psi_{kk})^v$  [136], where  $\Psi_{kk}$  is  $(k, k)$ th element of the covariance

matrix. The second raw moment is

$$P_2 = E\left(T_v(\mathbf{x})^2\right) = \sum_{k=1}^N \sum_{l=1}^N E\left(|x_k|^{2v} |x_l|^{2v}\right). \quad (82)$$

In the noise-only case [136]

$$E\left(|x_k|^{2v} |x_l|^{2v}\right) = (v!)^2 (\Psi_{kk})^v (\Psi_{ll})^v \sum_{i=0}^v \binom{v}{i}^2 \lambda_{kl}^{2i}, \quad (83)$$

where

$$\lambda_{kl}^2 = |\Psi_{kl}|^2 / (\Psi_{kk} \Psi_{ll}). \quad (84)$$

To find the third raw moment  $P_3$  of the decision variable it is necessary to evaluate the following  $6v$ -order multivariate moment:  $E\left(|x_k|^{2v} |x_l|^{2v} |x_m|^{2v}\right)$ . It was calculated with the partial derivation method; refer to [136] for details of the method. Note that the partial derivation method used here is rather tedious to apply in some cases.

Finally, the variance  $V = P_2 - P_1^2$  and the skewness

$$y = (2P_1^3 - 3P_1P_2 + P_3) / (V^{3/2}) \quad (85)$$

are calculated.

The results presented above are sufficient for threshold setting. However, parts of the results are also derived using real-valued random variables since they are easier to handle and there are more results concerning them. The received vector  $\mathbf{x}$  can be expressed in real variables with [137]

$$\hat{\mathbf{x}} = \hat{\mathbf{A}} \hat{\mathbf{n}}, \quad (86)$$

where

$$\hat{\mathbf{x}} = \begin{bmatrix} \text{Re}(\mathbf{x}) \\ \text{Im}(\mathbf{x}) \end{bmatrix}, \quad \hat{\mathbf{n}} = \begin{bmatrix} \text{Re}(\mathbf{n}) \\ \text{Im}(\mathbf{n}) \end{bmatrix} \quad (87)$$

and

$$\hat{\mathbf{A}} = \begin{bmatrix} \text{Re}(\mathbf{A}) & -\text{Im}(\mathbf{A}) \\ \text{Im}(\mathbf{A}) & \text{Re}(\mathbf{A}) \end{bmatrix} \quad (88)$$

The  $\hat{\mathbf{n}}$  is a real zero-mean Gaussian random vector with the covariance matrix  $\frac{\sigma^2}{2} \mathbf{I}_{2N}$ . Vector  $\hat{\mathbf{x}}$  is a  $2N$ -element zero-mean Gaussian random vector with the covariance matrix  $\mathbf{\Omega} = \frac{\sigma^2}{2} \hat{\mathbf{A}} \hat{\mathbf{A}}^T$ . The moment-generating function is  $\phi(t) = \exp\left(\frac{1}{2} t^T \mathbf{\Omega} t\right)$ . By differentiating the moment-generating function, it is possible to obtain the multivariate moments. For example,  $E\left[\hat{x}_k^2 \hat{x}_l^2\right] = \Omega_{k,k} \Omega_{l,l} + 2\Omega_{k,l}^2$ , and  $E\left[\hat{x}_k^3 \hat{x}_l\right] = 3\Omega_{k,k} \Omega_{k,l}$  [138]. In [138], a general expression using the hafnian of the covariance matrix is given.

Let us first discuss the case  $v = 2$ . Now, the first raw moment requires finding

$$\begin{aligned} E\left[|x_k|^4\right] &= E\left[\left(\text{Re}(x_k)^2 + \text{Im}(x_k)^2\right)^2\right] \\ &= E\left[\text{Re}(x_k)^4 + \text{Im}(x_k)^4 + 2\text{Re}(x_k)^2 \text{Im}(x_k)^2\right]. \end{aligned} \quad (89)$$

Therefore,

$$P_1 = \sum_{k=1}^N (3\Omega_{k,k}^2 + 3\Omega_{k+N,k+N}^2 + 2\Omega_{k,k}\Omega_{k+N,k+N} + 4\Omega_{k,k+N}^2). \quad (90)$$

Similarly, the second raw moment requires solving

$$\begin{aligned} E \left[ |x_k|^4 |x_l|^4 \right] &= E \left[ \left( \text{Re}(x_k)^4 + \text{Im}(x_k)^4 + 2\text{Re}(x_k)^2 \text{Im}(x_k)^2 \right) \right. \\ &\times \left. \left( \text{Re}(x_l)^4 + \text{Im}(x_l)^4 + 2\text{Re}(x_l)^2 \text{Im}(x_l)^2 \right) \right] \\ &= E \left[ \text{Re}(x_k)^4 \text{Re}(x_l)^4 + \text{Re}(x_k)^4 \text{Im}(x_l)^4 + 2\text{Re}(x_k)^4 \text{Re}(x_l)^2 \text{Im}(x_l)^2 \right. \\ &\quad + \text{Im}(x_k)^4 \text{Re}(x_l)^4 + \text{Im}(x_k)^4 \text{Im}(x_l)^4 + 2\text{Im}(x_k)^4 \text{Re}(x_l)^2 \text{Im}(x_l)^2 \\ &\quad + 2\text{Re}(x_k)^2 \text{Im}(x_k)^2 \text{Re}(x_l)^4 + 2\text{Re}(x_k)^2 \text{Im}(x_k)^2 \text{Im}(x_l)^4 \\ &\quad \left. + 4\text{Re}(x_k)^2 \text{Im}(x_k)^2 \text{Re}(x_l)^2 \text{Im}(x_l)^2 \right] \end{aligned} \quad (91)$$

which can be evaluated by calculating the appropriate multivariate moments. The resulting expression is lengthy and it is not shown here. However, the procedure for obtaining multivariate moments of complex random variables using real-valued random variables can be seen.

When  $v = 1$ , derivation is easier than in the general case, due to the expression

$$\begin{aligned} T_1(\mathbf{x}) &= \sum_{k=1}^N |x_k|^2 = \mathbf{n}^H (\mathbf{A}^H \mathbf{A}) \mathbf{n} \\ &= \text{Re}(\mathbf{n}^H \mathbf{A}^H \mathbf{A} \mathbf{n}) = \hat{\mathbf{n}}^T (\hat{\mathbf{A}}^T \hat{\mathbf{A}}) \hat{\mathbf{n}}, \end{aligned} \quad (92)$$

where the last expression is a real Gaussian quadratic form. The mean, variance and skewness can be calculated based on (92) and the properties of the real and symmetric Gaussian quadratic forms [139, 140].

## 7.2 Shifted log-normal approximation

The shifted log-normal approximation uses

$$P(x) = \frac{1}{\sqrt{\zeta^2} (x-c) \sqrt{2\pi}} e^{-(\log(x-c)-\lambda)^2/(2\zeta^2)}, \quad (93)$$

where  $\lambda$ ,  $\zeta^2$  and  $c$  are the parameters of the shifted log-normal approximation. Based on the knowledge of the mean  $P_1$ , the variance  $V$ , the skewness  $y$  from (85), and using the method of moments, these parameters are found to be ([132, 25])

$$\zeta^2 = \log \left( 1 + \left( \frac{1}{2} \sqrt[3]{4y + 4\sqrt{4+y^2}} - 2/\sqrt[3]{4y + 4\sqrt{4+y^2}} \right)^2 \right), \quad (94)$$

$$\lambda = -\frac{1}{2}\zeta^2 + \frac{1}{2} \log \left( \frac{V}{e\zeta^2 - 1} \right), \quad (95)$$

and the shift parameter

$$c = P_1 - e^{\left(\lambda + \frac{1}{2}\zeta^2\right)}. \quad (96)$$

The threshold corresponding to the shifted log-normal approximation can be found by using the inverse of the log-normal cumulative distribution function and adding the shift parameter. The threshold becomes

$$\eta = e^{\left(\sqrt{\zeta^2}Q^{-1}(P_{\text{FA,DES}}) + \lambda\right)} + c, \quad (97)$$

where  $Q$  is the tail integral of the Gaussian PDF. Note that thresholds can be precalculated and then scaled based on the currently valid noise variance estimate. Similarly, an approximation to the probability of the false alarm  $P_{\text{FA}}$  for a given threshold can be presented as

$$P_{\text{FA}} \approx Q \left( \frac{\log(\eta - c) - \lambda}{\sqrt{\zeta^2}} \right). \quad (98)$$

### 7.3 Contiguity-based detector

In [107], several contiguity based PLDs have been proposed. A certain amount of adjacent bins (values 2 and 3 have been used in [107]) are summed together. This smoothes the periodogram (FFT) spectrum estimate. The averaged spectrum estimate is used in calculation of the power-law statistic. Consider the  $T_{f2}$  detector that sums two adjacent bins. In this case, the decision statistic is

$$T_{f2,v} = \sum_{j=1}^N U_j^v = \sum_{j=1}^N \left( |x_{j-1}|^2 + |x_j|^2 \right)^v, \quad (99)$$

where  $U_j = |x_{j-1}|^2 + |x_j|^2$  and bins are indexed modulo  $N$ . In [107], the exact mean and variance of the decision statistic (99) have been derived assuming that an orthogonal transform has been used. Here, the following procedure is used. First, a general expression is written for the first three moments. This expression is then expanded. Finally, the expected values of the terms in the expression are evaluated using the partial derivation method [136]. For example, the general expression for the mean is  $E(T_{f2,v}) = \sum_{j=1}^N E \left( \left( |x_{j-1}|^2 + |x_j|^2 \right)^v \right)$ . When  $v = 2$ ,

$$E(T_{f2,2}) = \sum_{j=1}^N \left[ E \left( |x_{j-1}|^4 \right) + 2E \left( |x_{j-1}|^2 |x_j|^2 \right) + E \left( |x_j|^4 \right) \right] \quad (100)$$

and the resulting terms can then be evaluated with the partial derivation method. The second raw moment,  $E\left(T_{f2,v}^2\right)$ , is

$$\begin{aligned} & E\left(\sum_{k=1}^N\left(|x_{k-1}|^2+|x_k|^2\right)^v\sum_{l=1}^N\left(|x_{l-1}|^2+|x_l|^2\right)^v\right) \\ &= \sum_{k=1}^N\sum_{l=1}^N E\left(\left(|x_{k-1}|^2+|x_k|^2\right)^v\left(|x_{l-1}|^2+|x_l|^2\right)^v\right). \end{aligned} \quad (101)$$

For example, when  $v = 1$ ,  $E\left(T_{f2,1}^2\right)$  is

$$\begin{aligned} & \sum_{k=1}^N\sum_{l=1}^N\left[E\left(|x_{k-1}|^2|x_{l-1}|^2\right)+E\left(|x_{k-1}|^2|x_l|^2\right)\right. \\ & \left.+E\left(|x_k|^2|x_{l-1}|^2\right)+E\left(|x_k|^2|x_l|^2\right)\right], \end{aligned} \quad (102)$$

where the terms can be evaluated with the partial derivation method. This same approach can be used to calculate all the necessary moments of the decision variable. In [107], the mean and variance of the decision variables  $T_{f2,1}$  and  $T_{f2,2}$  have been evaluated assuming an orthogonal transform. The results obtained using the more general expressions presented here were verified to be exactly equal to those in this special case.

## 7.4 Numerical results

Figs. 39–41 show the simulation results and the theoretical approximations for the probability of the false alarm  $P_{\text{FA}}$  versus the threshold. In the simulations, the FFT length was  $N = 256$  and a Hamming window was used. The number of Monte-Carlo loops used in the simulations was  $5 \times 10^7$ . It can be seen from Fig. 39 that when  $v = 1$  and  $P_{\text{FA,DES}} = 10^{-3}$ , the Gaussian approximation gives a threshold of roughly 128. Based on the simulation results, it is seen that this is too low, the correct threshold is slightly over 130. The threshold based on the shifted log-normal approximation is accurate even when  $P_{\text{FA,DES}}$  is very small. It is observed from Fig. 40 that when  $v = 2$ , the shifted log-normal approximation can be used when  $P_{\text{FA,DES}}$  is to the order of  $10^{-5}$ . It can be seen from Fig. 41 that when  $v = 3$ , the shifted log-normal approximation can be used when  $P_{\text{FA,DES}} \geq 10^{-3}$ . It is noted that when  $v$  increases, the accuracy of the shifted log-normal approximation decreases as the probability of a false alarm diminishes. Note that in a typical situation, a value  $v = 2$  would probably be used because it gives a balanced performance for different signal types [31]. In the case of the  $T_{f2}$  detector with  $v = 2$ , the simulation results showed that the threshold is accurate when  $P_{\text{FA,DES}} \geq 10^{-5}$ .

It is interesting to compare the accuracy of the threshold setting method presented here to the method presented in [107] in the special case where an orthogonal transform (FFT without windowing) is used. A comparison was performed with the  $T_{f2}$  detector,  $N = 256$  and  $v = 1$  or  $v = 2$ . The results in the case of  $v = 1$  were as good as those obtained in [107, Fig. 5]. In fact, both results are practically equal. Fig. 42 shows results when  $v = 2$  is used. In this case, some of the terms were found to be extremely cumbersome to calculate using the partial derivation method. Therefore, when evaluating the more complicated

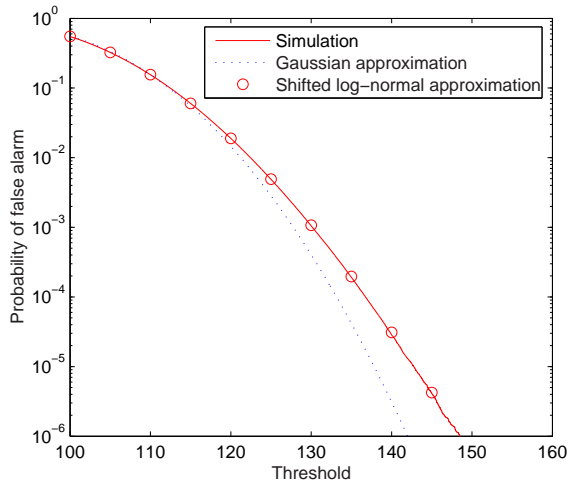


**Fig. 39.** Simulation results and theoretical approximations for the probability of a false alarm,  $N = 256$ , Hamming window,  $v = 1$ .

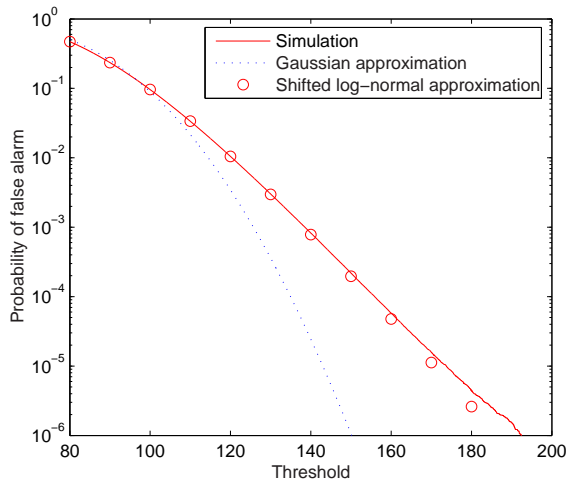


**Fig. 40.** Simulation results and theoretical approximations for the probability of a false alarm,  $N = 256$ , Hamming window,  $v = 2$ .

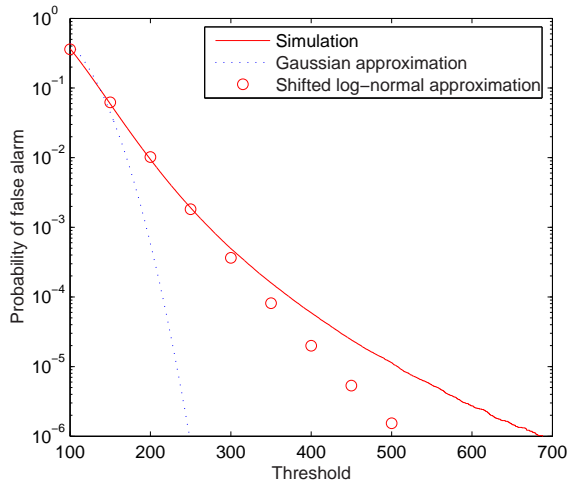


**Fig. 41.** Simulation results and theoretical approximations for the probability of a false alarm,  $N = 256$ , Hamming window,  $v = 3$ .

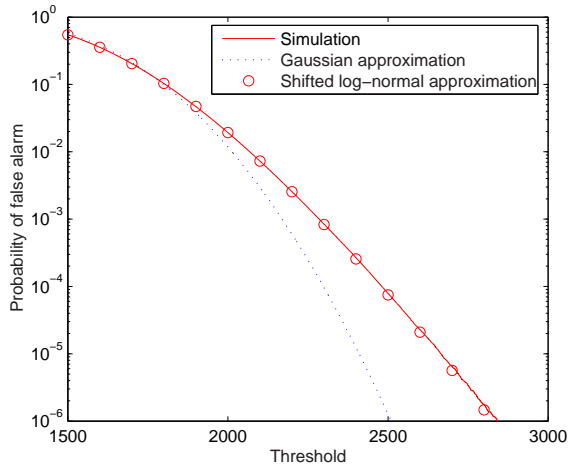


**Fig. 42.** Simulation results and theoretical approximations for the probability of false alarm,  $N = 256$ , no window, contiguity-based  $T_{f2}$  detector with  $v = 2$ .

Table 1. Windowing Losses (Hamming window).

|                                  | Direct sequence signal | Narrowband signal |
|----------------------------------|------------------------|-------------------|
| Radiometer                       | 1.5 dB                 | 1.5 dB            |
| Nuttall ( $v = 2$ )              | 1.3 dB                 | 0.9 dB            |
| Nuttall ( $v = 3$ )              | 0.9 dB                 | 0.6 dB            |
| Contiguity $T_{f_2}$ ( $v = 2$ ) | 1.7 dB                 | 1.3 dB            |

terms, symbolic differences were used instead of symbolic derivatives. By comparing the results to those given [107] for the saddlepoint approximation, it was observed that the method presented here had slightly better accuracy.

Figs. 43(a)–43(b) show the simulated miss probabilities when the signal to be detected is a sinusoidal signal. The theoretical miss probabilities [9] are also presented for the total-power radiometer (PLD with  $v = 1$ ) in addition to the simulation results. It can be seen that the PLD with  $v = 2$  has significantly better performance than the conventional total-power radiometer. The PLD with  $v = 3$  is somewhat better than the PLD with  $v = 2$ . The contiguity-based  $T_{f_2}$  detector with  $v = 2$  has roughly same performance as the conventional PLD with  $v = 2$  when no windowing was used. In the case where windowing is used, the  $T_{f_2}$  detector has a slightly worse performance. The windowing loss associated with the total-power radiometer is 1.5 dB. The windowing loss is the additional SNR required to get the same performance with windowing as with the case without windowing (or the rectangular window is used). The windowing loss with  $v = 2$  is approximately 0.9 dB. This means that the PLD with  $v = 2$  suffers less from windowing than the total-power radiometer. The loss associated with the PLD with the power-law parameter  $v = 3$  was 0.6 dB and the loss associated with the  $T_{f_2}$  detector with  $v = 2$  was 1.3 dB.

Figs. 44(a)–44(b) show the simulated miss probabilities when the signal to be detected is a DS signal. In this case, the total-power radiometer has the best performance. The PLD with  $v = 2$  and the  $T_{f_2}$  detector with  $v = 2$  also have a rather good performance. The PLD with  $v = 3$  has the worst performance. The windowing loss associated with the total-power radiometer was 1.5 dB. The windowing loss associated with the PLD with  $v = 2$  was 1.3 dB. This means that in the case of a wideband signal, the PLD with  $v = 2$  has only 0.2 dB smaller windowing loss than the total-power radiometer. The windowing loss when  $v = 3$  is used, was 0.9 dB and the loss, when the  $T_{f_2}$  detector with  $v = 2$  is used was 1.7 dB. These results are summarized in Table 1. Simulations were also performed with a 4-term Blackman-Harris window. In this case, losses were higher than with the Hamming window, roughly 2–3 dB depending on the parameters.

## 7.5 Conclusions

A new method for setting the threshold of a power-law detector that uses a non-orthogonal transform was proposed and analyzed. The simulation results showed that the accuracy

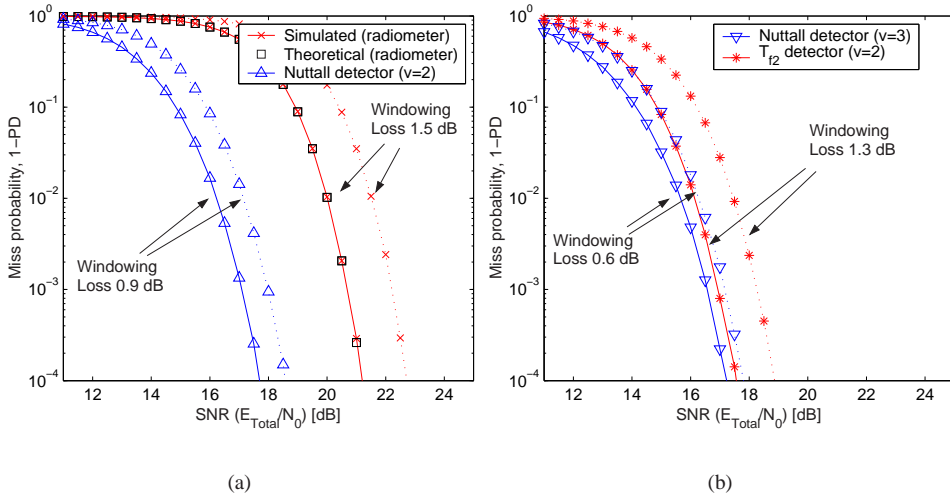


**Fig. 43.** Simulated miss probabilities,  $P_{FA,DES} = 10^{-3}$ , sinusoidal signal,  $N = 256$ . Solid lines are results without windowing and dotted lines are results with a Hamming window. (a)  $v = 1$  (radiometer) and  $v = 2$  (b)  $v = 3$  and  $T_{f2}$  detector with  $v = 2$ .

of the threshold depends on the power-law parameter. In the case of a typical value of the power-law parameter, the method can be used even when the required probability of the false alarm is to the order of  $10^{-5}$ . The simulation results showed that the windowing loss associated with the Hamming window is 0.6–1.7 dB depending on the power-law parameter and the signal to be detected.

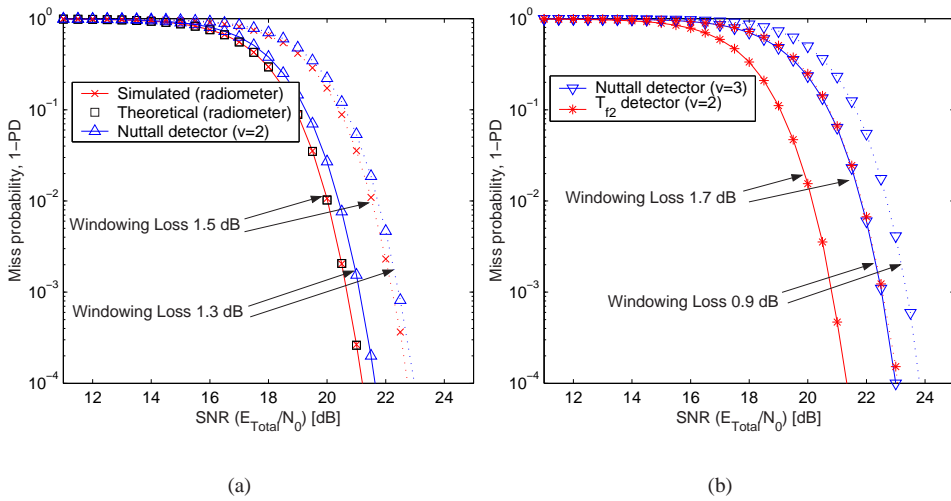


**Fig. 44.** Simulated miss probabilities,  $P_{\text{FA,DES}} = 10^{-3}$ , DS signal,  $N = 256$ . Solid lines are results without windowing and dotted lines are results with Hamming window. (a)  $v = 1$  (radiometer) and  $v = 2$  (b)  $v = 3$  and  $T_{f_2}$  detector with  $v = 2$ .

## 8 Conclusions and future work

In this thesis, energy based detectors were developed and analyzed. The relevant literature was reviewed in Chapter 2. Signal models for a digital receiver and a channelized radiometer were presented in Chapter 3.

The effects of quantization on the total power radiometer were considered in Chapter 4. Two cases were studied: (1) the noise power is unknown; and (2) the noise power is known. In case (1) the focus was on analyzing the CA-CFAR threshold setting strategy with different scaling factors. In case (2), three different threshold setting strategies were studied and compared. Numerical examples demonstrated that the threshold corresponding to the Gaussian quantization noise assumption performed surprisingly well and that 3 or 4 quantization bits are typically required for obtaining the desired false alarm probability. In future work, the effects of quantization on other detection structures could be studied. The effects of a power (variance) mismatch between reference samples and the actual noise on different detection structures could be compared. Additionally, new CFAR methods could be applied and/or developed for cases with a small dynamic range, i.e., a large saturation (overload) probability. For example, bi-parametric CFAR strategies estimating both the granular noise and the saturation (overload) noise could be investigated. Automatic gain control strategies could be studied and optimized especially for the digital total power radiometer. Interference mitigation could be applied prior to energy detection, especially in scenarios with narrow-band or impulsive interference sources that would otherwise render the energy detector useless. It might be worthwhile investigating the performance loss of systems using a general purpose receiver, where the in-phase and quadrature channels are separately quantized, compared to more specialized systems using envelope quantization. The addition of noise / dither could be investigated since the performance of a suboptimal detector may, in some special cases, be improved by adding noise [141].

Detection of frequency hopping signals, assuming time synchronism, was studied in Chapter 5. The logical OR-sum channelized radiometer, the sum-sum channelized radiometer, the max-sum channelized radiometer and the optimal detector using frequency sweeping were analyzed. Numerical examples demonstrated that if the number of hops observed per decision is large, frequency sweeping degrades the performance compared to a system that does not apply frequency sweeping with or without fading. If the number of hops observed is small, sweeping can be necessary to get the desired performance.

When the channel was fading, the best performance was obtained using fast sweeping. Without fading, the maximum based intercept receiver had the best performance, unless the POI was small. When the POI was large, the performance of the maximum based receiver was close to that of the optimal receiver. In the case of fading, logical OR-sum and sum-sum receivers had better performance than the maximum based receiver. The assumption of time synchronism was reasonable, since otherwise analytical results are much more complicated. Radiometer outputs from  $K$  detection phases within a hop interval were grouped together before applying, for example, logical-OR combining. In future work, the advantages of this grouping — as opposed to simply processing the  $K$  detection phases separately — could be studied in a more realistic case without time synchronism. Systems using an estimate of the SNR in order to improve detection could be investigated. A sequential procedure could be applied.

CFAR strategies, in the context of the channelized radiometer, were studied in Chapter 6. The methods studied were CA, OS, and iterative CFAR methods (FCME+CA, CA+CA, BCME+CA). The numerical results showed that iterative CFAR methods can improve the signal detection performance when some reference cells are corrupted and contain signal(s) in addition to noise. In most cases, the FCME+CA detector had the best detection performance, closely followed by the CA+CA detector. In some cases, the FCME+CA provided a somewhat larger false alarm probability than the desired value. The BCME+CA detector had a worse performance than both of these methods. The conventional OS detector also performs well, assuming its parameter is correctly chosen. Actually, when the SNR was small, the OS detector had the best performance. In future work, the performance of systems using CMLD scaling factors after censoring should be investigated and compared with systems using CA or TM scaling factors after censoring. Different methods of mapping the assumed number of interferers to the scaling factor could be studied (see Section 2.4.1). More detailed comparison could be made regarding also different numbers of multiple targets — perhaps with different strengths — with and without fading, and with different time-frequency products. It is expected that the CMLD and TM scaling factors will offer better false alarm performance than the CA scaling factors with small time-frequency products. In addition to simulation results, the performance of the iterative CFAR methods in the presence of inhomogeneous samples should be analytically studied. For example, assuming that interference is strong enough, the ordering of the reference samples can be approximated to be equal to separately ordering the noise-only samples and the samples containing interference, so that the samples containing interference always occupy the top-rank places [75]. Possible performance losses of systems using censoring directly for CFAR, relatively to the discussed two-stage systems could be analyzed. One could study Nitzberg's [88] idea that cells where target is decided to be present should not be included in the reference sets of future tests. Additional CFAR strategies could be explored. For example, it is expected that the clutter map CFAR will have good performance in stationary environments. The effects of post-detection processing / combining local decisions could be investigated.

Threshold setting of the power-law detector using windowing was studied in Chapter 7. A new method for setting the threshold of a power-law detector that uses a non-orthogonal transform was proposed and analyzed. The simulation results showed that the accuracy of the threshold depends on the power-law parameter. In the case of a typical value of the power-law parameter, the method can be used even when the required probability of

a false alarm is to the order of  $10^{-5}$ . The simulation results showed that the windowing loss associated with the Hamming window is 0.6–1.7 dB depending on the power-law parameter and the signal to be detected. In future work, more computationally efficient methods for calculating the moments of decision variable could be searched. Overlapping windows could be studied for reducing the windowing loss [112]. It might be worthwhile to extend the analysis to include the CFAR power-law detector as well.

The results in this thesis have significantly advanced the understanding of energy or power based detectors in single antenna systems. First, a study of quantized total power radiometer performance with and without noise level estimation was presented. Then, the sweeping channelized radiometer with several total power radiometer channels was analyzed, without noise level estimation. Several methods were studied for combining the local decisions. For simplicity, the standard (ideal) radiometer model, without quantization, was applied. Next, the channelized total power radiometer using novel noise level estimation methods was studied. For simplicity, the analysis was limited to a case without post-detection processing. Finally, a new threshold setting method was proposed for a system making local decisions with the windowed power-law detector, without noise level estimation.

## References

1. Bayes T (1764) An essay towards solving a problem in the doctrine of chances. *Philosophical Transactions of the Royal Society of London* 53: 370–418.
2. Neyman J & Pearson ES (1933) On the problem of the most efficient tests of statistical hypotheses. *Philosophical Transactions of the Royal Society of London, Series A*. 231: 289–337.
3. Van Trees HL (1968) *Detection, Estimation, and Modulation Theory, Part I*. John Wiley & Sons.
4. Kay SM (1998) *Fundamentals of statistical signal processing. Volume II: detection theory*. Prentice Hall, Upper Saddle River, New Jersey.
5. Hippenstiel RD (2002) *Detection theory: applications and digital signal processing*. CRC Press LLC, Boca Raton, Florida.
6. Poor HV (1998) *An introduction to signal detection and estimation, 2nd edition*. Springer-Verlag, Berlin, Germany.
7. Proakis JG (1995) *Digital Communications, 3rd edition*. McGraw-Hill, Inc., Singapore.
8. Schleher DC (1986) *Introduction to electronic warfare*. Artech House, Norwood, MA.
9. Dillard RA & Dillard GM (1989) *Detectability of Spread-Spectrum Signals*. Artech House, Norwood, MA.
10. Mills RF & Prescott GE (1995) Waveform design and analysis of frequency hopping LPI networks. *Proc. IEEE Military Communications Conference*. San Diego, CA, 2: 778–782.
11. Miller LE, Lee JS & Torrieri DJ (1993) Frequency-hopping signal detection using partial band coverage. *IEEE Transactions on Aerospace and Electronic Systems* 29: 540–553.
12. DiFranco JV & Rubin WL (1980) *Radar Detection*. Artech House, Dedham, MA.
13. Batchelder L (1965) Sonics in the sea. *Proceedings of the IEEE* 53: 1310–1319.
14. Sahai A, Hoven N & Tandra R (2004) Some fundamental limits on cognitive radio. *Proc. Annual Allerton Conference on Communications, Control, and Computing*. Monticello, Illinois.
15. Haykin S (2005) Cognitive radio: Brain-empowered wireless communications. *IEEE Journal on Selected Areas in Communications* 23: 201–220.
16. Cabric D, Mishra SM & Brodersen RW (2004) Implementation issues in spectrum sensing for cognitive radios. *Proc. Annual Asilomar Conference on Signals, Systems and Computers*. Pacific Grove, CA, 1: 772–776.
17. Reggiani L & Maggio GM (2005) Rapid search algorithms for code acquisition in UWB impulse radio communications. *IEEE Journal on Selected Areas in Communications* 23: 898–908.
18. Gibson JD & Melsa JD (1975) *Introduction to Nonparametric Detection with Applications*, vol. 119 of *Mathematics in science and engineering*. Academic Press, New York, NY.
19. Gandhi PP & Kassam SA (1988) Analysis of CFAR processors in nonhomogeneous background. *IEEE Transactions on Aerospace and Electronic Systems* 24: 427–445.
20. Hillenbrand J, Weiss TA & Jondral FK (2005) Calculation of detection and false alarm probabilities in spectrum pooling systems. *IEEE Communications Letters* 9: 349–351.

21. Oppermann I, Hämäläinen M & Inatti J (2004) UWB Theory and Applications. John Wiley & Sons.
22. Oppermann I, Stoica L, Rabbachin A, Shelby Z & Haapola J (2004) UWB wireless sensor networks: UWEN – a practical example. *IEEE Communications Magazine* 42: S27–S32.
23. Lehtomäki JJ, Juntti M, Saarnisaari H & Koivu S (2005) Threshold setting strategies for a quantized total power radiometer. *IEEE Signal Processing Letters* 12: 796–799.
24. Lehtomäki JJ & Juntti M (2005) Detection of frequency hopping signals using a sweeping channelized radiometer. *Signal Processing*, Elsevier Publishing Company 85: 2030–2043.
25. Lehtomäki JJ (2003) Maximum based detection of slow frequency hopping signals. *IEEE Communications Letters* 7: 201–203.
26. — (2003) Performance comparison of multichannel energy detector output processing methods. *Proc. Seventh International Symposium on Signal Processing and Its Applications*. Paris, France, 1: 261–264.
27. Lehtomäki JJ, Juntti M & Saarnisaari H (2004) Detection of frequency hopping signals with a sweeping channelized radiometer. *Proc. Annual Asilomar Conference on Signals, Systems and Computers*. Pacific Grove, CA, 2: 2178–2182.
28. Nemsick LW & Geraniotis E (1992) Adaptive multichannel detection of frequency-hopping signals. *IEEE Transactions on Communications* 40: 1502–1511.
29. Lehtomäki JJ, Juntti M & Saarnisaari H (2005) CFAR strategies for channelized radiometer. *IEEE Signal Processing Letters* 12: 13–16.
30. — (2004) Power-law based intercept receiver with nonorthogonal transforms. *Proc. IEEE Military Communications Conference*. Monterey, CA, 3: 1402–1408.
31. Lehtomäki JJ (2004) Detection of spread spectrum signals using a power-law based intercept receiver. *Proc. IEEE Vehicular Technology Conference*. Milan, Italy, 3: 1480–1484.
32. Henttu P & Aromaa S (2002) Consecutive mean excision algorithm. *Proc. IEEE International Symposium on Spread Spectrum Techniques and Applications*. Prague, Czech Republic, 2: 450–454.
33. Urkowitz H (1967) Energy detection of unknown deterministic signals. *Proceedings of the IEEE* 55: 523–531.
34. Shnidman DA (2002) Determination of required SNR values. *IEEE Transactions on Aerospace and Electronic Systems* 38: 1059–1064.
35. Marcum J (1960) A statistical theory of target detection by pulsed radar. *IRE Transactions on Information Theory* 6: 59–267.
36. Mills RF & Prescott GE (1996) A comparison of various radiometer detection models. *IEEE Transactions on Aerospace and Electronic Systems* 32: 467–473.
37. Kelly EJ, Lyons DH & Root WL (1963) The sensitivity of radiometric measurements. *SIAM Journal of Applied Mathematics* 11: 253–257.
38. Sonnenschein A & Fishman PM (1992) Radiometric detection of spread-spectrum signals in noise of uncertain power. *IEEE Transactions on Aerospace and Electronic Systems* 28: 654–660.
39. Cai KV, Phan V & O'Connor RJ (1989) Energy detector performance in a noise fluctuating channel. *Proc. IEEE Military Communications Conference*. Boston, MA, 1: 85–89.
40. Gevargiz J, Das PK & Milstein LB (1989) Adaptive narrow-band interference rejection in a DS spread-spectrum intercept receiver using transform domain signal processing techniques. *IEEE Transactions on Communications* 37: 1359–1366.
41. Davidovici S & Kanterakis EG (1989) Radiometric detection of direct-sequence spread-spectrum signals using interference excision. *IEEE Journal on Selected Areas in Communications* 7: 576–589.
42. Polydoros A & Weber CL (1985) Detection performance considerations for direct-sequence and time-hopping LPI waveforms. *IEEE Journal on Selected Areas in Communications* 3: 727–744.
43. McKinstry DR & Buehrer RM (2002) Issues in the performance and covertness of UWB communications systems. *Proc. Midwest Symposium on Circuits and Systems*. Tulsa, Oklahoma, 3: 601–604.
44. Gardner WA (1988) Signal interception: a unifying theoretical framework for feature detection. *IEEE Transactions on Communications* 36: 897–906.

45. Hill DA & Felstead EB (1995) Laboratory performance of spread spectrum detectors. IEE Proceedings – Communications 142: 243–249.
46. Sousa MJ (1992) Limitations of crosscorrelation radiometer performance. Proc. IEEE Military Communications Conference. San Diego, CA, 3: 816–821.
47. Eaddy DA, Kadota TT & Seery JB (1984) On the approximation of the optimum detector by the energy detector in detection of colored Gaussian signals. IEEE Transactions on Acoustics, Speech, and Signal Processing 32: 661–664.
48. MacMullan SJ (1994) The effect of multipath fading on the radiometric detection of frequency hopped signals. Proc. IEEE International Symposium on Spread Spectrum Techniques and Applications. Oulu, Finland, 1: 243–247.
49. Kostylev VI (2002) Energy detection of a signal with random amplitude. Proc. IEEE International Conference on Communications. New York, NY, 3: 1606–1610.
50. Digham FF, Alouini MS & Simon MK (2003) On the energy detection of unknown signals over fading channels. Proc. IEEE International Conference on Communications. Anchorage, AK, 5: 3575–3579.
51. Ohlson JE & Swett JE (1973) Digital radiometer performance. IEEE Transactions on Aerospace and Electronic Systems 9: 864–874.
52. Fischman MA & England AW (1999) Sensitivity of a 1.4 GHz direct-sampling digital radiometer. IEEE Transactions on Geoscience and Remote Sensing 37: 2172–2180.
53. Koivu S, Saarnisaari H & Juntti M (2004) Quantization and dynamic range effects on the energy detection. Proc. Nordic Signal Processing Symposium. Espoo, Finland, 264–267.
54. — (2004) Comparison of quantized power-law based intercept receivers. Proc. IEEE Military Communications Conference. Monterey, CA, 3: 1345–1351.
55. Gandhi PP (1996) Data quantization effects in CFAR signal detection. IEEE Transactions on Aerospace and Electronic Systems 32: 1277–1289.
56. Dillard RA (1979) Detectability of spread-spectrum signals. IEEE Transactions on Aerospace and Electronic Systems 15: 526–537.
57. Shnidman DA (2004) Binary integration with a cascaded detection scheme. IEEE Transactions on Aerospace and Electronic Systems 40: 751–755.
58. Torrieri DJ (1992) Principles of Secure Communication Systems, 2nd edition. Artech House, Norwood, MA.
59. Schwartz M (1956) A coincidence procedure for signal detection. IRE Transactions on Information Theory 2: 135–139.
60. Harrington JV (1955) An analysis of the detection of repeated signals in noise by binary integration. IRE Transactions on Information Theory 1: 1–9.
61. Dillard GM (1967) A moving-window detector for binary integration. IEEE Transactions on Information Theory 13: 2–6.
62. Dinneen GP & Reed IS (1956) An analysis of signal detection and location by digital methods. IRE Transactions on Information Theory 2: 29–38.
63. Tsui JB (1992) Microwave receivers with electronic warfare applications. Krieger publishing company, Malabar, Florida.
64. Mills RF & Prescott GE (2000) Detectability models for multiple access low-probability-of-intercept networks. IEEE Transactions on Aerospace and Electronic Systems 36: 848–858.
65. — (1995) Waveform design and analysis of frequency hopping LPI networks. Proc. IEEE Military Communications Conference. San Diego, CA, 2: 778–782.
66. Levitt BK, Cheng U, Polydoros A & Simon MK (1994) Optimum detection of slow frequency-hopped signals. IEEE Transactions on Communications 42: 1990–2000.
67. Beaulieu NC, Hopkins WL & McLane PJ (1990) Interception of frequency-hopped spread-spectrum signals. IEEE Journal on Selected Areas in Communications 8: 853–870.
68. Levitt BK, Simon MK, Polydoros A & Cheng U (1993) Partial-band detection of frequency-hopped signals. Proc. IEEE Global Telecommunication Conference. Houston, Texas, 4: 70–76.
69. Höring HC (1998). Probability of intercept for frequency hop signals using search receivers (i). News from Rohde & Schwarz 160 - 1998/TV - Radiomonitoring.
70. — (1999). Probability of intercept for frequency hop signals using search receivers (ii). News from Rohde & Schwarz 161 - 1999/I - Radiomonitoring.

71. Bharadwaj A & Townsend JK (2001) Evaluation of the covertness of time-hopping impulse radio using a multi-radiometer detection. Proc. IEEE Military Communications Conference. Vienna, VA, 1: 128–134.
72. Snelling WE & Geraniotis E (1994) Analysis of compressive receivers for the optimal interception of frequency-hopped waveforms. IEEE Transactions on Communications 42: 127–138.
73. Guida M, Longo M & Lops M (1993) Biparametric CFAR procedures for lognormal clutter. IEEE Transactions on Aerospace and Electronic Systems 29: 798–809.
74. Klemola O & Lehto A (1998) Tutkatekniikka [in Finnish], 2nd edition. Otatieto, Helsinki, Finland.
75. Lops M (1996) Hybrid clutter-map / L-CFAR procedure for clutter rejection in nonhomogeneous environment. IEE Proceedings – Radar, Sonar and Navigation) 143: 239–245.
76. Ritcey JA (1986) Performance analysis of the censored mean-level detector. IEEE Transactions on Aerospace and Electronic Systems 22: 443–453.
77. Kim CJ, Han DS & Lee HS (1993) Generalized OS CFAR detector with noncoherent integration. Signal Processing, Elsevier Publishing Company 31: 43–56.
78. Gandhi PP & Kassam SA (1994) Optimality of the cell averaging CFAR detector. IEEE Transactions on Information Theory 40: 1226–1228.
79. Rohling H (1983) Radar CFAR thresholding in clutter and multiple target situations. IEEE Transactions on Aerospace and Electronic Systems 19: 608–621.
80. Gandhi PP & Kassam SA (1989) An adaptive order statistic constant false alarm rate detector. Proc. IEEE International Conference on Systems Engineering. Fairborn, USA, 85–88.
81. Rickard JT & Dillard GM (1977) Adaptive detection algorithms for multiple-target situations. IEEE Transactions on Aerospace and Electronic Systems 13: 338–343.
82. Holm JR & Ritcey JA (1991) The optimality of the censored mean-level detector. IEEE Transactions on Information Theory 37: 206–209.
83. Ozgunes I, Gandhi PP & Kassam SA (1992) A variably trimmed mean CFAR radar detector. IEEE Transactions on Aerospace and Electronic Systems 28: 1002–1014.
84. Shnidman DA (1995) Radar detection probabilities and their calculation. IEEE Transactions on Aerospace and Electronic Systems 31: 928–950.
85. Lim CH & Lee HS (1993) Performance of order-statistics CFAR detector with noncoherent integration in homogenous situations. IEE Proceedings F 140: 291–296.
86. Han DS & Lee HS (1993) Performance of modified order statistics CFAR detectors with noncoherent integration. Signal Processing, Elsevier Publishing Company 31: 31–42.
87. Smith ME & Varshney PK (2000) Intelligent CFAR processor based on data variability. IEEE Transactions on Aerospace and Electronic Systems 36: 837–847.
88. Nitzberg R (1986) Clutter map CFAR analysis. IEEE Transactions on Aerospace and Electronic Systems 22: 419–421.
89. Lops M & Orsini M (1989) Scan-by-scan averaging CFAR. IEE Proceedings F 136: 249–254.
90. Weiss M (1982) Analysis of some modified cell-averaging CFAR processors in multiple-target situations. IEEE Transactions on Aerospace and Electronic Systems 18: 102–114.
91. Goldman H & Bar-David I (1988) Analysis and application of the excision CFAR detector. IEE Proceedings F 135: 563–575.
92. Conte E, Longo M & Lops M (1989) Analysis of the excision CFAR detector in the presence of fluctuating targets. IEE Proceedings F 136: 290–292.
93. Goldman H (1990) Performance of the excision CFAR detector in the presence of interferers. IEE Proceedings F 137: 163–171.
94. Barbov B, Lomes A & Perkalski E (1986) Cell-averaging CFAR for multiple-target situations. IEE Proceedings F 133: 176–186.
95. Barkat M, Himonas SD & Varshney PK (1989) CFAR detection for multiple target situations. IEE Proceedings F 136: 193–209.
96. Himonas SD & Barkat M (1992) Automatic censored CFAR detection for nonhomogeneous environments. IEEE Transactions on Aerospace and Electronic Systems 28: 286–304.
97. Melvin WL & Wicks MC (1997) Improving practical space-time adaptive radar. Proc. IEEE National Radar Conference. Syracuse, NY, 48–53.
98. Saarnisaari H & Henttu P (2003) Impulse detection and rejection methods for radio systems. Proc. IEEE Military Communications Conference. Boston, MA, 2: 13–16.

99. Saarnisaari H, Henttu P & Juntti M (2005) Iterative multidimensional impulse detectors for communications based on the classical diagnostic methods. *IEEE Transactions on Communications* 53: 395–398.
100. Vartiainen J (2005) Concentrated signal extraction using consecutive mean excision algorithms. *Proc. Finnish Signal Processing Symposium*. Kuopio, Finland, 87–90.
101. Juntti M, Saarnisaari H, Vartiainen J, Lehtomäki J & Myllylä M (2005) Diagnostic methods - general purpose tools for concentrated signal processing. *Proc. International Workshop on Convergent Technologies (Invited paper)*. Oulu, Finland.
102. Vartiainen J, Lehtomäki J, Aromaa S & Saarnisaari H (2004) Consecutive mean excision interference suppressor in direct sequence systems. *Proc. Nordic Radio Symposium*. Oulu, Finland.
103. Farrouki A & Barkat M (2005) Automatic censoring CFAR detector based on ordered data variability for nonhomogeneous environments. *IEE Proceedings – Radar, Sonar and Navigation* 152: 43–51.
104. Weisstein EW (2005). Power sum. From MathWorld—A Wolfram Web Resource. <http://mathworld.wolfram.com/PowerSum.html>.
105. Fawcett JA & Maranda BH (1991) The optimal power law for the detection of a Gaussian burst in a background of Gaussian noise. *IEEE Transactions on Information Theory* 37: 209–214.
106. Nuttall AH (1995) Near-optimum detection of random signals of unknown location, structure, extent, and strength. *Proc. OCEANS '95*. San Diego, CA, 3: 1659–1664.
107. Wang Z & Willett PK (2001) All-purpose and plug-in power-law detectors for transient signals. *IEEE Transactions on Signal Processing* 49: 2454–2466.
108. Frey M & Andescavage D (1998) An analytical theory for power law detection of bursty targets in multiplicative noise. *IEEE Transactions on Signal Processing* 46: 2837–2841.
109. Tandra R & Sahai A (2005) Fundamental limits on detection in low SNR under noise uncertainty. *Proc. Signal Processing Symposium (WirelessCom)*. Maui, USA.
110. Chen B, Willett P & Streit R (1999) Transient detection using a homogeneity test. *Proc. IEEE International Conference on Acoustics, Speech, and Signal Processing*. Phoenix, AZ, 5: 2769–2772.
111. Stoica P & Moses RL (1997) *Introduction to Spectral analysis*. Prentice Hall, Upper Saddle River, New Jersey.
112. Young JA (1999) Performance metrics for windows used in real-time DFT-based multiple-tone frequency excision. *IEEE Transactions on Signal Processing* 47: 800–812.
113. Abramowitz M & Stegun IA (1964) *Handbook of Mathematical Functions with Formulas, Graphs, and Mathematical Tables*. U.S. Government Printing Office, Washington, District of Columbia.
114. Cimini, Jr LJ & Kassam SA (1983) Data quantization for narrowband signal detection. *IEEE Transactions on Aerospace and Electronic Systems* 19: 848–858.
115. Hansen VG (1974) Optimization and performance of multilevel quantization in automatic detectors. *IEEE Transactions on Aerospace and Electronic Systems* 10: 274–280.
116. Gersho A (1978) Principles of quantization. *IEEE Transactions on Circuits and Systems* 25: 427–436.
117. Marco D & Neuhoff DL (2005) The validity of the additive noise model for uniform scalar quantizers. *IEEE Transactions on Information Theory* 51: 1739–1755.
118. Sripad AB & Snyder DL (1977) A necessary and sufficient condition for quantization errors to be uniform and white. *IEEE Transactions on Acoustics, Speech, and Signal Processing* 25: 442–448.
119. Widrow B, Kollár I & Liu MC (1996) Statistical theory of quantization. *IEEE Transactions on Instrumentation and Measurement* 45: 353–361.
120. Kollár I & Blair JJ (2004) Improved determination of the best fitting sine wave in ADC testing. *Proc. Instrumentation and Measurement Technology Conference*. Como, Italy, 829–834.
121. Piepmeier JR & Gasiewski AJ (2001) Digital correlation and microwave polarimetry: Analysis and demonstration. *IEEE Transactions on Geoscience and Remote Sensing* 39: 2392–2410.
122. Willett P & Warren D (1992) The suboptimality of randomized tests in distributed and quantized detection systems. *IEEE Transactions on Information Theory* 38: 355–361.
123. Han YI & Kim T (1997) Randomized fusion rules can be optimal in distributed Neyman-Pearson detectors. *IEEE Transactions on Information Theory* 43: 1281–1288.

124. Weisstein EW (2005). Gamma distribution. From MathWorld—A Wolfram Web Resource. <http://mathworld.wolfram.com/GammaDistribution.html>.
125. Høst-Madsen A & Händel P (2000) Effects of sampling and quantization on single-tone frequency estimation. *IEEE Transactions on Signal Processing* 48: 650–662.
126. Dillard RA & Dillard GM (1996) Likelihood-ratio detection of frequency-hopped signals. *IEEE Transactions on Aerospace and Electronic Systems* 32: 543–553.
127. Cheng U, Simon MK, Polydoros A & Levitt BK (1994) Statistical models for evaluating the performance of coherent slow frequency-hopped M-FSK intercept receivers. *IEEE Transactions on Communications* 42: 689–699.
128. — (1995) Statistical models for evaluating the performance of noncoherent slow frequency-hopped M-FSK intercept receivers. *IEEE Transactions on Communications* 43: 1703–1712.
129. Chung CD (1994) Generalised likelihood-ratio detection of multiple-hop frequency-hopping signals. *IEE Proceedings – Communications* 141: 70–78.
130. Ng W & Beaulieu NC (1994) Noncoherent interception receivers for fast frequency-hopped spread spectrum signals. *Proc. Canadian Conference on Electrical and Computer Engineering, Halifax, Canada*, 348–351.
131. de Mello ERB, Bezerra VB & Khusnutdinov NR (2001) Ground state energy of massive scalar field inside a spherical region in the global monopole background. *Journal of Mathematical Physics* 42: 562–581.
132. Read KLQ (1998) A lognormal approximation for the collector’s problem. *American Statistician* 52: 175–180.
133. Swerling P (1960) Probability of detection for fluctuating targets (originally published in 1954 as RAND research memo RM-1217). *IRE Transactions on Information Theory* 6: 269–308.
134. Preisig JC & Johnson MP (2001) Signal detection for communications in the underwater acoustic environment. *IEEE Journal of Oceanic Engineering* 26: 572–585.
135. Cao G (1993) Bayesian Nonparametric Mixture Modeling. Ph.D. thesis, Institute of Statistics and Decision Sciences, Duke University.
136. Miller KS (1969) Complex Gaussian processes. *SIAM Review* 11: 544–567.
137. Neeser FD & Massey JL (1993) Proper complex random processes with applications to information theory. *IEEE Transactions on Information Theory* 39: 1293–1302.
138. Triantafyllopoulos K (2003). A remark on the central moments of the multidimensional Gaussian distribution. University of Bristol, preprint STA03-2. <http://www.ncl.ac.uk/math/research/publications/statistics/>.
139. Lancaster HO (1954) Traces and cumulants of quadratic forms in normal variables. *Journal of the Royal Statistical Society – Series B* 16: 247–254.
140. Ghazal GA (1996) Recurrence formula for expectations of products of quadratic forms. *Statistics & Probability Letters* 27: 101–109.
141. Kay S (2000) Can detectability be improved by adding noise? *IEEE Signal Processing Letters* 7: 8–10.